Steel weight reduction in offshore wind jacket structures by wrapped FRP joints

M.P.A. (Marc) van Vliet

TU Delft

Steel weight reduction in offshore wind jacket structures by wrapped FRP joints

by

M.P.A. (Marc) van Vliet

to obtain the degree of Master of Science
at the Delft University of Technology,
to be defended publicly on Friday December 20, 2019 at 15:00.

Student number:	4150945	
Project duration:	February 11, 2019 – December 20, 2019	
Thesis committee:	Dr. M. (Marko) Pavlović,	TU Delft CEG (Steel and Composite Structures), chair
	Prof. dr. P. G. (Peter) Steeneken,	TU Delft 3mE (Precision and Microsystems Eng.), supervisor
	MSc. M. (Marco) Vergassola	TU Delft CEG (Offshore Engineering), supervisor

An electronic version of this thesis is available at `http://repository.tudelft.nl/`.

TU Delft

Summary

This report investigates the potential reduction of steel weight for offshore wind turbine supporting jacket structures, if conventional welded joints are replaced by innovative wrapped FRP joints. This new type of connection is under development by Dr. Marko Pavlović at the Delft University of Technology, and shows outstanding fatigue performance compared to welded counterparts. As jacket structures suffer highly cyclic load, member thickness of current jackets is governed by the fatigue performance of welds. Due to the superior fatigue performance of wrapped FRP joints, substantial weight benefit is expected to be made.

The study examines a jacket supported 5 MW wind turbine located in 50-meter water depth in the North Sea. The structure and model are based on the UpWind project. The model includes soil-structure interaction by non-linear depth-dependent springs along with foundation piles.

Fatigue limit state (FLS) and ultimate limit state (ULS) are simulated by respectively five and three scenarios. The scenarios consider different combinations of wind (speed and direction), waves (height, period and direction) and current (speed and direction). Six 10-minute simulations are performed for each scenario with different wind turbulence and wave irregularity seeds. Wind and waves are applied in a single simulation, and normal force N and bending moments M_{ip} and M_{op} time series are recorded at a selection of elements.

The time series are post-processed in a self-written MATLAB procedure. For FLS, detailed fatigue analyses of welded joints are performed by evaluating crown and saddle hotspot stress, according to DNVGL-RP-C203. For every time step, the hot spot stress is calculated by applying geometry and load-dependent stress concentration factors (SCFs). Rainflow counting is applied, and the resulting stress range is projected on the details' S-N curve to evaluate the damage. Linear Palmgren-Miner is applied to accumulate damage. A similar procedure, including stress concentration at thickness transition, is applied to calculate fatigue of elements. For ULS, welded joints are checked for chord face and punching shear failure. Members are checked for tension yielding, local buckling and global buckling. ULS calculations are performed for all time steps and according to Eurocode manuals.

The unity check of both FLS and ULS is calculated for each individual member. Next, the member thickness is manually optimised to obtain the most optimal use of material. This optimisation is performed for three different cases with both mild S355 steel and high strength S690 steel. The welded steel structure, case 1, acts as a reference. The unwelded structure, case 2, is the lightest structure if joint fatigue does govern design. Case 3 gives the wrapped FRP structure and includes fatigue results obtained from small scale lab tests. Additionally, due to limited production length of steel tubular elements, it includes circumferential welds in the legs.

The potential jacket weight reduction if wrapped FRP joints are applied is large, and the governing unity check shifts from fatigue to global buckling. For mild steel, the reduction of steel weight is more than 50%. The additional reduction of mass for high strength steel is low and not economical. The eigenfrequency of the wrapped FRP structure is viable, as it is outside operating frequencies.

The results for the wrapped FRP structure are based on two major assumptions. Firstly, satisfactory joint performance can be obtained, and secondly, this can be accomplished by increasing wrapping thickness only. These assumptions should be verified by future experiments to support the weight reduction statement.

In conclusion, the potential benefit of wrapped FRP joints to offshore wind turbine supporting jacket structures is large, and future experiments will show if, or to what extent, the full potential can be exploited.

Contents

Glossary

List of Acronyms

FLS	=	Fatigue Limit State
FRP	=	Fibre Reinforced Polymer
GB	=	Global Buckling
HSS	=	High Strength Steel
LB	=	Local Buckling
MS	=	Mild Steel
MSL	=	Mean Sea Level
SCF	=	Stress Concentration Factor
ULS	=	Ultimate Limit State

Acknowledgements

Selecting a research project to mark the end of an unforgettable study career is a complicated task. Now, after finishing the project, I am delighted to have chosen to graduate on an innovation which may replace conventional welding for tubes. I never expected to graduate on an offshore wind-related topic, but it is a choice I definitely not regret.

I am very grateful for a lot of people of which I will highlight a few. First, I want to thank Eveline, the master coordinator of Mechanical Engineering. From the moment I decided to combine Mechanical and Civil Engineering in a double degree, your support was vital to arrange all complicated paperwork.

Next, I want to thank my graduation supervisors for all coaching and feedback during the meetings. Peter, special thanks for your feedback and your open mind to supervise a project not closely related to your daily research. Marco, big thanks for helping me out with offshore related questions and for the use of the essential offshore simulation software. Finally, I would like to express my gratitude to Marko. It was an honour to bring your idea one (small) step closer to reality. The bi-weekly meetings were very motivating, and the feedback kept me on track to work towards the main goal.

Furthermore, I want to thank all friends who helped me through the day-in-day-out graduation. Special thanks for my Civil Engineering *Studoc* friends Kaj, Tim, Geert and Berend. Both the feedback and the laid-back coffee breaks definitely helped me. Besides, many thanks to Yvo and Thijs for preparing me to expect the worst. In the end, it was not that bad, but having this in mind, kept me positive.

Off course this acknowledgement is not complete before I express my gratitude to my parents. I cannot thank you enough for all the opportunities and support you gave me during the extended study period. Last but not least, I would like to thank my girlfriend, Marlies. I really found rest and relaxation in the moments we spent together. It was crucial for the successful completion of the research.

Marc van Vliet

Delft, December 10, 2019

Structure of report

Chapter 1 gives a thorough literature study concerning fibre reinforced polymer, the degradation of properties in seawater and wrapped FRP joints. The essential points are collected and discussed in the conclusion.

Chapter 2 gives a thorough literature study concerning support structures, loads, and the design procedure for offshore wind turbine support structures. The essential points are collected and discussed in the conclusion.

Chapter 3 focusses on the research questions to be answered and gives the motivation of this study.

Chapter 4 contains all relevant information regarding structural and load modelling. Besides, it contains the calculation procedure and cases to be analysed.

Chapter 5 shows the results of the simulations and calculations. Both main results are discussed, as well as detailed outcomes concerning the dependency on seeds, the relative influence of normal force and moments, the most harmful wind-wave scenarios and the influence of hydrodynamic loading.

Chapter 6 gives a critical view on results by listing and commenting on the assumptions, simplifications and modelling choices. Besides, results are clarified by evaluating model and calculation sensitivities.

Chapter 7 answers the research questions, gives the overall conclusion, and sums up the recommendations for future work.

The Appendix includes a comparison to the UpWind project, the GH Bladed model input, the load properties, a description of analyses, the S-N curves, and the tables regarding main and detailed results.

1 Fibre reinforced polymer

In this chapter, information regarding fibre reinforced polymer (FRP) is given. Apart from the potential, the material behaviour, a short history and structural applications, a literature review regarding properties and their degradation in seawater is given. Next, an innovative method to join circular hollow sections by a wrapping of fibre reinforced polymer is introduced. This connection is the basis of this research. To conclude, some remarks are given concerning the application of wrapped fibre reinforced polymer joints in offshore environments.

1.1. Material

Fibre reinforced composites are unique, as they combine attractive properties. The combination of excellent strength-to-weight, stiffness-to-weight, fatigue performance and environmental durability is unmatched by regular steel, concrete and timber building material. On top of that, properties can be tailored to obtain orientation-specific properties. For the civil and maritime industry, the corrosion resistance is of great value as well.

1.1.1. Composition

To understand how this unique set of properties is obtained, the composition of the material should be looked at. FRPs are composite materials made from fibres and resin, each with significantly different physical and chemical properties. The fibres applied are strong and stiff, and the resin in which they are embedded weaker and less stiff. The fibres mainly determine the tensile strength and stiffness, while the matrix adds toughness and compressional strength to the brittle fibres. The composite shows stress-strain behaviour in between components behaviour and overall properties superior to those (see Fig. 1.1).

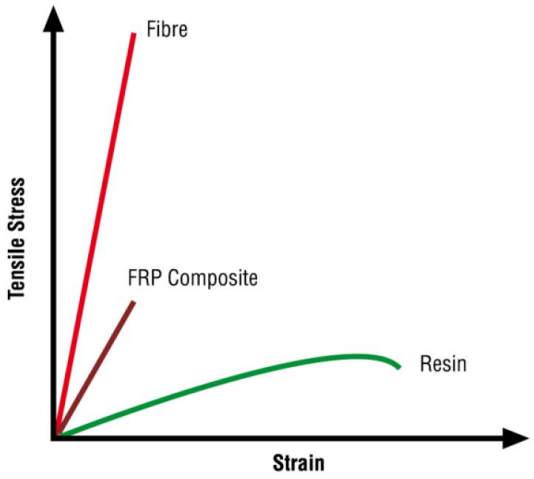

Figure 1.1: Stress-strain curve of fibres, resin and resulting composite [Gurit Holding AG, 2000].

Most common applied **fibres** are glass, carbon and aramid. They mainly differ in (tensile) strength and stiffness, but also in durability and price:

- **Glass fibres** are by far the most predominant fibres in the polymer industry and are obtained by extruding molten glass through bushings into continuous filaments [64]. In the sizing step, they are coated with additives, brought together in strands and wound onto a spool (see Fig. 1.2). The stiffness of E-glass fibres is around 70 GPa, the strength around 2 750 MPa and the ultimate strain around 4%. The fibres can be sensitive to alkaline environments and are used when low flexural modulus and high deflections do not limit use.

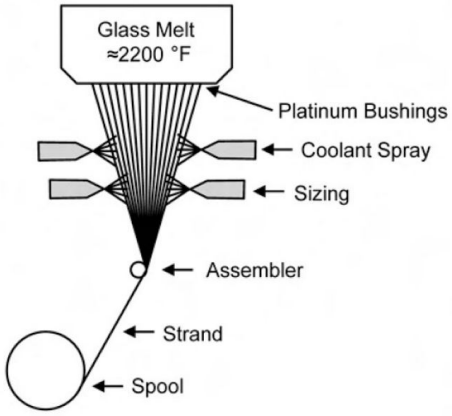

Figure 1.2: Production process of glass fibres used in glass fibre composites [Campbell, 2010].

- **Carbon fibres** contain at least 90% carbon and have high tensile strength, high modulus of elasticity, low creep and fatigue performance superior to glass fibres [61]. The PAN-, isotropic-pitch- and mesophase-pitch-based carbon fibres are produced by the spinning of the precursor, followed by stabilisation and carbonisation up to about 1300 °C (see Fig. 1.3). In the sizing step, the fibres undergo a surface treatment to improve the interaction with the matrix phase. The density of the fibres is around 30% lower, and they are up to 20 times more expensive compared to glass fibres. Both high modulus, intermediate modulus and high strength carbon fibre reinforced polymers (CFRP) exist. The variety is wide because the stiffness of the carbon fibres depends on the regularity, alignment and crystallinity of the fibres' atomic structure. Brittle high modulus carbon has a stiffness of around 400 GPa, a strength of around 4 700 MPa and an ultimate strain of around 0.6%. Note, the E-modulus is almost twice as large as the modulus of regular steel.

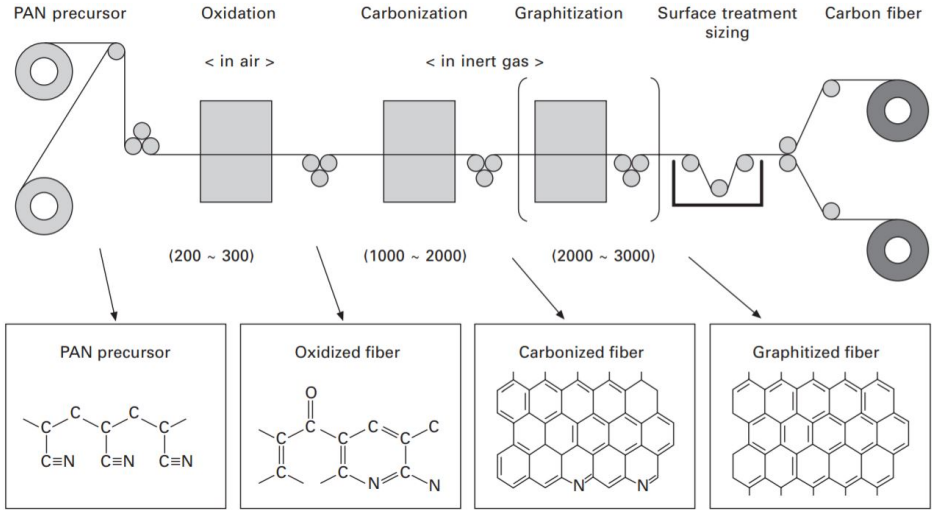

Figure 1.3: Production process of PAN-carbon fibres used in carbon fibre composites [Bunsell and Matsuhisa, 2009].

- **Aramid fibres** have strength and stiffness values in between glass and carbon fibres. The aramid fibre is a synthetic organic polymer produced by a spinning process of a solid fibre from a stock solution of polyamide. The synthetic fibres have excellent wear resistance and toughness, good chemical resistance and are very lightweight. On the contrary to glass and carbon fibres, aramid fibres do show plastic deformation in compression and ductility in tension. This is due to the fibrillation of the fibres [13]. However, due to their susceptibility to moisture degradation, they are not applicable in submerged conditions. [46, 59].

The **resin** positions, aligns and protects the fibres in a composite. Besides that, it transfers the load to and between the fibres and prevents them from buckling. Additionally, it provides toughness, damage tolerance, impact resistance and abrasion resistance. The matrix material can either be thermosetting or thermoplastic. Thermoplastic materials have a definite melting point, whereas thermosetting materials cure to produce an infusible solid material that does not melt when heated. Curing leads to polymerisation of thermoset resin, creating an infusible three-dimensional, rigid crosslinked structure. Thermoplastics are less suitable for civil structures, due to the inability to produce large structures, low fire resistance and large creep value. For thermosets, the value of glass transition temperature T_g is of great importance, as it determines the maximum usage temperature. At temperatures higher than T_g the polymer changes from a *glassy* to a *rubbery* state. At the same time, resin stiffness, compressive strength, shear strength and water resistance drop sharply. Vinyl ester, polyester, polyurethane, phenolic and epoxy are thermosetting of which the latter is mostly used for structural applications. It has a stiffness of around 3 GPa, a tensile strength of around 75 MPa and an ultimate strain of around 5%. Besides, it has extremely low shrinkage, good dimensional stability, high heat resistance, good fatigue behaviour, excellent resistance to (alkaline) environments and a low price [54, 56].

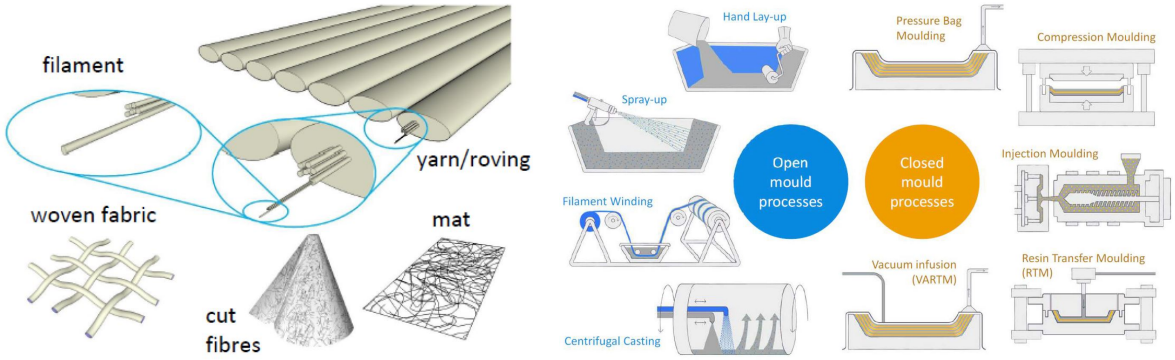

(a) Different fibre reinforcement types [Pavlović and De Putter, 2018].

(b) Batch wise processes to produce fibre reinforced composite products [Pavlović and De Putter, 2018].

Figure 1.4: Reinforcement types and the processes used to obtain fibre reinforced products.

Fibre reinforced plastic composites are strengthened by either short or long (continuous) fibres. The latter is of interest in this report. The reinforcement material is applied in small-diameter fibres to limit the influence of material flaws. Although the number of flaws in bulk and fibrous glass is the same, they will be restricted to a small number of fibres with the remainder exhibiting the materials theoretical strength. Therefore multiple parallel or bundled fibres will reflect more accurately the theoretical performance of the material. The fibres can be processed in a wide variety of reinforcements. Strands, yarns, rovings, mats and fabrics are produced and shown in Fig. 1.4a. Mechanical properties of composites with different types of reinforcement can vary strongly. The focus is on uni-directional fabrics; manufactured assemblies of long uni-directional fibres held in place by weaving, stitching or bonding. Many production processes are used to produce composites, of which most common are shown in Fig. 1.4b. Information about reinforcement types and production of fibre reinforced composites can be found in various literature, among [46].

Composites can be built up by multiple layers (plies) of continuous fibres oriented in a single direction (uni-directional plies) (see Fig. 1.5a). When plies are repeated and orientated in different directions, properties can be tailored. Common ply orientations are 0, 90 and +/- 45 degrees with respect to the main laminate direction. Plies generally have a thickness of 0.1 to 1 mm. By stacking, laminates of up to 100 mm can be produced. No fibres are orientated in through-thickness direction.

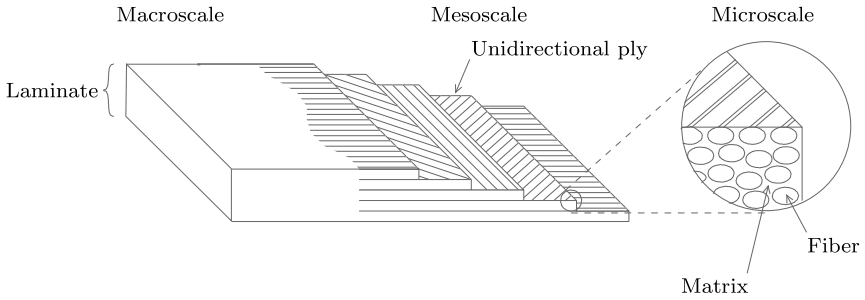

(a) Fibre reinforced polymer laminate consisting of five plies [Van der Meer, 2012].

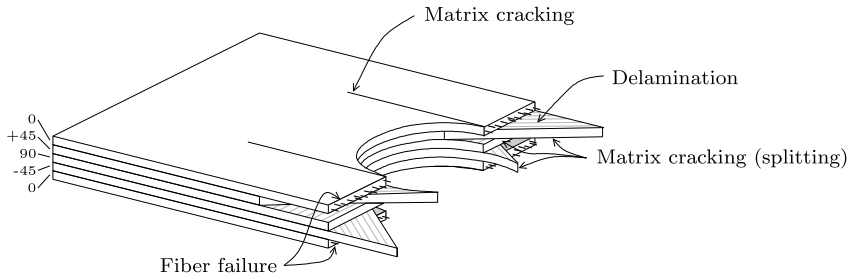

(b) Failure modes for a laminated composite [Van der Meer, 2012].

Figure 1.5: Laminated fibre reinforced plastic composite and corresponding failure modes.

As mentioned and shown in Fig. 1.1, the strength and stiffness of composites is a combination of both components. Strengths of more than 2 500 MPa are within reach, depending on composition (see Fig. 1.6). The properties can be tailored by the type of fibres, the type of resin, the type of reinforcement, the orientation of fibres, the number of fibres and the production process. The fibre-volume fraction $V_f = V_{fibres}/V_{total}$ is typically around 50% depending on the production process. Higher fibre-volume fraction composites shown more stiff fibre-like behaviour. For a single layer uni-directional composite, the linear-elastic stage is followed by a brittle rupture failure of the fibres (see Fig. 1.6). The absence of fibre yielding causes this. For layered composites, a wide range of failure modes can be observed (see Fig. 1.5b). The presence of ductility is of great importance for structural applicability, as structures should *warn* before failing. Ductility and plasticity can be increased to some extent by stacking rotated plies, but should always be considered closely.

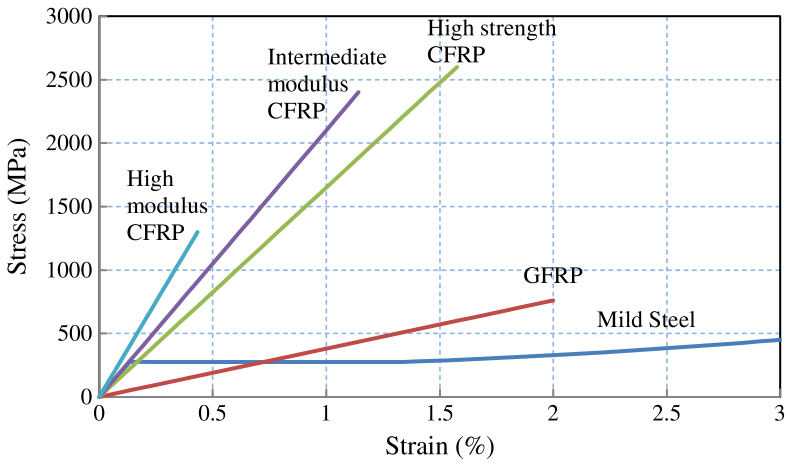

Figure 1.6: Typical FRP composite and mild steel stress-strain curves [Teng, 2012].

High performance of FRP composites could only be achieved if fibres and resin work well together. Fibre and matrix materials should be chosen for their interfacial properties. These properties can be analysed from different structural levels; molecular, micro, meso and macro (see Fig. 1.5a). At the molecular level, the fundamental interaction between fibres and matrix is due to van der Waals forces, acid-base interactions and chemical bonds (mainly covalent bonds). These forces, bonds and interactions determine the work of adhesion [76]. Due to the different bonding and interaction processes on a molecular scale, a fibre reinforced composite with a void-free compatible resin-fibre combination shows outstanding performance. At the micro-level, interfacial interaction is described by parameters characterising load transfer through the interface, like bond strength and interfacial shear strength. Surface roughness is a micro-level phenomenon which can enhance friction and mechanical interlocking. The mesoscale takes the actual distribution of fibres in the matrix into account, and at the macro level, the composites are characterised as bulk material.

1.1.2. Fatigue behaviour

Fatigue is the process of damage accumulation in a material due to repetitive loading. Usually, so-called Wöhler S-N curves relating stress and number of cycles to failure are used to represent fatigue performance. In general, FRP composites show good fatigue behaviour compared to steel, but the anisotropy and variety of composite materials make generalising a complicated task. Besides that, it depends on parameters like loading rate, temperature, humidity, mean stress and load frequency. Composites show very different behaviour for cyclic tension-tension, tension-compression and compression-compression loading. For loading in the main fibre direction, Vassilopoulos and Keller [69] and many others found reversed loading being most critical and tensile-tensile loading least critical. The effect of the mean stress level is very critical for the fatigue life of any composite material. Fibres govern material properties in tension, while matrix and matrix-fibre interaction are governing for compression. The inability to estimate and model behaviour accurately results in high safety factors. Compared to steel, FRP generally has a less steep S-N curve. However, FRP has no endurance limit; a value of stress or strain below which there is no fatigue damage accumulation.

1.1.3. Hybrid composites

The vast majority of composites consists of single fibre and single matrix material. Hybrid composites consist of two or more types of reinforcing fibres in one or more types of matrices. Combining both glass and carbon fibres could be beneficial to obtain a mix of advantageous properties. Shan et al. [62] tested glass and glass-carbon epoxy composites in water. Improved fatigue life and reduced environmental degradation were found for the hybrid specimen for loading up to 65% of ultimate tensile strength. The corrosion resistance of carbon fibres led to better retention of structural integrity. As carbon fibres are effected less by seawater than glass fibres, hybrid glass-carbon composites could be an attractive alternative for offshore applications. Joints could be tailored with carbon fibres at most severe loaded parts and at layers in direct contact with seawater.

1.2. Short history

A brief historical overview of the use of composites shows which industries benefited from the promising material first. The development started at the beginning of the 1940s, with the need for high-strength, lightweight materials [53]. The high strength of glass fibres was discovered and ways to produces composite materials were investigated.

The earliest application of GFRP was a fibreglass boat. In 1944, the first fibreglass aircraft was produced at the Wright-Patterson Air Force Base. By stacking sheets of uni-directional fibres in multiple orientations, directional properties were tailored. Later applications included helicopter blades and sports car bodies.

In the early 1960s, the first carbon and boron fibres were developed. The higher strength and stiffness led to new applications. The F-4 Jet produced in 1969 was equipped with boron fibres and in 1971, DuPont introduced Kevlar. The latter material contains aramid fibres and is still used for bulletproof military equipment like helmets and vests.

Since the 1970s, carbon fibres composites are common for sports gear like racing helmets, tennis rackets, racing bikes and golf clubs. Production methods and costs evolved over the years, making fibre reinforced polymers viable for a large variety of sectors, including in the civil industry.

1.3. Structural applications

Due to the mentioned unique combination of properties, many structural applications arose for both new constructions and rehabilitation of existing structures. The ease of application, the ability to provide direction-dependent properties and the possibility to follow irregular shapes make the material especially suitable for repair and strengthening.

1.3.1. New constructions

Bridges with short span and low imposed loads are well suited to be constructed from FRP. In the municipality of Rotterdam, the first FRP pedestrian bridge was delivered in 2009 (see Fig. 1.7a). Currently more than 90 full-FRP bridges are present in Rotterdam [25, 32].

The service life of existing bridges could be prolonged by replacing old decks with a lightweight FRP deck. As the deck weight decreases, higher live load levels are accommodated without the need to strengthen columns and foundation. An example is the historic Rugg Bridge in the United States. The deck weight was reduced from 90 to just over 30 $\mathrm{kg\,m^{-2}}$ (see Fig. 1.7b) [68].

(a) Full-FRP pedestrian bridge in Rotterdam [Fibercore, 2013].

(b) Replacement of Rugg Bridge deck (US), originally built in 1938 [Composite Advantage, 2018].

Figure 1.7: A full-FRP bridge and a bridge deck composed of fibre reinforced polymer.

Regular structural I, H, CHS, RHS and angle steel profiles could be replaced by similar shaped pultruded FRP profiles. Improved corrosion and chemical resistance makes this an attractive alternative for steel in aggressive environments.

To solve corrosion problems in reinforced concrete, glass or carbon fibre polymer bars can be applied (see Fig. 1.8a). Concrete reinforced with FRP bars has increased durability and service life. Fibre reinforced concrete, concrete with fibres blended through the concrete mix, is another invention to attain corrosion resistant and ductile reinforced concrete. For the latter, glass fibres are applied without polymer resin (see Fig. 1.8b).

(a) From left to right GFRP, C-GFRP and CFRP reinforcement bars [Prokeš, 2018].

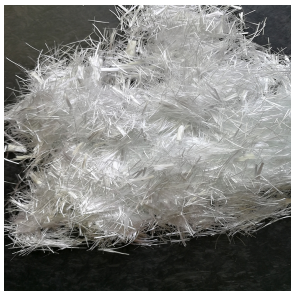

(b) Glass fibres used to construct fibre reinforced concrete [Alibaba, 2019].

Figure 1.8: Fibre reinforced polymer bars, and fibres used to reinforce corrosion-resistant concrete.

In the offshore industry, fibre reinforced polymer composites are used for a wide range of purposes including walkways, flooring, pipes, risers, tanks and vessels [29]. Besides, blades of wind turbines and tidal energy converters make use of fibre reinforced polymer. Compared to wind turbine blades, the latter have moderate dimensions (see Fig. 1.9). Due to pricing, glass fibres are currently most common. As the price of carbon

fibres is currently lowering, and the dimensions and resulting forces on blades are increasing, the use of carbon fibres gets more attractive. Especially due to their superior strength, stiffness, fatigue performance and environmental resistance [16].

Figure 1.9: Various tidal energy converters with FRP blades [Dawson et al., 2018].

1.3.2. Rehabilitation of existing structures

The flexural strength of existing structures can be increased by FRP bars or strips. Common applications are bridge decks, parking garage floors and floor slabs. A recent example of flexural FRP strengthening of floors is the NoMa House in Amsterdam. After the collapse of a parking garage in the Dutch city of Eindhoven on May 29th 2017, many bubble-deck floors were required to be strengthened. In the NoMa House, the moment capacity of some floors was enhanced by CFRP strips (see Fig. 1.10a). Besides flexural strengthening, FRP is used for shear strengthening of beams. For this application, FRP is attached to the webs (see Fig. 1.10b). Wrapping of a column is performed to enhance the axial load carrying capacity, shear resistance, ductility and energy dissipation (see Fig. 1.10c).

(a) Flexural strengthening of floor in NoMa House [Van Vliet, 2018].

(b) Shear strengthening of parking garage floor [Alkhrdaji, 2018].

(c) Wrapping of concrete column [Hamakareem, -].

Figure 1.10: Strengthening of concrete slabs, beams and columns for respectively flexure, shear and axial capacity.

Flexural and shear strengthening of steel structures is similar to concrete structures. Additionally, as slender steel compression members are susceptible to buckling, buckling strengthening can be applied. Because of the high stiffness, carbon fibre polymers are the preferred option.

FRP overlays on walls can be used to decrease susceptibility to earthquakes. The overlay increases the ductility and plastic capacity of buildings. Similar seismic strengthening is applied to bridge columns. Studies have shown that carbon-epoxy retrofits can be just as effective as conventional steel retrofits [68].

FRP overlays are used to protect structures against fire, blast, impact and corrosion. The most common application, however, is the repair of steel pipelines damaged by corrosion or impact. The traditional solution is covering the damaged region by welding a steel patch, or to remove a damaged section and replace it by a new one. As welding a steel patch underwater is a cumbersome process, the industry sought for more light, fast and easy to handle alternatives. Both GFRP and CFRP patching or wrapping have proven to be effective. When carbon fibre is applied, the layer in direct contact with steel should be composed of glass fibres. In this way, galvanic corrosion between dissimilar metals is prevented [61]. Several examples of pipeline repair methods by FRP exist and are shown in Fig. 1.11.

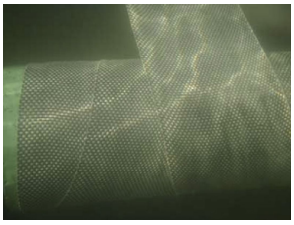

(a) Repair by wrapping of flexible FRP composite [Green, 2010].

(b) Repair by ClockSpring sleeve mechanism [ClockSpring, 2019].

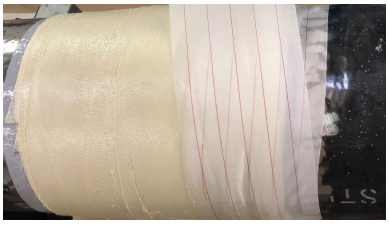

(c) Repair by water activated FRP wrapping [ClockSpring, 2019].

Figure 1.11: Different fibre reinforce polymer products and processes to strengthen damaged offshore pipes.

1.4. Degradation in seawater

In this section, the degradation of FRP in seawater is elaborated on. First, environmental factors influencing durability are shown, and moisture degradation is elaborated on more closely. Next, the degradation of FRP properties in (sea)water environments according to DNV-GL and JRC composite codes is discussed. As the codes either lack data or give very conservative values, scientific research is consulted. An overview is given regarding moisture effects on static and fatigue performance of laminates, as well as on FRP-steel adhesive joints.

1.4.1. Decay mechanisms

Mechanical properties of FRP can be affected by moisture, UV, temperature, chemicals and microbiological attack. Influencing factors on FRP-steel joints are schematically shown in Fig. 1.12. In an offshore environment, moisture attack is most harmful and therefore focussed on. Note, decay is a synergistic process, meaning the combined effect of multiple degradation mechanisms is greater than their individual effect. Research on hygrothermal decay, a combination of heat and moisture, is common, and results show increased decay for higher temperatures.

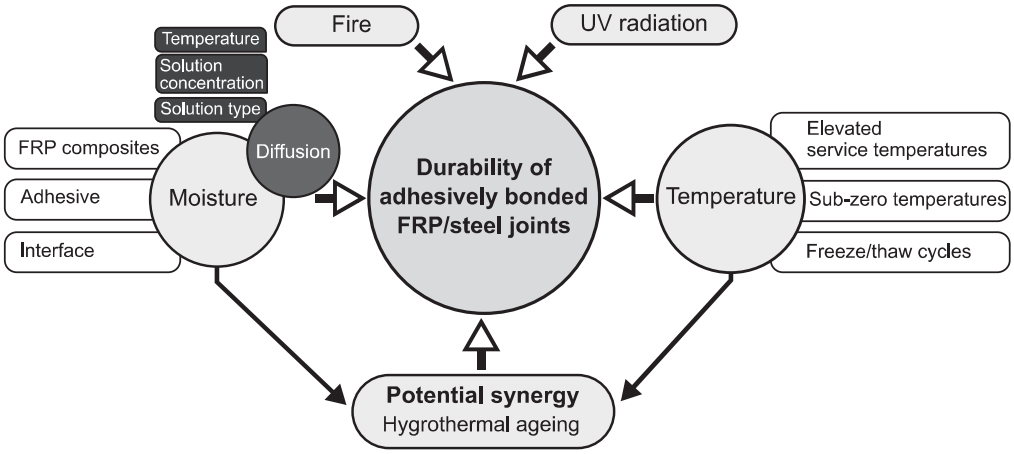

Figure 1.12: Schematic of environmental factors influencing the durability of adhesively bonded FRP-steel joints [Hesmati et al., 2015].

Moisture absorption of fibre reinforced plastics can be split up in three mechanisms [54]:

- **Direct diffusion** of water molecules through the matrix and in some cases through the fibres. This process generally follows Fickian behaviour.
- **Capillary flow** of water molecules along with the fibre-matrix interface followed by diffusion from the interface into the resin. The latter is a consequence of the breakdown of chemical bonds between fibres and matrix caused by water attack at the interface.
- **Diffusion through micro-cracks**, voids, pores and defects in the material.

Typical water absorption is graphically shown in Fig. 1.13. In the early stages, water absorption obeys Fick's law meaning a reduced absorption rate is seen when saturation is approached. The rate is mainly driven by a difference in moisture concentration between environment and material, but not solely. Besides, material properties (fibre type, resin type, fibre volume fraction, fibre orientation), environmental factors (stress level, relative humidity and temperature) and load influence behaviour. The water uptake leads to swelling, (swelling) stresses and possibly to cracking. Due to cracking, moisture diffusion along fibre direction and presence of voids in the matrix, non-Fickian behaviour is observed in later stages of decay. Moisture concentration increases rapidly, and mechanical properties degrade strongly.

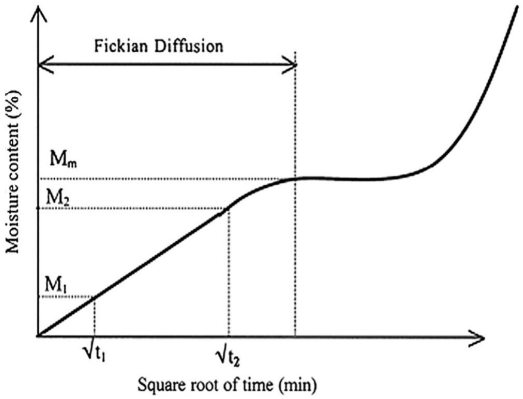

Figure 1.13: Typical water absorption profile of FRP composites, consisting of initial Fickian behaviour followed by strongly non-Fickian absorption [Nayak et al., 2016].

Frequently applied glass-epoxy composites show a high degree of non-Fickian behaviour due to a high rate of diffusion, caused by a large amount of OH-groups in epoxy [54]. Besides swelling stresses, absorption of water leads to plasticization, entailing a changing polymer structure making it more flexible. This process reduces the glass transition temperature T_g; a material property that is strongly influencing mechanical properties. Significant strength reduction is caused by loss of adhesion between glass fibres and epoxy, leading to interlaminar cracking and increased moisture uptake.

1.4.2. Composite standards

Two different codes regarding the use of composites are consulted to get insight into the current procedures to design and calculate with fibre reinforced polymers. Of main interest are the static, dynamic and fatigue performance after long-term immersion in (sea)water.

DNVGL-ST-C501

This standard, developed by DNV GL, gives requirements and recommendations for the structural design of composite components [22]. Fibre and matrix dominated properties are considered separately and may decay by different amounts.

Mechanical properties under long-term static and cyclic loads may differ from short-term values, especially in harmful environments. Influenced by cyclic fatigue, the E-modulus tends to reduce mainly due to cracking of matrix under tensile fatigue loads. The standard states that the E-modulus in main fibre direction should be reduced by 10% for glass and carbon fibres for 10^6 cycles, while the E-modulus of the matrix in transverse direction should be reduced to zero. No quantitative data is given for creep. For low and normal safety class, the effects of creep and stress relaxation may be ignored if the maximum stress does not exceed 10% of the characteristic strength and the loading time does not exceed 10^4 hours.

For most properties, operating temperature is assumed not to affect properties if at least 20 degrees Celcius below T_g of the matrix. The effect of water on properties is given for 10^6 cycles or 10 years. The effect on glass fibre composite properties is given in Tab. 1.1. Note, it only gives a reduction for fibre dominated properties in the main fibre direction. The effect on other properties is unknown and should be obtained by experiments. The code states that the effect of seawater is generally smaller than freshwater, but no quantification is given.

Table 1.1: Reduction of long-term fibre dominated properties of glass fibre composites in water. Values representative for the main fibre direction only [DNVGL, 2017].

Property	Reduction
E-modulus	10%
Tensile strength	10%
Compressive strength	10%
Ultimate strain	None
Fatigue stress range	10%

As only few quantifiable reduction factors for long-term properties are given, experiments can be performed to obtain mechanical properties. Tests should be performed with a configuration which resembles reality as close as possible for e.g. configuration, curing conditions, surface treatment, size, load, lay-up and environment. Material properties may be documented by the following methods:

- Direct measurements;
- Qualification against representative data;
- Qualification against manufacturers data;
- Qualification against data from the open literature;
- Qualification by component testing.

Testing can be performed either for (i) qualification based entirely on tests and for (ii) updating or verification of the analysis. When testing according to (i) is performed, for short-term properties, at least 3 specimens shall be tested and for long-term properties at least 10. For testing according to (ii) the minimum number of tests for short term properties is between 1 and 3, while for long term properties minimum 1 or 2 survival test must be performed. For the latter, the number of tests depends on the safety class. ASTM and ISO describe preferred test methods for laminates.

JRC report
The Joint Research Centre (JRC) report, *Prospect for new guidance in the design of FRP*, gives rules and standards for designing with FRP [4]. Conversion factors taking the environment into account are given. The total conversion factor is depending on the limit state and is calculated by:

$$\eta_c = \eta_{ct} \cdot \eta_{cm} \cdot \eta_{cv} \cdot \eta_{cf}$$

in which η_{ct} accounts for temperature, η_{cm} for humidity, η_{cv} for creep and η_{cf} for fatigue. For ultimate limit state (ULS) strength verification, $\eta_{ct} = 0.9$ and $\eta_{cm} = 0.7$ for a composite continuously exposed to water in combination with UV. The value of η_{cv} depends on fibre and resin type, fibre lay-up and content, temperature, type of loading (normal or shear stress), load duration and the verification (strength or stiffness). For long term loading $\eta_{cv} = 0.5 - 0.6$. Note, the conversion factor for creep effects has to be applied to the sustained part of the load only. Fatigue conversion factor $\eta_{cf} = 0.9$, if the number of cycles exceeds 5 000 and the peak stress from cyclic and permanent load exceeds 15% of the materials design strength. If not, $\eta_{cf} = 1$. Combining conversion factors values gives a drastic degradation of 70% of the original properties ($\eta_c < 0.3$).

1.4.3. Scientific results

The codes give an incomplete set (DNVGL-ST-C501 [22]) or a very conservative estimate (JRC [4]) of FRP properties when in seawater for a long time. Besides, properties are given regarding FRP instead of FRP-steel joints. Therefore, scientific research is consulted, and findings are given in this section. As there is a large amount of variety between FRP composites, this section focusses on a selection of composites. Based on their affordability and structural use, the main focus is on epoxy-based resins reinforced with glass fibres.

- **Effect of moisture on fibres**
  It is generally known that hydrophilic glass fibres can be damaged by prolonged exposure to water, while hydrophobic carbon fibres are not degraded by water [28, 40]. Degradation of glass fibres is dependent on the coating of fibres, matrix adhesion and matrix cracking [38]. Mourad et al. [48] immersed

glass fibre epoxy-polyurethane composites in 65 °C seawater for one year and found no fibre damage. In general, moisture decay of FRP is not governed by moisture degradation of fibres.

- **Effect of moisture on resin**
  Moisture can change resin through plasticization, swelling, cracking and hydrolysis [31]. Moisture increases ductility while reducing the strength and elastic modulus of resins. Resins for offshore should have predictable long term properties to guarantee to function during service life. Epoxy resin was found most suitable, as only for this resin, mechanical properties stabilise after moisture saturation (see Fig. 1.14) [28].

- **Effect of moisture on static mechanical properties of FRPs**
  Hydrophobic fibres embedded in a moisture-resistant matrix does not guarantee good long-term performance. The durability of fibre reinforced polymers in seawater depends on fibre-matrix compatibility and stability of interfacial adhesion [31]. Fibre dominated properties like tensile strength are generally less affected by seawater than matrix dominated properties like interlaminar shear strength. A general statement about moisture content and degradation of properties cannot be identified, due to the fundamentally different damaging mechanisms at the fibre-matrix interface for individual FRP composites [31]. Nevertheless, several experimental results are discussed:

  Garcia-Espinel et al. [28] studied the effect of seawater on glass fibre reinforced plastics for marine civil engineering constructions. Water uptake and mechanical properties of glass-epoxy, glass-polyester, glass-vinyl ester and glass-polyurethane composites immersed in seawater for more than 100 days were compared. For glass-epoxy, the flexural strength was reduced by 35% and the tensile strength by 24% after 90 days (see Fig. 1.14).

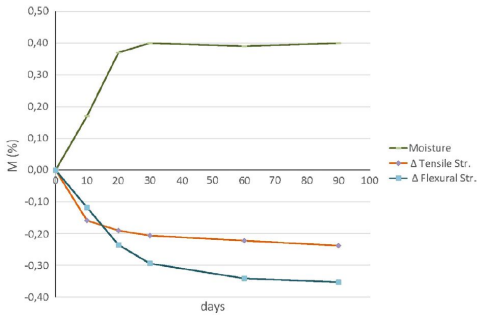

Figure 1.14: Water intake versus mechanical properties of glass-epoxy composite at 25 °C. Mechanical properties degrade by 20-40% and stabilise after moisture saturation [Garcia-Espinel et al., 2014].

Koots et al. [38] tested glass-polyester, glass-vinyl ester, carbon-polyester and carbon-vinyl ester composites exposed to 30 °C seawater for two years. Polyester composites showed mass change towards zero after saturation, while vinyl-ester composites showed continuous mass change. For both polyester-based composites, the flexural modulus was reduced by 10-20% at saturation, while flexural strength was reduced by 20-40%. The flexural modulus and strength of vinyl ester composites at saturation reduced by respectively 30% and 40-50%. Mode I interlaminar fracture toughness of composites was not affected significantly by seawater immersion.

Patel et al. [54] studied the effect of 8 days immersion in 60 °C distilled water, NaCl-water and seawater on characteristic properties of glass-epoxy composites. The resulting performance reduction is greater for matrix compared to fibre dominated properties. The interlaminar shear strength (ILSS) is decreased by roughly 8 per cent in seawater and by about 15 per cent in distilled water and NaCl-solution. Smaller decay in seawater compared to (distilled) water is found in many studies. According to Alia et al. [2], deposited salt constitutes a physical barrier to the ingress of water. Few studies showed higher absorption in distilled water, which was explained by high seawater pH, resulting in micro cracking of resin and resin-fibre interface [40].

Mourad et al. [48] studied the degradation of glass-epoxy composites after one year of exposure to seawater. No significant change in tensile strength and modulus was observed at ambient temperature. Reduction of mechanical properties for glass-epoxy was observed at 65 °C and for glass-polyurethane composites at both temperatures.

Fang et al. [24] reported decay of mechanical properties of glass-polyester composites after six months immersion in seawater at room temperature. Tensile and flexural strength decreased by 13.8% and 9.8% respectively and E-modulus by 4.6%. Moisture absorption and degradation of mechanical properties in seawater were smaller than in water.

Dawson et al. [16] investigated the reduction of tensile strength and interlaminar shear strength for glass-epoxy specimens aged in 40 °C seawater and deionised water for eight months. Weight gain and decay of mechanical properties were highest in deionised water (see Fig. 1.15). A linear correlation was found between weight gain at saturation and tensile strength in the fibre direction. No correlation could be found between weight gain and ILSS.

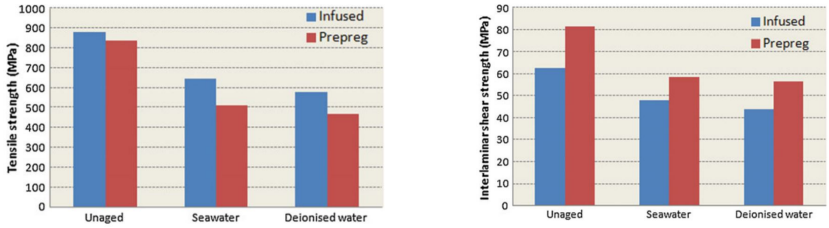

Figure 1.15: Tensile strength in fibre direction and interlaminar shear strength for 8 months aged glass-epoxy composites in seawater and deionized water of 40 °C. Decay in deionised water is larger compared tot decay in seawater. Both tensile strength and interlaminar shear strength are affected considerably [Dawnson et al., 2018].

Hesmati et al. [31] compared research of FRP composites exposed to environmental conditions. In Fig. 1.16, all values are normalised to unaged properties. As mentioned, results vary considerably.

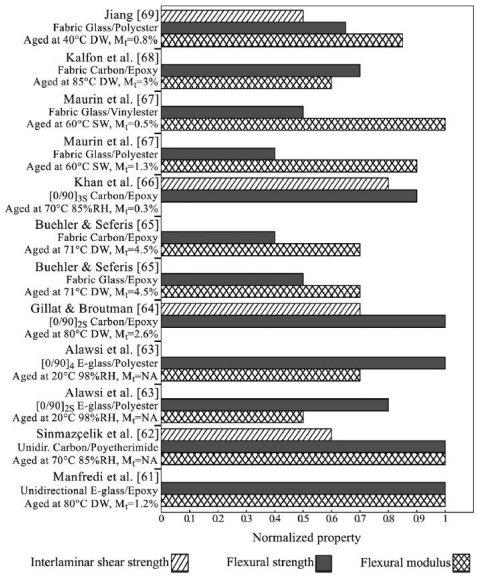

Figure 1.16: Experimental data of environmental effects on flexural and interlaminar shear strength of FRP composites. Degradation varies considerably between research. NA = not available, M_t = moisture content, DW = distilled water, SW = salt water [Hesmati et al., 2015].

- **Effect of moisture on fatigue behaviour of FRPs**
  Fatigue behaviour of fibre reinforced composites is sensitive to ageing by moisture. Like decay of static properties, the decay of fatigue properties is strongly influenced by the composition and the compatibility of fibres and resin. S-N curves of seawater immersed specimens are obtained by a downward shift and slope change of dry experimental curves. Some results of studies regarding fatigue behaviour are given to illustrate common decay:

  Poodts et al. [57] performed fatigue tests of polyester and vinyl ester glass fibre composites in 15 °C marine environment. Results show a minor difference in ultimate strength (6% for glass-vinyl ester and

7% for glass-polyester) and no change in flexural modulus between dry and 22-week immersed specimen. Fatigue tests performed in water showed longer fatigue life for both immersed and un-immersed specimens. According to the authors, this is explained by the improved heat transfer provided by the wet environment. No appreciable difference in fatigue behaviour was seen between immersed and un-immersed specimen tested in air.

Gibson et al. [29] reported research on fatigue performance of GFRP composites of polyester, vinyl ester and phenolic. Flexural fatigue tests were performed under both immersed and un-immersed conditions. Some of the specimens were preconditioned in 35 °C seawater for six months. The fatigue strain limit was defined based on maximum surface strain and was about 0.6-0.8%. Preconditioning showed a minor effect on fatigue performance of both vinyl ester and phenolic, but a major effect on low cycle fatigue for polyester composites. Joints aged under ambient conditions showed significantly improved fatigue life, explained by enhanced curing.

Boisseau and Peyrac [8] studied the fatigue behaviour of different composites immersed in 50 °C seawater for 8 months. Fatigue tests showed a large variance between composites, but a correct prediction by log-log Basquin law (see Fig. 1.17a). Composite 2 (carbon-epoxy) showed no change in fatigue life, while composite 3 (glass-polyester/epoxy) showed a clear degradation of fatigue life after seawater immersion. Composite 1 (glass-epoxy) showed degradation only for high stress - low cycle fatigue. Similar flattening of the S-N curve for immersed specimens is found by Kensche et al. [36] and Boisseau et al. [9]. Kensche also showed better fatigue performance for CFRP compared to GFRP. Besides, he found steepening of S-N curves for high-fibre content composites.

Dawson et al. [16] cited earlier, also investigated fatigue behaviour of 9-month immersed and un-immersed glass-epoxy composites. Water showed adverse effects on fatigue behaviour, while no significant difference was observed between water and seawater (see Fig. 1.17b). This research showed that ageing is the major factor while the environment is of minor importance.

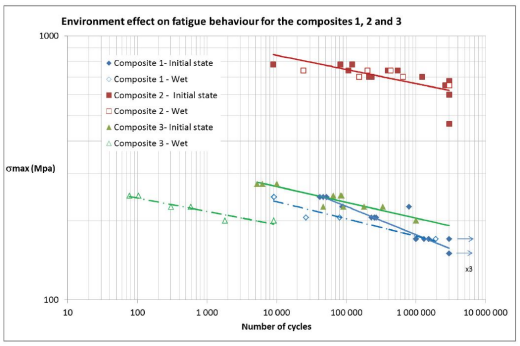

(a) Fatigue life of different composites (1. glass-epoxy (blue), 2. carbon-epoxy (red) and 3. glass-polyester/epoxy (green)) before and after 8 month immersion in 50 °C seawater on log-log axis. For the glass-epoxy composite, flattening of the S-N curve is seen, as well as improved fatigue life for low stress cycles [Boisseau and Peyrac, 2015].

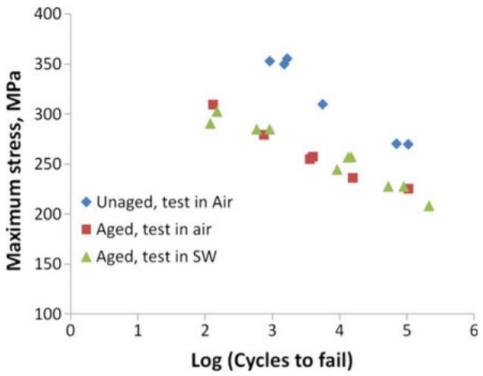

(b) Fatigue life of glass-epoxy composite before and after 9 month immersion in 40 °C seawater on log-lin axis. No difference in fatigue performance is observed between air and seawater ageing [Dawson et al., 2018].

Figure 1.17: Fatigue test results shown in S-N diagrams for different composites and ageing conditions.

- **Effect of moisture on FRP-steel joints**
  The long-term strength of adhesive FRP-steel joints in moist conditions depends mainly on the degradation of interfaces. According to literature, degradation of adhesive is of minor importance, and failure locus almost always switches from cohesive within adhesive, to at or near the interfaces [31]. As the FRP-adhesive interface is stable under moist conditions, joint durability is mainly governed by the adhesive-steel interface. Strength degradation of joints whose failure took place at the adhesive-steel interface is found to be as high as 90%, while it is less than 25% for all other failure modes [31]. While numerous studies showed loss of strength in moist adhesively bonded joints, some did not. A hypothesis of a critical moisture content below which no joint degradation takes place is formulated [11, 30]. It is recommended to use adhesives with ultimate moisture content below 2%.

  The steel-adhesive interface is affected by water molecules attracted and absorbed by an ultra-thin oxide layer of steel. The transport of moisture to the interface leads to weakening of intermolecular adhesive forces, and (cathodic and galvanic) corrosion of steel substrate. Corrosion leads to loss of adhesion between adhesive and steel adherent. Galvanic corrosion occurs when two dissimilar materials with sufficient electro potential difference are bridged together by an electrolyte like (sea)water. Multiple studies showed the existence of galvanic corrosion between CFRP and mild steel [5, 6, 12]. Applying a layer of GFRP or a thicker layer of epoxy (>0.5 mm) between steel and CFRP is proven to be successful while adding glass fibres to adhesive does not improve bond durability [14, 66].

  The steel-adhesive interface bond strength benefits from the mechanical interlocking of adhesive or polymer and rough steel. Grinding and sandblasting the steel substrate surface instead of only hand-sanding increases average shear strength by at least 40% [63]. Grit blasting, in combination with silane coupling agents, is well studied and proven to be effective. Dawood and Rizkalla [15] studied the performance of steel-CFRP joints subjected to harsh accelerated ageing of wet/dry cycles in NaCl solution for six months under sustained loading. Durability with pre-treatment of steel surface with silane coupling agent showed mostly no degradation of bond strength. Linghoff and Daumes [45] did found degradation under a very harsh accelerated ageing scenario, caused by corrosion of steel surface.

  Sustained loading effects on FRP-steel joints are investigated by [15, 44]. Loading the joint by 35% of dry joint strength did not result in experimental ageing after six months.

- **Effect of UV-radiation on FRPs**
  FRPs in offshore can be exposed to and degraded by UV-radiation (see Fig. 1.12). UV-light leads consecutively to (i) loss of surface gloss, (ii) surface discolouration, chalking and pitting and (iii) erosion leading to topmost fibres becoming visible. Kumar et al. [39] evaluated the degradation of carbon fibre reinforced epoxy by ultraviolet radiation and moisture. The author observed that a combination of seawater and UV is more harmful due to their synergistic effect. Matrix dominated properties are affected the most, resulting in a reduction of transverse mechanical properties. Transverse tensile strength is decreased by 29% after only 1 000 hours of cyclic exposure to UV radiation and condensation. UV-degradation could be overcome by applying UV-resistant paint, coating or resin.

- **Effect of microbiological degradation on FRPs**
  A decay mechanism in offshore environments not shown in Fig. 1.12, is microbiological degradation. Wagner et al. [73] analysed the susceptibility of fibre reinforced polymer composites to microbiological degradation. Different composites, resins and fibres were exposed to different types of bacteria. Epoxy and vinyl ester resins, carbon fibres, and epoxy composites were not adversely affected by microbial species. The bacteria did degrade the organic surfactant of glass fibres.

- **Effect of temperature on FRPs**
  Elevated temperatures affect the performance of fibre reinforced polymers, mainly due to the degradation of matrix properties at temperatures close to the glass transition temperature. FRP joints show a bilinear relation between temperature and strength/stiffness. For temperatures well below T_g of resin and above 0 °C, mechanical properties are enhanced due to post-curing. For service temperatures close to or above T_g, a strong reduction of resin dependent properties like interlaminar shear strength is seen. Also, moisture ingression rate increases considerably [31]. Guidelines recommend adhesives with T_g at least 15 °C above operating temperature. Note, resin curing slows down with lower temperatures. For some situations, heating might be needed to speed up curing.

Accelerated ageing makes use of increased temperatures to decrease moisture immersion time of specimen. This should be done with care, cause at higher temperatures damage mechanisms could develop which do not occur during service conditions [31]. As a result, durability may be underestimated.

Sub-zero temperatures can cause FRP matrix embrittlement, matrix hardening, matrix micro-cracking and fibre-matrix bond degradation [1]. Changes in FRP constituents and the difference in thermal expansion coefficient between fibre and matrix are responsible. For carbon fibre composites, this is more critical due to the negative thermal expansion of the fibres and positive thermal expansion of resin.

- **Effect of freeze/thaw cycling on FRPs and FRP-steel joints**
  Freeze/thaw cycling in general results in less than 20% reduction of tensile modulus and strength of FRP, but could lead to severe stress if water fills voids and cracks [1]. Degradation of properties can be limited to a large extent by a compatible resin-fibre combination. Freeze/thaw cycling in FRP-steel joints can lead to increased damage if the thermal expansion of steel and adhesive are dissimilar.

1.5. Wrapped FRP joints

As mentioned, FRP is commonly used to strengthen existing steel structures. In recent years, researchers looked into strengthening circular hollow section (CHS) joints. Lesani et al. [41–43] performed research on CHS T-stub connections strengthened by GFRP. Strengthening of the brace member showed increased ultimate capacity for axial loading and reduced chord ovalisation. Fu et al. [27] investigated the strengthening of CHS gap K-joints by CFRP and found increased ultimate axial load capacity and strongly enhanced ductility.

Mentioned research used fibre reinforced polymer to strengthen welded joints by applying it over and around the weld. Wrapped FRP joints under development by Dr. M. Pavlović at the Delft University of Technology, connect CHS members without welding. This idea is innovative, and no literature is available on this topic. First experiments with glass fibre reinforced polymer on axial and X-joints show promising results [55]:

- **Axial joints**
  The initial stiffness of wrapped FRP and welded axial joints are similar, and the static resistance of the fist-mentioned is 71-96% of the yield resistance of the welded joint. The requirement for CHS joints is a static resistance larger than the member yield resistance. With further optimisation of the thickness and the length of wrapping, this criterion is within reach. Ductility of the joint is lower but present, and all three specimens experienced adhesive failure.

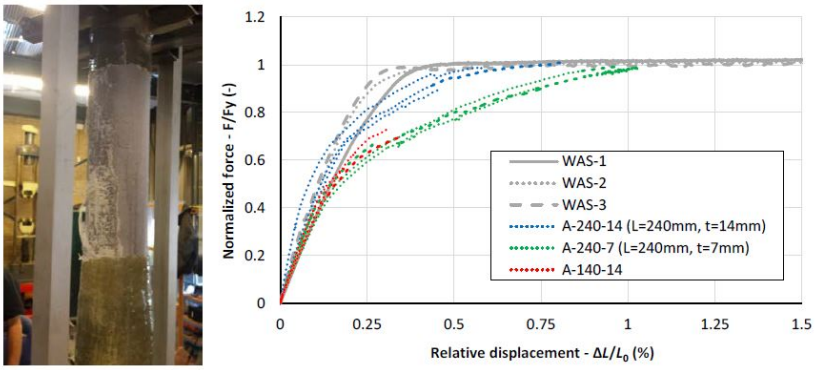

Figure 1.18: Left picture shows slip failure mode and right diagram comparison of force-displacement curves for both welded (WAS-.) and wrapped FRP (A-...-..) axial joints. The green and blue lines indicate wrapped joints with a wrapping length of 240 mm. They have the ultimate force close to the welded joints (grey lines). Also, the initial stiffness of the wrapped joints is similar to the welded. Lower maximum relative displacement indicates reduced ductility of wrapped joint [Pavlović et al., 2018].

- **X-joints**
  The initial stiffness of the wrapped FRP X-joint is almost three times the stiffness of the welded X-joint, and the static resistance is 87-92% of the yield resistance of the welded joint. The increased initial stiffness is due to reduced ovalisation. The joint possesses significant ductility compared to common

values for adhesively bonded joints. The failure mode is adhesive for two specimens and FRP wrapping failure for the third specimen.

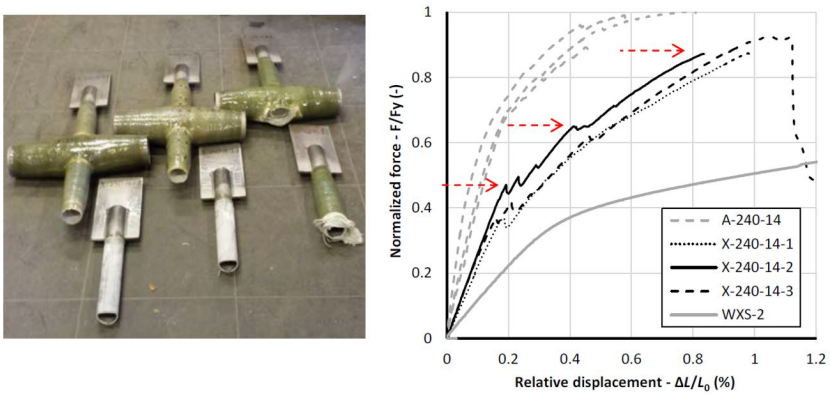

Figure 1.19: Left picture shows adhesive failure (2x) and FRP wrapping failure (1x) and right diagram comparison of force-displacement curves for both welded and wrapped FRP X-joint. Wrapped X-joints have higher initial stiffness compared to welded counterparts [Pavlović et al., 2018].

Current and future experiments will prove static and fatigue performance in harsh marine conditions. FEM modelling will be used to provide better insight and to optimise wrapped joints. Experiments of static and fatigue performance in seawater will give properties and feasibility of wrapped FRP joints for offshore wind turbine jacket supporting structures.

1.6. Conclusion

Since the first use of fibre reinforced polymers for aeroplanes and boats, plastic composites gained interest from the civil industry. Especially the high specific strength, high specific stiffness, and ease of application made it suitable for repair and strengthening of civil structures. Later, bridge decks and complete lightweight bridges were built with this revolutionary material. The need for a flexible, lightweight and easy to apply repair system for submerged corroded steel pipes, led to increased knowledge regarding long-term material properties in harsh offshore environments. Interest in (fatigue) behaviour of glass and carbon fibre plastic composites for wind turbine blades and tidal energy converters, boosted further understanding regarding material degradation.

Wrapped FRP joints under development at the Delft University of Technology connect steel circular hollow sections without welding, but instead by wrapping a fibre reinforced polymer around the joining area. A literature review on fibre reinforced polymers showed the challenge of predicting long term material behaviour in hostile environments. The enormous variety in material composition, fundamentally different and not fully understood degradation mechanisms, and material-specific failure modes are responsible. As a result, only rough and conservative estimates of long-term material properties for wrapped FRP joints can be made.

The research did show some general and useful insight in the degradation of properties. Glass fibres are applicable in offshore composites if surrounded by a compatible resin of which epoxy is most suitable for marine environments, mainly due to stable mechanical properties after saturation. Interfacial strength and stability are of great importance, and for FRP-steel joints, the steel-adhesive interface is generally governing due to corrosion. Performance of these joints is proven to be enhanced by grit blasting of the steel surface and the addition of silane to the resin. Strength and stiffness of fibre reinforced plastic composites can degrade considerably, and the effect of seawater is generally less severe than distilled water. Coatings can successfully protect FRP against UV-degradation and susceptibility to microbiological decay is low. Elevated temperatures close to glass transition temperature cause major degradation of mechanical properties, while low temperatures cause embrittlement and stresses induced by different thermal expansion. Freeze/thaw cycles can be detrimental when water fills voids and cracks. Fatigue behaviour of immersed reinforced plastic composites can generally be estimated by shifting down and flatten unaged S-N curves on a log-log coordinate system.

Combining glass and carbon fibres, so-called hybrid composites, by smart stacking order, orientation and location, could improve fibre reinforced polymer properties. Adding a small number of carbon fibres could enhance fatigue performance and environmental durability while keeping cost at an acceptable level.

The application of wrapped FRP joints in jacket structures, as an alternative for fatigue sensitive welded joints, is promising. Before being used in wind turbine supporting jacket structures, experiments should be performed to show both short and long-term performance regarding strength, stiffness and fatigue in seawater. Tests performed should mimic reality as close as possible concerning load (force and moments), composite composition (fibre and resin type), test set-up (joint geometry and scale) and test conditions (temperature, ageing and fluid of immersion). Accelerated ageing should be done with care, as high temperatures could lead to both conservative and un-conservative estimates. As codes and standards lack data, test results are the only way to get accurate long-term properties and to obtain convincing conclusions regarding the applicability of wrapped FRP joints in offshore.

In the next chapter, the results of a literature study regarding offshore wind turbine supporting jacket structures are presented. It will give insight into the current procedure to design and analyse jackets, as well as the way to deal with a wide variety of loading situations.

2

Jacket support structures

In this chapter, the current design approach for offshore wind turbine support structures is discussed. Though the focus is on jacket structures, the majority of the procedure is generally applicable. As an introduction, a short description of the need for offshore wind is given, followed by an enumeration of current supporting structures. Next, information about soil conditions and wind and wave loading is given. In the subsequent section, the focus is on the design procedure and limit states. Among other things, information is given about dynamic behaviour and loading scenarios. Finally, the chapter is summarised, and major findings related to the design of a jacket offshore wind support structure are given.

2.1. Offshore wind energy

The publication of *Our Common Future (1987),* also known as the Brundtland Report, raised awareness of climate change and encouraged the commitment of both citizens and governments to take action. Following, politicians signed various international agreements to limit temperature rise to 1.5 degrees Celsius above pre-industrial levels. To reach this target, the share of renewable energy needs to be increased strongly. The current global share of renewable energy is around 20 per cent, of which wind power is responsible for around one per cent (see Fig. 2.1) [75]. To limit sensitivity to seasonal and yearly environmental variability, an energy mix consisting of different sources is preferred. Wind energy is one of these sources, and much research and activity are seen in this field.

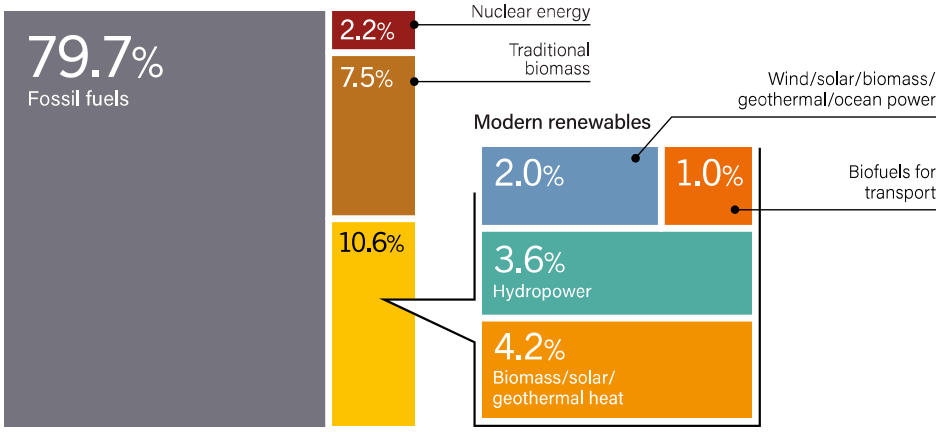

Figure 2.1: Estimated renewable energy share of total energy consumption in 2017 [REN, 2019].

Wind energy can be harvested both on- and offshore. In 2018, around 10 per cent of the total wind energy generated in Europe, was installed offshore [37]. Onshore wind turbines encounter societal resistance due to noise, and visual impact and land are scarce in relation to the sea area. Consequently, and because of more reliable and powerful wind at sea, offshore wind farms gain popularity.

2.2. History, trends and support structures

As a definition, a windmill or wind turbine is a device that converts wind energy to rotational energy by means of blades. Already since the eleventh century, windmills decorate the Dutch scenery. In the early days, they were used to ease labour-intensive processes like milling grain, pumping water or sawing wood. Since the nineteenth century, wind turbines converting wind energy into electricity are built. However, large-scale electricity production is not observed before the end of the twentieth century. Since below 1 MW capacity turbines were installed in the 1990s, research boosted current (2018) average installed capacity to almost 7 MW (see Fig. 2.2). The trend of increased capacity continues, as General Electric introduced a 12 MW turbine in March 2018. The turbine with a 220-meter rotor is installed on the Maasvlakte in Rotterdam in October 2019 for five years of testing.

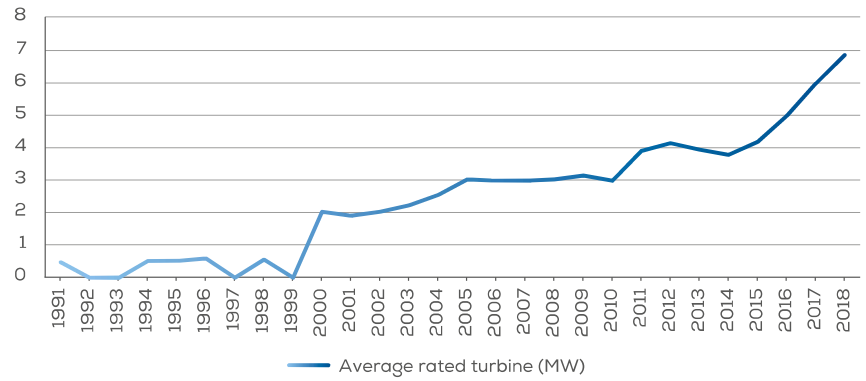

Figure 2.2: Yearly average rated capacity of newly installed offshore wind turbines [WindEurope, 2019].

Not just the capacity of wind turbines increases at a high pace. Also, the size of wind farms is fast-growing (see Fig. 2.3). The first offshore wind farm, Vindeby in Denmark, was constructed in 1991 and consisted of 11 turbines of 0.45 MW. Since September 2018, the 659 MW Walney Windfarm extension in the United Kingdom is the largest operational wind farm. In the first quarter of 2020, this number will be doubled by the 174-turbine Hornsea One Project, having a capacity of 1 200 MW.

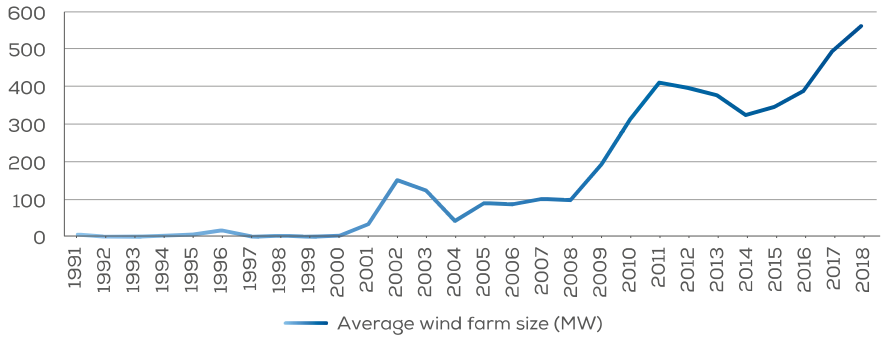

Figure 2.3: Average size of commercial offshore wind farms in construction and grid-connected in the given year [WindEurope, 2019].

The third clear trend is related to distance to shore and water depth. Vindeby and Hornsea wind farms are respectively 2 and 120 km offshore with water depths of respectively 4 and 30 meters. This trend is expected to continue as about 80% of Europe's potential offshore wind resource is situated in a sea of at least 60 meters deep [26]. Currently, the vast majority of offshore wind turbines is placed in water depths up to 40 meters [60].

Floating turbines are a hot research topic, as it has the potential to utilise almost the complete sea area. The dynamic behaviour in harsh wind and wave conditions is of main concern. Multiple concepts exist and are being checked for viability. In October 2017, the first commercial wind farm of 6x5 MW turbines was commissioned in 220-meter-deep water. This Hywind wind farm in Scotland shows promising results and survived a hurricane in the first months [26]. The floating wind farm industry is still in its early stages, and lots of research is needed before a widespread application is possible.

For fixed support structures, the supporting structure is defined as the structure that supports the turbine, holds it in place and transfers the loads from the turbine to the ground. For clarity reasons, the supporting structure is divided into multiple elements. The tower is the tubular element on top of which the turbine is installed, the substructure the part extending from the bottom of the tower to the seabed, and the foundation is the part in direct contact with the soil (see Fig. 2.4) [17].

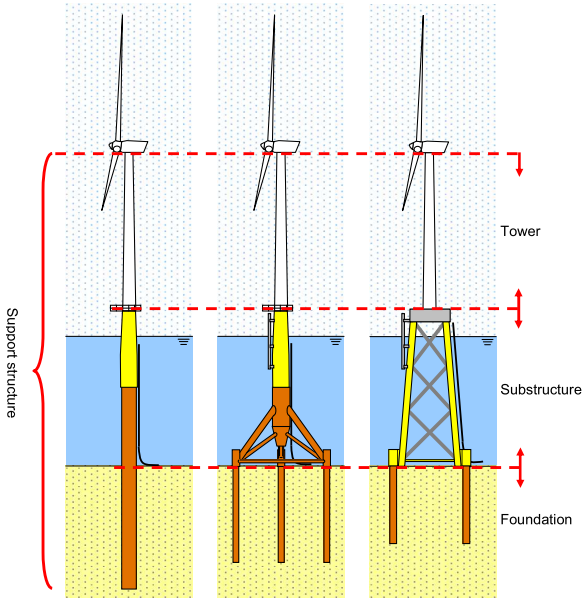

Figure 2.4: Definition of support structure and main components [De Vries et al., 2011].

The most used substructure is a single large diameter tube, the monopile. Currently, more than 75 percent of the almost 5 000 offshore wind substructures are monopiles [60]. The choice is less obvious in advance in deeper waters and for larger turbines. The most common substructures are shown in Fig. 2.5 and elaborated on next:

- **Monopiles** are made of steel plates of typically more than 150 mm thick, forming a 4-8 meter diameter tube. The length is typically around 60 meters and is influenced by water depth, soil and loading conditions. Depending on the seabed, monopiles are either driven by large impact or vibratory hydraulic hammers or grouted into sockets drilled into the rock. The vertical loads are transferred to the seabed by wall friction and tip resistance. The horizontal wind and wave load on the supporting structure are transferred to the soil by bending moments. To maintain bearing capacity during design service life, scour protection is applied. Scour is the transportation of sand particles from the original location, to a location downstream. Due to the presence of the monopile, the flow is disturbed and scour is intensified. If no scour protection is applied, so-called scour holes would develop, resulting in reduced bearing stability.

  The mass of a monopile structure increases quadratically with water depth [17]. This is partly caused by the large diameter needed to obtain a sufficiently high eigenfrequency, and partly by the increased thickness needed to sustain the increased dynamic load due to the increased diameter.

  Standard monopiles are used for water depths up to 30 meters, while *XXL* monopiles are designed to support larger turbines in deeper water. According to a report from the Renewable Consulting Group at the end of 2017, monopiles will stay the preferred foundation choice for water depths up to at least 40 meters [58]. This is the result of the constant development of monopiles. Still, soil conditions, structural stiffness and corresponding dynamic performance limit use in deeper waters. Due to the simplicity of fabrication, ease of installation and corresponding low cost, monopiles are currently the most applied support structure for offshore wind turbines.

- **Tripod** substructures are based on monopiles but have three-legged steel frames supporting the lower portion of the pile. The construction is anchored by piles through sleeves at the end of each of the tripod

legs. Tripods are used in water depths of over 30 meters and are suitable up to 50 meters [77]. Compared to monopiles, tripods have better overturning moment resistance, need shallower foundation piles and need less scour protection. The latter due to mainly axial instead of bending loading of foundation piles. However, monopiles are easier to construct, have fewer fatigue issues and can be transported more efficiently.

- **Jackets** are very common in the oil and gas industry and are the second most used substructure for offshore wind turbines. At the end of 2018, 446 jacket substructures for grid-connected wind turbines were present in Europe [60]. The structure typically consists of four mildly tilted legs interconnected by slender diagonal members (braces), to form a 3-dimensional lattice structure. The diameter of the legs is more than one meter, with a thickness of about 50 mm. The structure is anchored to the seabed by piles, which are mainly loaded by axial force. Jackets are said to be applicable for water depths of 30 to 80 meters [77]. Strictly speaking, a division should be made between (truss) tower and jacket structures. Truss towers are anchored to the seabed by piles through pile sleeves (like tripods), whereas jacket structures are connected to the seabed by piles through the legs connected at the top. Although there is a difference in the way forces are transferred to the foundation, in practice, often no distinction is made between these two formulations. Jacket structures supporting wind turbines are usually anchored by driven or drilled piles of 0.8-2.5 meter in diameter through pile sleeves, so strictly truss towers. Still, the term jacket substructure is used in literature and throughout this report.

  The mass of a jacket structure increases linearly with water depth, and due to member placement away from the neutral line, the structure comprises a higher stiffness over mass ratio than monopiles [17]. This ratio, influencing the eigenfrequency, can be tweaked by varying global structural layout. Of major importance is the distance between the piles at the seabed, the so-called base width. The eigenfrequency of the supporting structure is crucial to support wind towers in deeper waters, while at the same time accommodating increasing mass and dimensions of wind turbines. Moreover, due to reduced cross-section dimensions compared to monopiles, jackets are less affected by waves and current. Transportation is moderately difficult, and maintenance and fabrication costs are high. Due to the high degree of pre-assembly, installation costs are relatively low. Fatigue resistance is of great interest and protective coatings, and cathodic protection should be applied.

- **Tripile** structures consist of three vertical steel piles, connected above water level by a transition piece. Like jacket and tripod, the foundation piles mainly carry axial forces, the stiffness of the structure can be significantly enhanced by the global layout, and fatigue resistance of welded joints is crucial. Piles are driven in the seabed like monopiles, without the need for separate foundation piles. Tripiles are currently used in the BARD offshore 1 Wind Farm with 40-meter water depth [67].

- **Gravity based** structures consist of a slender steel tube fixed in a large reinforced concrete foundation. Due to the use of concrete, this type of foundation is very heavy. The weight of the base should be sufficient to resist overturning moments caused by environmental conditions. This type of foundation is used for the Thornton Bank offshore wind farm in 28-meter water depth [77]. Transportation and installation are challenging due to the dimensions and weight. Even though concrete is relatively cheap, gravity-based solutions are expensive. Due to the absence of piles, decommissioning is easy.

- **Full truss towers** are jacket-like truss structures, spanning the complete height from the seabed to wind turbine. Opposed to jacket structures, no standard circular wind tower is used. This reduces complexity and failure modes induced by the transition between lattice supporting structure and circular wind turbine tower. Besides, the full-height braced structure gives more freedom in stiffness over mass ratio, important for facilitating increased turbine size and capacity [17]. Downsides are the sensitivity to torsional loading, the increased number of fatigue sensitive joints, the amount of workmanship and the design of the truss tower - rotor joint.

The mentioned structures are fixed to the seabed by driving either the main supporting structure (monopile and tripile) or foundation piles (e.g. jackets and tripods) into the seabed. Another foundation solution is the use of suction piles/buckets. A suction bucket is relatively short in relation to the diameter and is pulled downward by a pressure difference, obtained by pumping water out of the suction bucket. As a result, this concept is more suitable for deeper waters. Tension and bending capacity are commonly lower than driven piles and limit wide use.

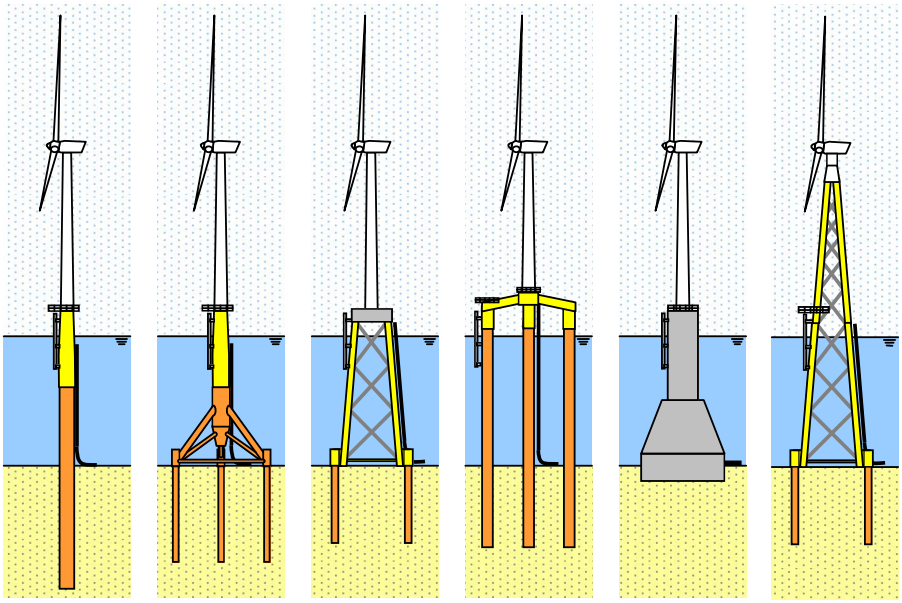

Figure 2.5: Wind turbine supporting structures. From left to right: monopile, tripod, jacket, tripile, gravity-based substructure and full lattice tower [De Vries et al., 2011].

2.3. Environmental data and loads

Characteristics of soil and data regarding environmental loads should be known to design of an offshore wind turbine support structure. Soil data is needed to check foundation strength, to evaluate eigenfrequencies and to obtain correct load effects. Environmental loading is used to formulate load scenarios and to evaluate structural performance. Wind and waves exert the major part and current, and marine growth adds to this. All input relevant for the design of jacket support structures is given and elaborated on this section.

2.3.1. Soil

Soil is a granular material of which the composition depends on the erosion of rocks or the accumulation of organic material. Both clay-like cohesive soils and sand-like non-cohesive soils exist. Due to (geological) history, properties are very inhomogeneous and location dependent. Therefore, location-specific data is gathered using sampling and cone penetration tests. For sandy soils, the angle of internal friction (ϕ) and the effective soil unit weight (γ') should be specified. For clay, the undrained shear strength (s_u) should be given.

Simplified soil modelling can be performed with distributed springs along the buried foundation length. For horizontal (lateral) stiffness a $p-y$ relation is used, for vertical (axial) stiffness a $t-z$ relation. Another strategy is the use of an effective depth at which the structure is supposed to be simply supported. Literature suggests a length equal to a multitude of leg diameter.

2.3.2. Water level

Due to periodical tides and non-periodical storms, water level changes over time. Frequently used parameters are the Lowest Astronomical Tide (LAT) and Mean Sea Level (MSL). In combination with tidal range, storm surge and highest waves expected, LAT is used to determine the interface level of a support structure.

2.3.3. Waves

Waves can be sorted according to their period. Long-wavelength (12 or 24 hours) tidal waves are caused by tidal forces, originated by the gravitational pull of moon and sun. Wind waves are caused by wind acting on the sea surface. Their wavelength varies from a couple of minutes to less than a second and their height depends on wind speed, wind duration and the distance over which wind blows without a change in direction, the so-called fetch. Waves with periods between a minute and an hour are called surges and are caused by atmospheric and seismic forces. Measurements are performed mainly by buoys equipped with accelerometers and pressure sensors mounted at fixed underwater positions.

Regular waves can be described by the linear wave theory, in which the wave follows a sinusoidal shape. Real waves are irregular and variable in nature. Although individual waves can be identified, there is significant variability in height and period from wave to wave. Consequently, definitions of waves must be statistical or probabilistic. The most important parameter is the significant wave height, H_s. It is the mean of the largest 1/3 (33%) of waves recorded during the sampling period. Note, the significant wave height is a statistical measure, not intended to correspond to any specific wave. The largest wave in a 1000-wave sample is likely to be 1.86 times the significant wave height [74].

Two main approaches exist to treat realistic, complex waves: spectral analysis and wave-by-wave analysis. The more popular and powerful spectral analysis assumes waves can be considered as a superposition of many regular sinus waves, with different frequencies and amplitudes. It is a transformation from the time-domain to the frequency domain and is accomplished by the mathematical Fast Fourier Transform (FFT). It gives the distribution of wave energy over wave frequencies. The energy is a function of significant wave height, peak period and frequency and is proportional to the component amplitudes squared.

Attempts have been made to describe the ocean in specific conditions. Two frequently used wave spectra are the Pierson-Moskowitz and the JONSWAP spectrum. The former describes the sea in a fully developed state. This is a sea state produced by winds blowing steadily for a long time (roughly 10 000 wave periods) and over a large distance (roughly 5 000 wavelengths), giving waves in equilibrium with the wind. The spectrum is obtained from ships in the North Atlantic Ocean. In 1973, data was gathered for the North Sea in the Joint North Sea Wave Observation Project JONSWAP. It was found that the wave spectrum is never fully developed. To improve the fit to measurements, a correction factor γ was added to the Pierson-Moskowitz approximation. The main difference is a more pronounced peak (see Fig. 2.6). Depending on the definition used, the significant wave height H_s and the peak spectral period T_p should be specified to obtain the location-specific JONSWAP spectrum [65].

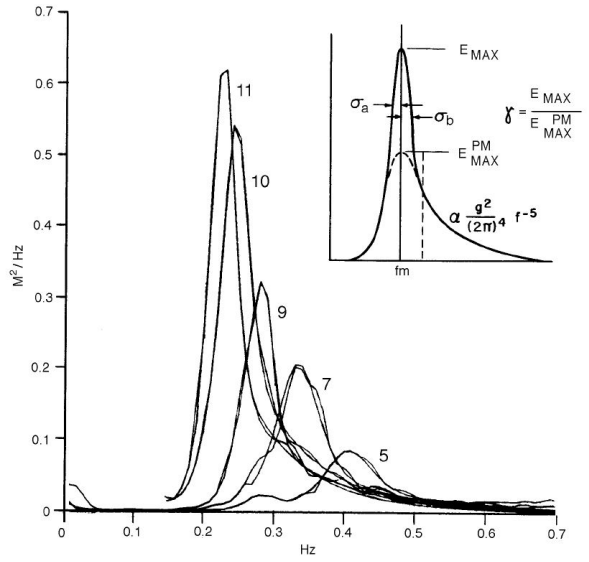

Figure 2.6: JONSWAP wave spectral density for different fetch lengths. In the top right corner, the difference between the peak of Pierson-Moskowitz and JONSWAP spectrum is shown, indicating correction factor γ [Stewart, 2011].

2.3.4. Wind

Wind originates from differences in atmospheric pressure. It is the renewable source responsible for power generation and exerts significant forces on both rotor and tower. Measurements are performed by masts and more recently by lidars. The latter performs wind measurements over a height up to about 300 meters. Mast and lidar data can be translated into wind speed at reference heights using power or logarithmic relations, representing the shear profile. Of main importance is the value at hub height (mid-rotor height). Besides the wind speed, also directional data should be supplied. Usually, this is done by a wind-rose.

At a fixed height (e.g. hub height), the average wind speed is commonly gathered for 10-minute time intervals. Over a long time, e.g. over a year, the 10-minute average wind speeds can be gathered and sorted on the probability of occurrence. This probability is proven to be well approximated by a Weibull distribution (see Fig. 2.7). Extrapolation of the mean wind speed can be performed to obtain values for a different return period.

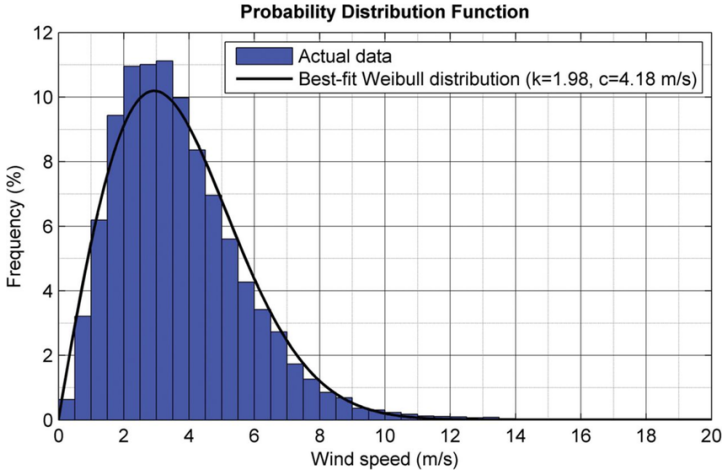

Figure 2.7: Typical Weibull approximation of wind speed data, fitted by Weibull shape factor k [Ricci et al., 2014].

The maximum wind speed (gusts) expected within the design life, can be assessed by ranking yearly maximum wind speeds in ascending order in a Weibull graph. The typically used 50-year value can be obtained by extrapolation and is used for the ultimate limit state analysis. A wind turbulence model, like the commonly used Kaimal spectrum, is used to account for local wind effects.

2.3.5. Wave-wind directionality

Wind and waves do not necessarily have similar directions. On top of that, extreme wind speeds and extreme waves do not necessarily coincide with extreme loads. Therefore, directional data is used to obtain more accurate results. Wind roses and wave roses can be used to find wind-wave misalignment.

2.3.6. Current

Currents may be caused by wind, tides, pressure gradients or density gradients. Near the water surface, the wind-induced current is generally governing, while in deeper layers tidal currents are. At the seabed, the current speed is assumed to be zero. The resulting profile can be approximated by a power, linear of bilinear profile. Current data is given in meters per second and provided by measurements. The data points are fitted with a Gumbel distribution to obtain a cumulative distribution function. Extrapolation is used to obtain maximum currents for long recurrence rates. For design, the recurrence period is usually 5 or 50 years.

2.3.7. Marine growth

Marine growth affects surface roughness, adds mass and increases the effective diameter of steel sections. The latter is of main importance as the wave forces exerted on the structure is a function of the member diameter. The growth depends on location and depth and guidance values are giving in DNVGL-ST-0437 (see Tab. 2.1) [20].

Table 2.1: Marine growth thickness [mm] as function of depth below water level and location [DNVGL, 2016].

Depth below MWL [m]	Central and Northern North Sea (56° to 59° N)	Norwegian Sea (59° to 72° N)
-2 to 40	100	60
> 40	50	30

2.4. Wind turbine characteristics

The behaviour of a wind turbine depends on the wind speed. Several curves are developed to indicate functioning over the complete wind speed range. They are based on the following key parameters:

- **Cut-in wind speed** is the wind speed at which a turbine starts to rotate and generate power. Usually between 3 and 4 m/s.
- **Rated wind speed** is the wind speed at which the power output reaches the limit that the electrical generator is capable of. At higher wind speeds, the power output is constant, which is commonly realised by a change of the blade angle (pitch control). The rated wind speed is typically between 10 and 15 m/s.
- **Cut-out wind speed** is the wind speed at which the forces and the risk of damage are considered too high. The rotor is brought to a standstill by brakes. The cut-out speed is usually around 25 m/s.

The power curve, rotor speed, pitch angle and trust force as a function of the wind speed are shown in Fig. 2.8, in which the vertical lines indicate the cut-in, rated and cut-out wind speed.

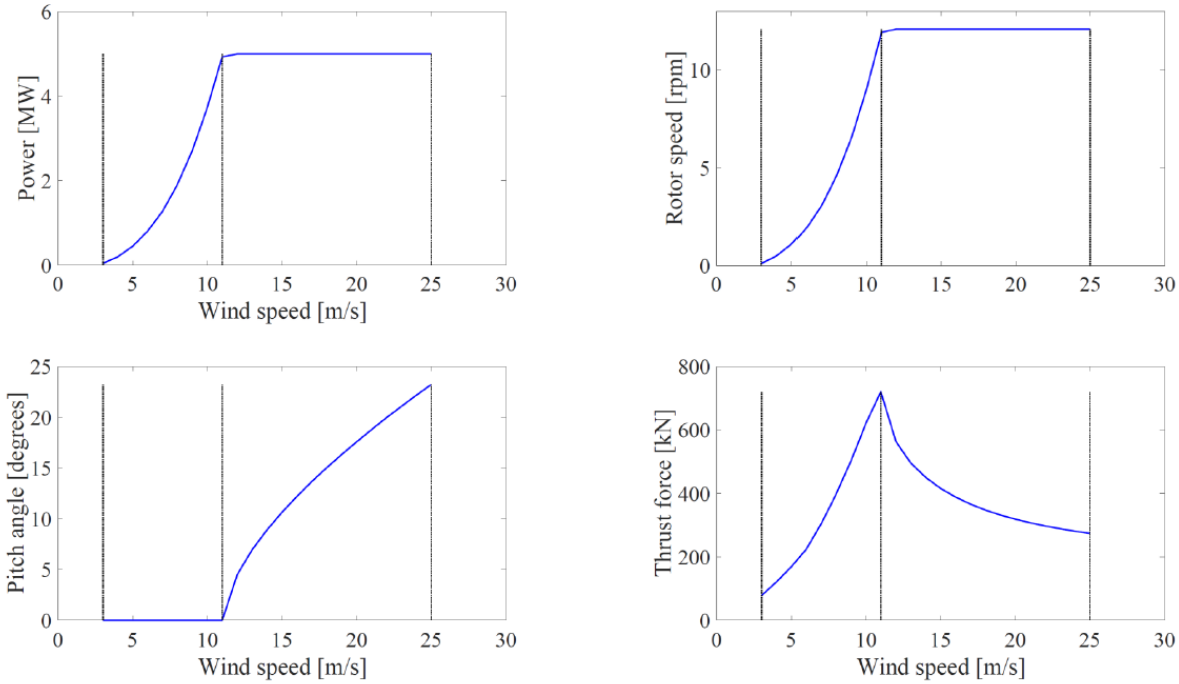

Figure 2.8: Power, rotor speed, pitch angle and thrust force as a function of wind speed for a pitch regulated wind turbine. The vertical black lines represent from left to right the cut-in, rated and cut-out wind speed [TU Delft, 2018].

To calculate the energy yield, both the power curve, the probability of wind speeds around hub height, and the rated capacity should be known. The rated capacity is the amount of energy the turbine would produce if it ran 100% of the time at optimal wind speeds. The capacity factor is the unitless ratio of the actual energy output to the maximum energy output over a given period. The capacity factor is determined by the availability of wind, the blade length, the size of the generator and the power demand. The latter is of great importance, as in more than 80 per cent of the time, the power generated by an offshore wind turbine is a control decision [3]. Supply of energy should match the demand to control the grid frequency. Typical capacity factors for offshore wind farms are around 0.35-0.45. From the capacity factor and the rated capacity, the electricity production of a wind turbine can be calculated.

Note, the power production of a wind farm is lower than what would be calculated by addition of standalone turbines. The tower, and to a larger degree the rotor, influences the flow velocity of air due to so-called wake effects. These wake effects can last for several rotor diameters. Turbines placed downwind operate in reduced wind speeds and increased turbulence, which results in lower energy production. Besides, the increased turbulence leads to increased loading. Modelling is performed to decrease wake effects as much as possible.

2.5. General design procedure

In this section, the general design procedure for offshore wind turbine support jacket structures is given. The majority of the procedure is generally applicable. First, an overview of the complete procedure is shown. Afterwards, load cases and frequency analysis are highlighted and discussed in detail.

2.5.1. Overview of procedure

The design of an offshore wind turbine support structure is complex and therefore, generally an iterative process. First, a preliminary design is made to find the global layout of the supporting structure. The design is based on on-site input like water depth and turbine input like operating frequencies. In this process, the eigenfrequency of the supporting structure is the main design driving parameter.

Next, coupled aero-hydro simulations are performed based on design scenarios. The scenarios are formulated by certification and standardisation companies like DNVGL and IEC. Different simulations are performed for extreme load analysis, the so-called ultimate limit state (ULS) and the fatigue load analysis, the so-called fatigue limit state (FLS). Many hundreds of load cases are simulated with a variety of wind speed and direction, wave height, period and direction, current speed and direction, operation conditions, fault scenarios etcetera. For the ULS, the harshest situation is looked at, while for the FLS, the expected load history during complete lifetime should be approximated as accurate as possible.

Load effects for both limit states are recorded and post-processed to perform strength, stability and fatigue checks of members and joints. If checks indicate insufficient or uneconomic resistance, the design is updated. If considerable changes are made, the eigenfrequency should be checked again, and loading simulations should be redone. An overview of the design process is schematically shown in Fig. 2.9.

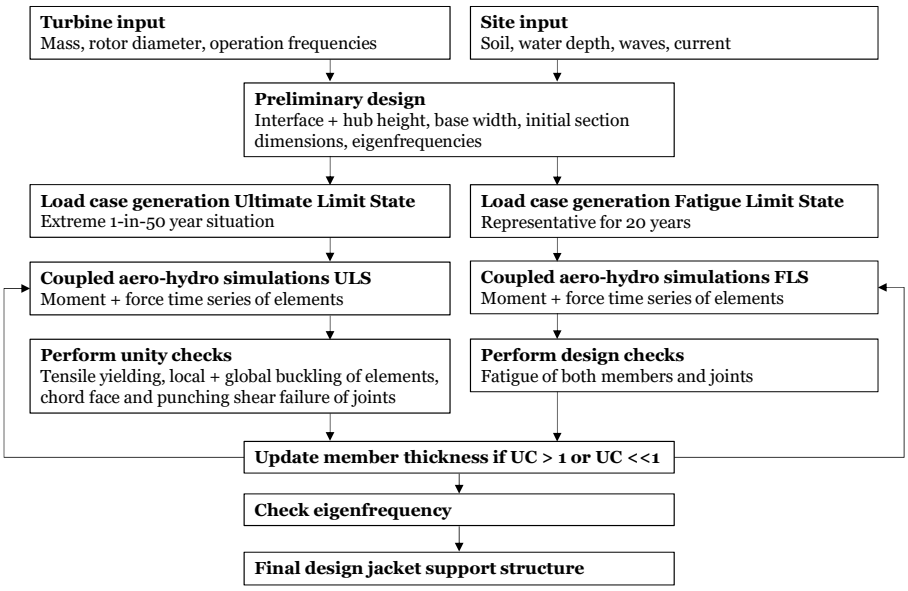

Figure 2.9: Work flow showing the steps and their order to design a jacket supporting structure for an offshore wind turbine. UC = Unity Check.

In the current industry, there is a division between the turbine (including tower) and substructure designer. Load effects at the interface between tower and substructure are exchanged and used as input for models. As the tower and the substructure interact, the resulting process is highly iterative.

2.5.2. Load case generation

The loading of wind turbine supporting structures is complex due to a variety of wind and wave load combinations, as well as due to different wind turbine conditions. In advance, it is not known which loading condition will cause most detrimental load effects. The design load cases should cover all expected operational as well as fault situations. The design load cases are defined by IEC61400-1 and IEC61400-3 and cover the following situations [33, 34]:

1. Power production;
2. Power production plus the occurrence of fault;
3. Start-up;
4. Normal shut-down;
5. Emergency shut-down;
6. Parked (standing still/idling);
7. Parked plus fault conditions;
8. Transport, assembly, maintenance and repair.

These load cases are implemented in time-domain simulations, taking into account wind, wave and current loads on the structural model, including their aero-hydrodynamic coupling.

2.5.3. Eigenfrequency analysis

The design of a wind turbine support structure is highly influenced by the selection of the wind turbine. The turbine choice determines the top mass and the operating frequencies, and it influences the eigenfrequencies of the complete structure. The latter is of great importance to ensure proper functioning. If natural frequencies overlap with either operating frequencies or loading frequencies, resonance occurs. At resonance, the response of the structure is larger than expected from a quasi-static case. As a result, the stress (range) will increase. The ratio between the dynamic response and the quasi-static response is quantified by the Dynamic Amplification Factor (DAF). The response of a structure with eigenfrequencies overlapping with loading frequencies is shown in Fig. 2.10.

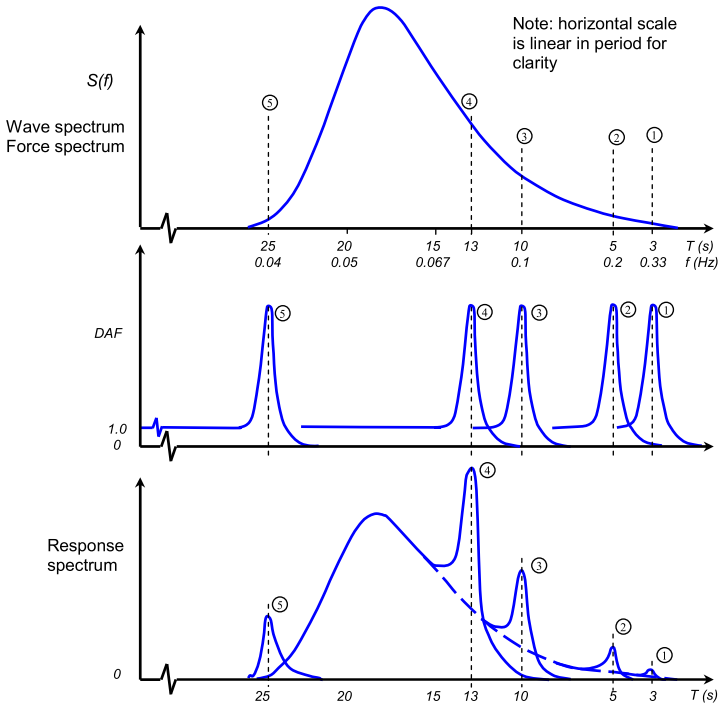

Figure 2.10: Structural response (bottom) for forcing frequencies (top) overlapping with eigenfrequencies (middle). If high energy forcing frequency overlaps with eigenfrequency, the structural response is amplified [De Vries et al., 2011].

Wind turbines operate at different wind speeds with rotating frequencies determined by cut-in speed, cut-out speed and control system. The rotor spinning at a given speed induces mass imbalances, causing a frequency known as 1P. In addition, blades of a wind turbine passing the tower induce an excitation equal to $n \cdot P$. For a regular 3-bladed wind turbine, this frequency is 3P. The frequency bands given by $f_{\text{cut-in}}$ to $f_{\text{cut-out}}$ (1P band) and $3 \cdot f_{\text{cut-in}}$ to $3 \cdot f_{\text{cut-out}}$ (3P band) indicate frequency ranges during operation. To avoid resonance, the eigenfrequency of the wind turbine support structure should be outside the frequency bands.

An overview of the frequency spectrum can be seen in Fig. 2.11. Here, also the three viable frequency ranges, known as soft-soft, soft-stiff and stiff-stiff are shown. The soft-soft range, with frequencies lower than the 1P frequency band, implies a very flexible structure. Moreover, the wave frequencies may lie in this region. The stiff-stiff range, with frequencies above the 3P band, implies a very stiff structure and therefore generally uneconomic for water depths around 50 meters. The soft-stiff region, between the 1P and 3P band, is currently the optimum range for design [10]. For safety reasons, the natural frequency should be separated from the frequency bands by at least 10%. Besides the first natural frequency, also higher eigenfrequencies should be outside the ranges.

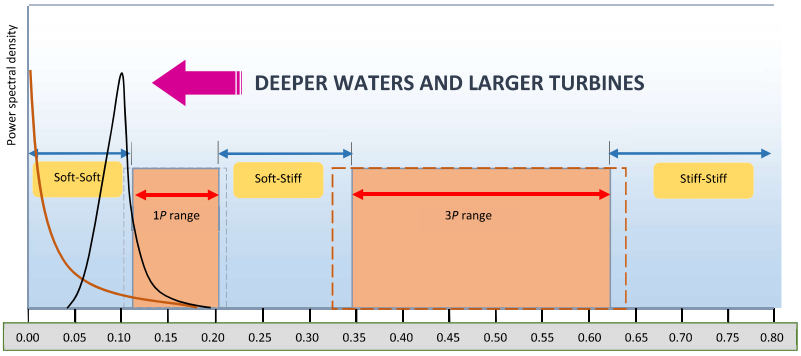

Figure 2.11: Forcing frequencies in Hertz against power spectral density for a three-bladed wind turbine. The orange line represents the wind and the black line the wave spectrum. The three eigenfrequency ranges for the supporting structure are shown [Bouzid et al., 2018].

2.6. Conclusion

The interest in renewable energy is increasing due to societal and political commitment to limit global warming. Wind is one of the renewable resources, and a shift is seen towards offshore placement of turbines. Trends show offshore wind turbines increase in size, parks increase in capacity and sites increase in water depth.

Currently, monopiles comprise the vast majority of wind support structures. Mass of mono-piles increases quadratically with depth, indicating future room for alternative fixed substructure concepts. Jackets consist of circular hollow sections in a lattice structure and show a linear increase of mass with depth. Due to the open structure and placement of members away from the centre of mass, a high stiffness over mass ratio and a relatively wave-transparent structure can be obtained. The eigenfrequency of the structure is influenced by the mentioned ratio and is of great importance to avoid resonance with forcing and operating frequencies.

Wind, waves and current exert the majority of forces on the construction. Load scenarios are formulated by certifying companies like DNV GL and IEC, which combine environmental actions in all realistic combinations. Operating conditions, start-up and shut-down are simulated in coupled aero-hydro simulations, and load effects are recorded for both ultimate and fatigue limit state. After the simulation, design checks are performed for both FLS and ULS. For the former, fatigue lifetime of joints is of main concern. For the latter, the strength of joints and strength and stability of members is checked. As the structural properties influence the load effects, the jacket design procedure is highly iterative.

3

Motivation and research questions

This report investigates the potential benefits of innovative wrapped FRP joints, under development by Dr. Marko Pavlović, for offshore wind turbine jacket support structures. The load on jacket structures is highly cyclic due to waves, but mainly due to wind acting on turbine blades. Usually, welding is performed to achieve a rigid connection between circular steel sections. Unfortunately, welded joints limit the strength and lifetime of the structure due to the following phenomena:

- Heat-induced during welding leaves **residual internal stresses** in the material. Tensile stress in and close to the weld, compressive stress further away from the weld. This residual stress has a negative influence on fatigue resistance.
- Local weld geometry leads to **stress concentration**. The shape of the weld influences the local stress. The worse the finishing and smoothness of the weld, the larger the stress concentration.

As a result, welded joints generally govern jacket design. To increase the resistance of the joint, member diameter or more commonly, member thickness is increased. This is performed over a certain length (a so-called can section), or over the complete member length. The former gives a more material-efficient structure, but increases labour and entails damage induced by additional welding.

To avoid welded joints, wrapped FRP joints can be used. Wrapped FRP joints connect circular hollow jacket members by wrapping layers of fibre reinforced polymer around the to-be-jointed members. No welding is performed for this connection method, and as a result, the detrimental phenomena enumerated before are either prevented or reduced. Due to the absence of welds and due to the outstanding fatigue performance of FRP material, the theoretical potential of these joints is large.

Experiments are performed at the Delft University of Technology to prove the actual performance. Tests on small scale X-joints indicate outstanding cyclic behaviour. As both theory and test show similar promising results, the main research questions of this report reads:

What is the potential steel weight reduction in offshore wind turbine supporting jacket structures, if regular welded joints are replaced by innovative wrapped FRP joints?

Additionally, the following sub-questions will be answered:

- *Which limit state (fatigue or ultimate) governs jacket member design and does this change when using wrapped FRP instead of welded joints?*
- *What is the potential additional steel weight reduction for both welded and wrapped FRP jointed jacket structures, if high strength S690 steel is used instead of mild strength S355 steel?*
- *What is the potential cost saving if wrapped FRP counterparts replace regular welded joints?*

4

Model, analyses and cases

The first part of this chapter contains all relevant details regarding the modelled structure and the applied load. The second section discusses the analyses and calculations performed to give a substantiated answer to the research questions. The final section elaborates on different design cases of the jacket support structure. The cases are set up to determine the potential of wrapped FRP joints.

4.1. Model

Environmental and turbine properties highly influence the potential benefit of wrapped FRP joints. Jacket structures are not applied in shallow water up to about 40 meters. Besides, the eigenfrequency, important to prevent displacement, force and stress amplification, is highly influenced by turbine mass.

The supporting structure, load conditions and foundation used, are based on the UpWind project [17]. This project, completed in March 2011, was aimed to investigate design limits for large wind turbines. It is one of the largest European funded wind energy projects with cooperation between universities, research institutes and companies. This project is chosen as a reference since all relevant data is available, and the water depth of 50 meters is suitable for application of jacket supporting structures. Differences to the UpWind project are summed up in App. A. The input settings of the GH Bladed simulation software can be seen in App. B.

4.1.1. Jacket structure, foundation and wind turbine

The general properties of the **jacket structure** can be found in Tab. 4.1, the member properties in Tab. 4.2 and a schematic view is shown in Fig. 4.1. The modelled OC4 jacket structure is a simplified version of the UpWind structure. In the UpWind structure, member thickness is locally increased around joints, while the OC4 structure has constant member thickness between joints. Excluding so-called joint cans has little influence on modelling results (change of the lowest eigenfrequency under 0.7%), while it reduces computational time strongly [17].

Table 4.1: Properties of the jacket structure.

Jacket structure	
Source	OC4/UpWind project [17, 71, 72]
Base width	12 m
Top width	8 m
Mass of transition piece	666 t
Levels of X-braces	4
Water depth	50 m
Interface height	20.15 m above MSL
Site	North Sea, between Great-Britain and the Netherlands
Structural damping	1% [72]

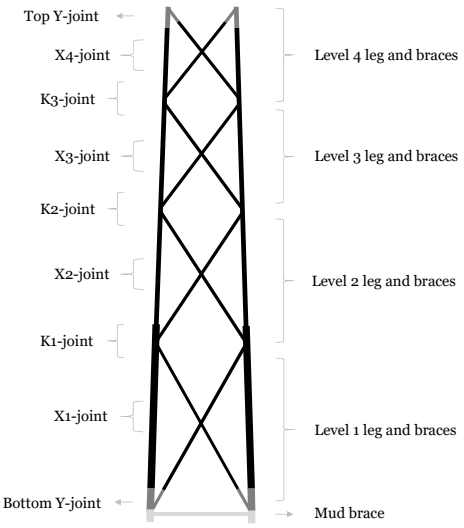

Figure 4.1: Modelled OC4 jacket structure with indication and tag of the analysed elements and joints. Line thickness indicates element thickness. Dark grey Y-joints and light grey mud brace are not within the scope of this project, and therefore not optimised. Light grey mud brace elements are not taken into account in the mass calculation.

Table 4.2: Member properties of the modelled jacket support structure.

	Outer diameter [m]	Thickness [mm]
Level 1 legs	1.2	50
Level 2, 3 and 4 legs	1.2	35
All level X- and mud braces	0.8	20

The general properties of the **foundation** can be found in Tab. 4.3 and Tab. 4.4. The soil is modelled with lateral non-linear $p-y$ springs and axial non-linear $t-z$ springs, according to DNVGL-RP-0126 [19]. Springs are depth-dependent and are applied every 2 meters. The pile tip resistance is included at 48 meter below seabed. The soil parameters are changed with respect to the UpWind project to remain within friction angle limits of soil spring model [18, 19]. As a result, interpolation is performed and extrapolation is avoided.

Table 4.3: Properties of the foundation structure.

Foundation	
Source	UpWind project [17]
Number of piles	4
Pile length	48 m
Minimum pile thickness	28 mm
Maximum pile thickness	60 mm
Soil	Layered sand
Modelling	Lateral $p-y$ and axial $t-z$ springs every 2 m along pile. Additionally, pile tip resistance at pile end.
Effective soil unit weight	10 000 $\mathrm{N\,m^{-3}}$

Table 4.4: Soil properties of the modelled foundation.

	Depth [m]	Friction angle [deg]
Layer 1	0 - 4	38
Layer 2	4 - 8	35
Layer 3	8 - 10	38
Layer 4	10 - 48	40

The general properties of the **wind turbine** can be found in Tab. 4.5 and the frequency diagram in Fig. 4.2. The same wind turbine is used in the UpWind reference project. The frequency diagram shows the rotor operating frequency (1P) and the blade-passing operating frequency (3P), including a 10% safety margin. Additionally, it shows forcing frequencies of wind and waves. To avoid resonance, the eigenfrequency of the complete structure (soil + jacket + wind turbine) should not overlap with the operating frequencies.

Table 4.5: Properties of the modelled wind turbine.

Wind turbine	
Source	NREL 5 MW [35]
Hub height	90.55 m above MSL
Nacelle mass	240 t
Rotor mass	110 t
Cut-in wind speed	3 m/s
Rated wind speed	11.4 m/s
Cut-out wind speed	25 m/s
1P frequency band	0.115 - 0.202 Hz (6.9 – 12.1 rpm)
3P frequency band	0.345 - 0.605 Hz (20.7 - 36.3 rpm)
Viable eigenfrequency range	0.222 – 0.311 Hz (10% margin taken into account (see Fig. 4.2))
Eigenfrequency modelled structure	0.272 Hz (lowest eigenfrequency)

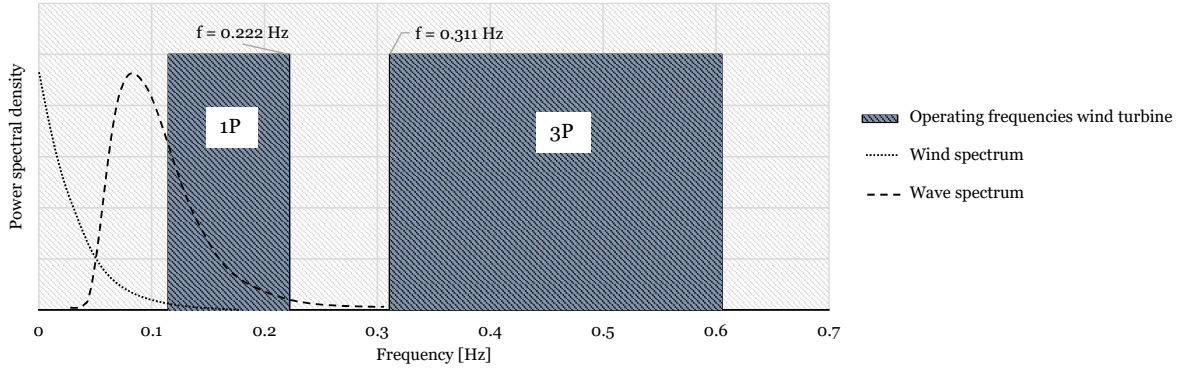

Figure 4.2: Eigenfrequency diagram of modelled NREL 5 MW wind turbine, with 1P-range indicating rotor frequency range and 3P-range indicating blade-passing frequency range. The vertical axis indicates power spectral density, the horizontal axis frequency. Dotted line indicates wind and dashed line indicates wave frequencies [Adapted from De Vries et al., 2011 and Bouzid et al., 2018].

Complete jacket supported offshore wind turbine:

The complete structure is modelled in the GH Bladed simulation software, and resulting structural layout can be seen in Fig. 4.3. The blue layer represents mean sea level, and the light-brown layer represents seabed.

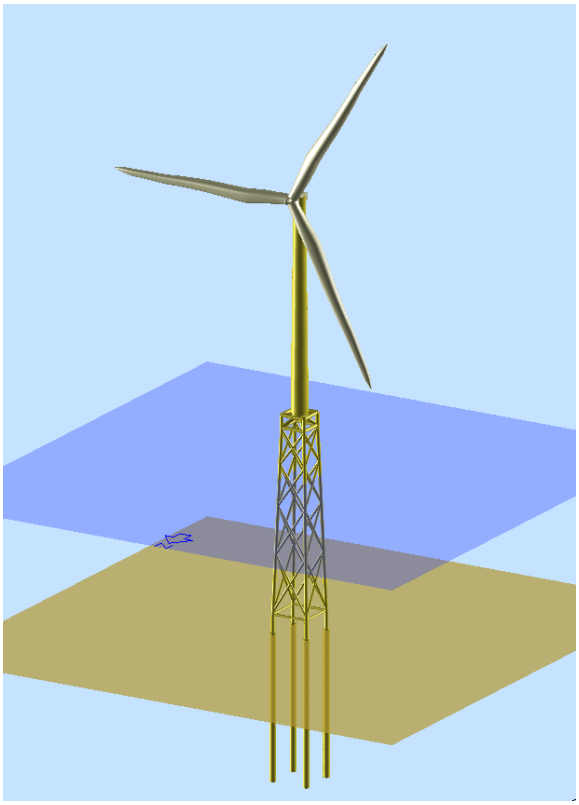

Figure 4.3: Wind turbine including jacket substructure and pile foundation as modelled in GH Bladed.

4.1.2. Load

The general properties of the **fatigue load** can be found in Tab. 4.6 and the modelled load scenarios in Tab. 4.7. These scenarios cover all wind speeds (with corresponding wave conditions) and are formed to reduce the number of simulations. For all five modelled load scenarios, six simulations with different seeds for wave irregularity and wind turbulence are performed. As a result, dependency on the chosen seed is reduced, and randomness is incorporated. After simulations are performed, data from all different seeds for a single load scenario are merged. In the fatigue calculations, the occurrence in lifetime is used to correct for the likeliness of the load scenarios. The fatigue load is representative for load during the full 20 years lifetime of the structure. Detailed information about the fatigue load can be found in App. C.

Table 4.6: Properties of the fatigue load.

Fatigue load	
Source	UpWind project [17]
Wind direction	0 degrees from North
Wind-wave misalignment	0 degrees
Modelled wind-wave scenarios	5 (see Tab. 4.7)
Amount of different wind-wave seeds	6
Total number of simulations	30
Length per simulation	800 s, first 200 s removed to get rid of start-up effects
Wind and waves simulated simultaneously	Yes
Members flooded	No
Marine growth	Yes (see Tab. 2.1)
Current	Yes, 0.6 m/s near-surface current, linearly decreasing with depth to zero at 20 meter water depth
Total lifetime	20 years

Table 4.7: Load scenarios simulated for fatigue load analysis. Binned wind speeds including the simulated wind speed, turbulence intensity, significant wave height, peak wave period and occurrence percentage. Numbers based on UpWind project [17].

Wind speed window [m/s]	Wind speed [m/s]	Turbulence intensity [%]	H_s [m]	T_p [s]	Occurrence in lifetime [%]
1 - 9	5	18.95	1.14	5.82	43
9 - 15	11.4	14.78	1.63	5.84	37.5
15 - 19	17	13.75	2.33	6.54	12.5
19 - 25	22	13.30	3.09	7.4	6
25 - 31	28	11.9	4.17	8.49	1

The general properties of the **extreme load** can be found in Tab. 4.8, the modelled load properties in Tab. 4.9 and the modelled scenarios in Fig. 4.4. Scenarios 1 and 2 are expected to be governing and scenario 3 was governing for most elements in UpWind. The extreme load is representative for an extreme storm with a 50-year return period. Detailed information about the extreme load can be found in App. C.

Table 4.8: Properties of the extreme load.

Extreme load	
Source	UpWind project [17]
Wind direction	0 or 45 degrees from North
Wind-wave misalignment	0 or 150 degrees
Modelled wind-wave scenarios	3 (see Tab. 4.9 and Fig. 4.4)
Amount of different wind-wave seeds	6
Total number of simulations	18
Length per simulation	700 s, first 100 s removed to set up yaw misalignment
Wind and waves simulated simultaneously	Yes
Members flooded	No
Marine growth	Yes (see Tab. 2.1)
Current	Yes, 0.6 m/s near-surface current, linearly decreasing with depth to zero at 20 meter water depth. Additionally, 0.6 m/s sub-surface current.
Wind and sea condition	50-year return period

Table 4.9: Extreme load properties used for all simulated ultimate limit state simulations. Numbers based on UpWind project [17].

Wind speed [m/s]	Turbulence intensity [%]	Current speed [m/s]	H_s [m]	T_p [s]	Yaw error [deg]
42.73	11.00	1.2	9.40	13.70	8

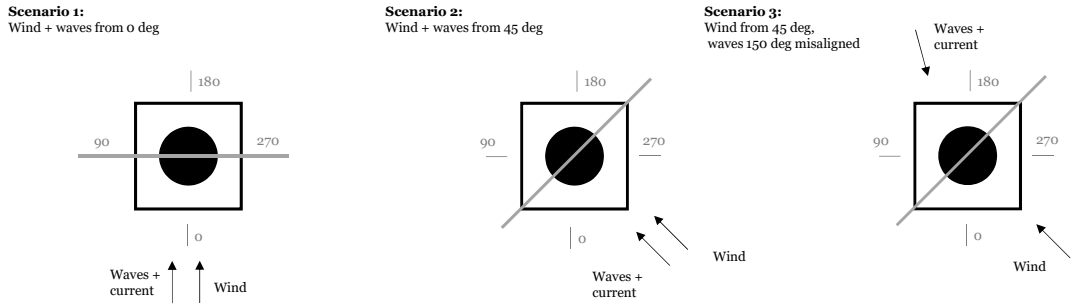

Figure 4.4: Modelled wave-wind scenarios to simulate extreme load. Zero degrees corresponds to the North.

4.2. Analyses and calculations

The wind turbine support structure, as shown in Fig. 4.3, is exposed to fatigue and extreme load conditions. Load effects (normal force N, in-plane moment M_{ip} and out-of-plane moment M_{op}) are recorded over time. Data is obtained both directly at the structural nodes and a certain distance away from the nodes. For the legs, this distance is $0.5D_{\text{leg}}$ from the weld and for the braces $1.5D_{\text{brace}}$ from the weld. This results in a distance of 1.8 to 3.2 meters from the joint node. This data is used to investigate member fatigue.

To reduce modelling time and to reduce data extraction time, data is not obtained at all joints and members, and due to practical reasons, ULS data is extracted at other planes than FLS data. Most data for the FLS analysis is extracted from the front plane, while most data from the ULS analysis is extracted from the three remaining planes.

FLS calculations are performed for all 6 uniplanar K-joints and 4 X-joints in the front plane (see Fig. 4.1 and Fig. 4.3). Additionally, 3 K-joints in the adjacent side plane (pointing West) are analysed. All members adjacent to the mentioned joints are checked for element fatigue.

ULS calculations are performed for 11 uniplanar K-joints (6 in the back plane, 3 in side plane (pointing East), 1 in the front plane and 1 in the side plane (bottom, pointing West)) and for 8 X-joints (4 in back plane and 4 in side plane (pointing West)). The latter two K-joints are included for comparison and reference. For member buckling and tension yielding, calculations are performed for 44 elements (32 braces in both back and side plane (pointing East) and 12 leg elements (North-East, South-East and East-West leg)).

The load factors and the material factors used can be seen in Tab. 4.10. The material factor for fatigue, $\gamma_M = 1.25$, is equivalent to DFF = 3 (Design Fatigue Factor, commonly used in offshore calculations [19]).

Table 4.10: Load factor and material safety factor for FLS and ULS calculations.

	FLS	ULS
Load factor γ_F	1.00	1.35
Material factor γ_M	1.25	1.15

4.2.1. Fatigue limit state

A thorough and detailed analysis is performed to calculate the fatigue damage of joints and members. The detailed step-by-step procedure can be found in App. D. In short, the procedure for joints is given below:

1. At every time step, **hot spot stresses** are calculated by combining forces and moments in all members around a joint. The hot spot stress is dependent on stress concentration factors (SCFs), which are a function of the geometry and the loading of the joint. The hot spots analysed are the crown heel, the crown toe and the saddle locations at both sides of the member (see Fig. D.1).
2. At a single hot spot, stresses for all time steps are combined to obtain a **stress-time series**.
3. At a single hot spot, rainflow counting is applied to transform the varying hot spot stress-time series, into a simple set of **stress ranges and counts**. The latter is called a histogram.
4. For a single stress range, the **single damage** is calculated by using the appropriate S-N curve.
5. For a single hot spot, linear Palmgren-Miner is used to add damages to calculate the **total damage**.

The procedure for members is similar to the procedure for joints, except for step 1. The four hot spot locations are four evenly spaced points around the member circumference, and the stress is calculated by the simple addition of normal stress and bending stress. If a thickness transition is present, this is accounted for by a stress concentration factor.

Hot spot stresses are obtained with stress concentration factors of DNVGL-RP-C203 [21], based on Efthymiou [23]. SCFs are used for both tubular K- and X-joints, as well as for members. SCFs for tubular joints are dependent on the geometry and the loading of the joint, while for members, this is only dependent on the geometry

of the thickness transition. All applied S-N curves (except for wrapped FRP joints) are representative for the performance of details in seawater with cathodic protection as given in DNVGL-RP-C203 [21] (see App. E). The fatigue resistance is a function of the member thickness by the thickness exponent k.

4.2.2. Ultimate limit state

ULS checks are performed for both joint failure (strength), tension yielding (strength), global buckling (stability) and local buckling (stability). A detailed step-by-step procedure for the ULS analysis of joints and members can be seen in App. D.

Welded joints are checked for chord face failure and punching shear failure according to EC1993-1-8 [49]. Members are checked for tension yielding according to EC1993-1-1 [51]. For wrapped FRP joints, joint failure is checked by tension yielding of elements. Global buckling of members is checked according to Annex A of EC1993-1-1 [51] and local buckling according to EC1993-1-6 [50].

4.3. Cases

Multiple cases are set up to investigate the potential steel weight reduction. The description of cases, including the calculation properties, can be seen in Tab. 4.11. Manual optimisation is performed for thickness only, and as a result, diameters are equal to values mentioned in Tab. 4.2. Thickness optimisation is performed in steps of 0.5 mm.

Table 4.11: Description of analysed cases, including calculation properties for fatigue and extreme resistance check of both members and joints.

Case description	FLS - Joint		FLS - Member		ULS - Joint	ULS - Member
	S-N curve	SCF	S-N curve	SCF		
Case 1 - Welded						
a) Mild steel	T	GEO + LD	C1	TT	CFF + PSF	LB + GB + TY
b) High strength steel	T	GEO + LD	C1	TT	CFF + PSF	LB + GB + TY
Case 2 - Unwelded						
a) Mild steel	-	-	B1	Unity	-	LB + GB + TY
b) High strength steel	-	-	BM4	Unity	-	LB + GB + TY
Case 3 - Wrapped FRP						
a) Mild steel	WFRP	Unity [a]	B1/C1 [b]	Unity	TY [c]	LB + GB + TY
b) High strength steel	WFRP	Unity [a]	BM4/C1 [b]	Unity	TY [c]	LB + GB + TY

FLS = Fatigue limit state
ULS = Ultimate limit state
SCF = Stress concentration factor
T, C1, B1, BM4 = S-N curves for details in seawater with cathodic protection (See App E) [21]
TT = Thickness transition [21]
GEO = Geometry [21]
LD = Load [21]
LB = Local buckling [50]
GB = Global buckling [51]
TY = Tension yielding [51]
CFF = Chord face failure [49]
PSF = Punching shear failure [49]
WFRP = Wrapped FRP joint experimental S-N curve

[a] Stress concentration factors already included in S-N curves. Wrapped FRP S-N curve is used to calculated wrapping thickness.

[b] Brace elements contain no welds and hence, curve B1 is used for mild steel, and curve BM4 is used for high strength steel. Leg elements do contain circumferential welds and fatigue curve C1 is used for both mild steel and high strength steel.

[c] Joint ultimate resistance of wrapped FRP joint is governed by tension yielding of adjacent elements.

Case 1: Welded structure
The most material-efficient jacket structure with regular welded connections. It functions as the reference structure and is the starting point to evaluate the potential weight reduction for wrapped FRP joints. The structure contains can sections and is evaluated with both mild S355 steel and high strength S690 steel (see Tab. 4.12).

Table 4.12: Steel types used including yield strength.

	f_y for t ≤ 40 mm [MPa]	f_y for t > 40 mm [MPa]
Mild S355 steel	355	335
High strength S690 steel	690	650

For members, fatigue curve C1 is used (tubular member - circumferential butt weld made from a single side machined or ground flush). For joints, fatigue curve T is used (tubular joints). Note, fatigue curves for welds are independent of base material yield strength. Fatigue curves can be seen in App. E and are given in DNVGL-RP-C203 [21].

Case 2: Unwelded structure
The most material-efficient unwelded jacket structure with idealised joints and constant member thickness (no welds, no cans). The joints are assumed not to govern design, and the structure functions as a boundary case to show the maximum potential steel reduction. In reality, the steel reduction could only be reached if wrapped FRP joints could be produced, which not govern design. The structure is evaluated with both mild S355 steel and high strength S690 steel.

For mild steel, fatigue curve B1, and for the high strength steel, fatigue curve BM4 is used for members (tubular member - non-welded sections). Fatigue curve BM4 has better fatigue properties compared to B1. Hence, fatigue performance is enhanced by high strength steel. Fatigue curves can be seen in App. E and are given in DNVGL-RP-C203 [21].

Case 3: Wrapped FRP structure
The most material-efficient steel structure with wrapped FRP joints. The steel structure contains no cans and brace thickness is similar to case 2. No welding is performed at tubular joints, but circumferential welding is performed for leg elements (fatigue curve C1). These welds are present as tubular elements are produced in lengths up to 12 meters, while leg elements have lengths up to 19 meters. For the second and third level legs, these welds are applied in low-moment regions in the middle of the elements. Fatigue curves can be seen in App. E and are given in DNVGL-RP-C203 [21].

The S-N curves for joints are deducted from lab experiments at the Delft University of Technology. Stress concentration factors are already included in the fatigue curve. According to experiments, FRP wrapping thickness of joints is based on stress in the brace only.

5

Results

This chapter reveals results from the performed simulations and gives answers to the research questions stated in Ch. 3. The first section states the procedure and starting points for the jacket design. Next section elaborates on the results regarding the steel weight reduction, the governing unity check, the benefit of high strength steel and the cost reduction. In the final section, results are analysed more closely, and interesting additional conclusions are given.

5.1. Procedure and starting points

As mentioned in the previous chapter, three different cases are analysed. Each case with mild S355 steel (case a) and high strength S690 steel (case b). Case 1 acts as a reference and gives the most material-efficient structure with current state-of-the-art welded joints. Case 2 is an idealistic boundary case and is the most material-efficient structure when no welding is performed, and when fatigue life of joints does not govern design. Case 3 is a more realistic case which takes experimental results of wrapped FRP joints into account. Additionally, welds are present in leg elements due to the limited production length of tubular steel elements.

For each case, individual members of the jacket structure are optimised to obtain a unity check as close to unity as possible. A unity check gives the ratio between action and resistance. For example, for tension yielding the action would be the acting stress ($\sigma_{\mathrm{Ed}} = \frac{N}{A} + \frac{M}{W}$) and the resistance would be the maximum allowable stress ($\sigma_{\mathrm{Rd}} = f_{\mathrm{y}}$). A unity check close to zero means resistance is much larger than acting stress, while a unity check of one indicates resistance and acting stress are equal. The latter is aimed for, as it implies optimal use of material.

For each element, four unity checks are obtained (see Tab. 4.11). Two fatigue checks to validate fatigue limit state (FLS), and two strength and stability checks to examine ultimate limit state (ULS):

- Fatigue resistance of joint (FLS - Joint);
- Fatigue resistance of member (FLS - Member);
- Ultimate resistance of joint (ULS - Joint);
- Ultimate resistance and stability of member (ULS - Member).

For each element, the maximum value of the four unity checks is brought as close to (but smaller than) unity as possible. This is done by varying the thickness. Starting points for the optimisation are the following:

- Optimisation is done for thickness only;
- Thickness is changed by steps of 0.5 mm;
- In all planes, brace members in a single level should have equal thickness;
- In all planes, leg members in a single level should have equal thickness.

These starting points are formulated to end up with a feasible and symmetric structure without an abundance of different member thicknesses.

5.1.1. Additional starting points case 1

The optimised welded structure of case 1 is the only jacket structure containing joint can sections. Additional starting points are related to this:

- In all planes, brace cans of a single X-joint should have equal thickness;
- In all planes, leg cans of a single K-joint should have equal thickness.

These starting points are to prevent additional welding in the joint centre, which would induce additional stress concentration.

5.2. Main results

The main research question of this thesis concerns the potential reduction of steel mass. The first subsection will elaborate on this. The second section will discuss the governing unity check per case and the third section elaborates on the benefit of high strength steel. Finally, the costs are discussed in the fourth section. The jacket design for all cases can be seen in Fig. 5.1. Quantitative results can be found in Fig. 5.2 and in detail in App. F.

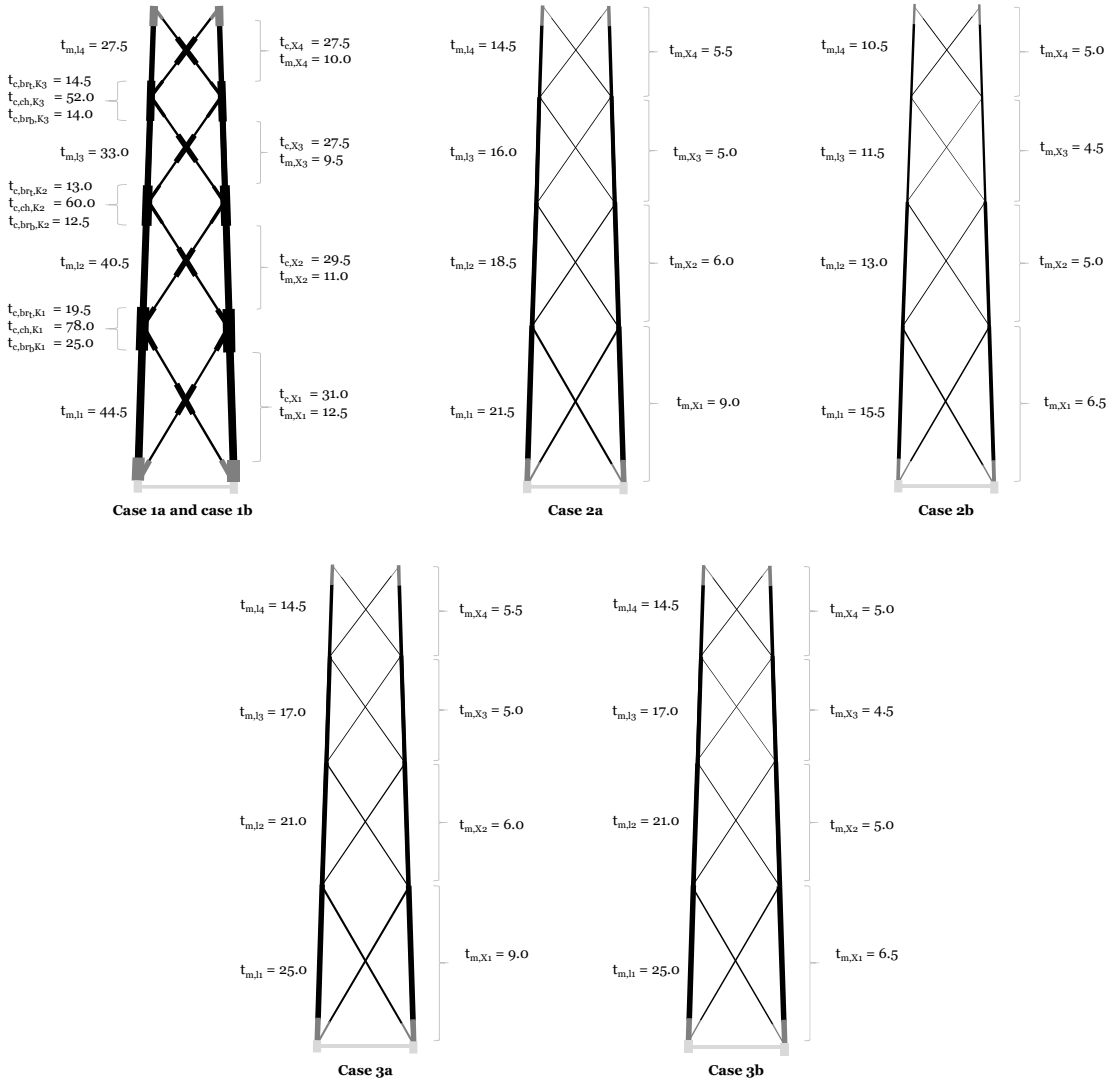

Figure 5.1: Schematic layout of jacket structures for all cases. Line thickness indicates element thickness. Dark grey Y-joints and light grey mudbrace are not optimised. Light grey elements are not taken into account in mass calculation. Subscript l indicates leg, X braces, m member, c can, br_t top brace, br_b bottom brace and ch chord. The number indicates the level.

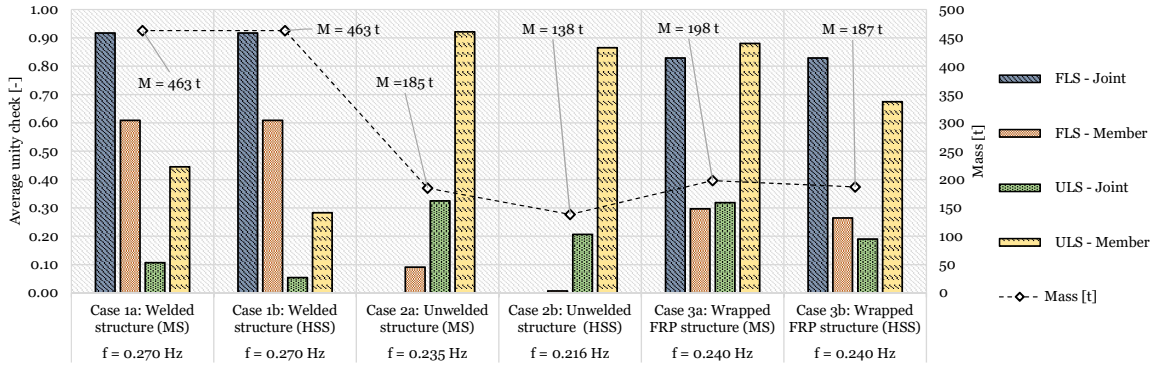

Figure 5.2: Graph showing steel weight and average unity checks for jacket structure case 1 (welded), case 2 (unwelded) and case 3 (wrapped FRP joint). Results are given for mild S355 steel (MS) and high strength S690 steel (HSS). The left vertical axis indicates the average value of the unity check and the right vertical axis shows the steel mass in tons. The first eigenfrequency f of the structure is shown to check the likelihood of resonance (see Fig. 4.2). Eigenfrequency of case 1 is obtained without can sections.

5.2.1. Steel weight reduction

The steel jacket weight is calculated with the exclusion of the light grey elements (elements below Y-joints) of Fig. 5.1. No simulation data is collected for those elements, and consequently, no unity check and updated element thickness could be calculated. As they are relatively thick in relation to the optimised elements, including them in the mass calculation would reduce the percentage weight reduction. As an educated guess could be made for the dark grey Y-joint cans, these are included. For case 1, these cans have the same thickness as cans of the most nearby K- or X-joint. For case 2 and 3, these elements have the same thickness as the member. The mass calculation procedure is validated with the UpWind project, and results agree to 99%.

As can be seen in Tab. 5.1, the potential weight reduction with respect to the welded structure is large; maximum 60% if mild steel is used and 70% if high strength steel is used. Note, no weight reduction is possible for the high strength steel welded structure (case 1b), as fatigue is governing and resistance of welds is independent of yield strength of base material. The weight difference between case 2 and case 3 is small for mild steel but considerable for high strength steel. This is due to the welds which govern leg thickness.

Table 5.1: Weight reduction of jacket support structure with respect to mild steel welded structure (case 1a). Black and dark grey element of Fig. 5.1 are taken into account.

Weight reduction with respect to case 1a - Welded structure (MS) [%]	
Case 1b - Welded structure (HSS)	NONE
Case 2a - Unwelded structure (MS)	60
Case 2b - Unwelded structure (HSS)	70
Case 3a - Wrapped FRP structure (MS)	57
Case 3b - Wrapped FRP structure (HSS)	60

Increasing the slenderness of elements reduces the eigenfrequency of the structure. To prevent amplification of displacement and stress, the eigenfrequencies should be separated from the forcing frequencies (wind and waves), and should be outside of the operating frequency ranges 1P and 3P (see Fig. 4.2). The optimised steel welded reference structure has a lowest eigenfrequency well away from resonance; $f_{\text{case1}} = 0.270$ Hz (see Fig. 5.2). The eigenfrequency $f_{\text{case2a}} = 0.235$ Hz is still outside the 1P domain, while $f_{\text{case2b}} = 0.216$ Hz is within the 10% safety margin. The eigenfrequency $f_{\text{case3}} = 0.240$ Hz of case 3a and case 3b is outside the operating frequencies. The reduced brace thickness of case 3b has a negligible influence on the lowest eigenfrequency.

The wrapping thickness for case 3 is given in Tab. 5.2. The values are based on preliminary tests of small scale specimens. They give a first indication of the minimum thickness of wrapping needed to have sufficient joint fatigue life. According to experiments, the values are based on brace fatigue only. The length of the wrapping for leg elements is 600 mm ($0.5D_{\text{leg}}$) and for braces 1200 mm ($1.5D_{\text{brace}}$).

Table 5.2: Minimum thickness of fibre reinforced wrapping to obtain sufficient fatigue resistance for K- and X-joints.

	FRP wrapping thickness [mm]	
	Bottom member	Top member
K1	25.5	22.5
K2	18.0	18.0
K3	19.5	19.5

	FRP wrapping thickness [mm]
X1	25.5
X2	22.5
X3	19.5
X4	22.5

5.2.2. Governing unity check

The benefit of wrapped FRP joints is related to the improved fatigue resistance of these joints. For this reason, it is relevant to check if the current state-of-the-art welded jacket structure (case 1) is indeed governed by fatigue. Furthermore, it is examined if the governing unity check changes for the unwelded and wrapped FRP jointed structure. Results are visible in the bar chart of Fig. 5.2.

Welded structure

This case is governed by both fatigue of joints and fatigue of elements. Due to the presence of joint cans, unity check of joints and unity check of elements can be optimised individually. However, while the average fatigue unity check for joints is close to unity, the average fatigue unity check for elements is for various reasons around 0.6 (see Fig. 5.2). First, the element spans from can to can, while a single side governs the thickness. The average unity check drops when the unity check of the non-governing side is low. Besides, the unity check for fatigue is highly dependent on thickness, and a reduction of 0.5 mm is relatively larger for thin elements than for thick joint cans. For example, the unity check for $t_{m,X2} = 11$ mm is just 0.76, while a thickness reduction of 0.5 mm yields a unity check exceeding 1 (see App. F and Fig. 5.1).

Unwelded structure

This case is governed by global buckling of elements. Due to the assumption of non-governing joint fatigue, the unity check of joints is not shown in Fig. 5.2. The average unity check for global buckling (ULS - Member) is close to unity for both cases 2a and 2b. For case 2b, it is slightly lower, due to the mentioned argument concerning the increased effect of thickness reduction for thin elements.

Wrapped FRP structure

This case is governed by both member buckling (braces), member fatigue (legs), and joint fatigue (joints). The presence of circumferential (C1) welds in legs, makes fatigue governing for the three lowest leg levels. As braces are not welded, dimensions are governed by global buckling. The wrapping thickness is governing for joint fatigue and can be tailored to obtain sufficient fatigue resistance (see Tab. 5.2).

5.2.3. Benefit of high strength steel

High strength steel has equal stiffness, but increased strength compared to mild steel. Consequently, the ULS joint resistance and the buckling unity check improve. For welded structures, it is seldom used as the strength of the base material does not influence the fatigue life of welds. The fatigue resistance of the unwelded base material does improve for high strength steel.

Welded structure

As case 1a and case 1b have equal member thickness, the influence of high strength steel on unity checks can be seen. Steel mass can not be reduced as can and member thickness is governed by fatigue, and the S-N curve for welds does not depend on the yield strength of base material (see Fig. 5.2). The unity checks for extreme resistance of joints (chord face failure and punching shear failure) does reduce by almost 50 per cent, and the global buckling unity check reduces by more than 35% (see Tab. 5.3). The latter percentage is smaller, as yield strength influences resistance more than stability.

Table 5.3: Benefit of high strength steel with respect to mild steel for the optimised welded structure (case 1a versus case 1b). Dimensions for both cases are the same.

Unity check reduction case 1b with respect to case 1a: Benefit of HSS [%]	
FLS - Joint	NONE
FLS - Member	NONE
ULS - Joint	49
ULS - Member	36

Unwelded structure

For unwelded base material, the fatigue unity check of members is influenced (see Fig. 5.2). High strength steel has a larger fatigue resistance compared to mild steel. As buckling of elements is governing for case 2, this increased fatigue resistance is of minor importance and does not influence design.

Mass reduction due to high strength steel can be seen when comparing case 2a with case 2b (see Fig. 5.2). The total weight for case 2 can be reduced by 25% if high strength steel is used.

Wrapped FRP structure

The fatigue unity check of brace elements is influenced by high strength steel, but the fatigue unity check of welded leg members not. Besides, the tension yielding and the buckling resistance of members is influenced positively.

Mass reduction by using high strength steel for case 3 is minimal, as only the thickness of unwelded braces could be reduced.

5.2.4. Cost reduction

In the end, costs are a major factor for the viability of wrapped FRP joints in practice. Therefore, steel, cutting and welding costs for the optimised welded (case 1) and the wrapped FRP (case 3) structure are calculated. The difference indicates the budget to produce wrapped FRP joints. If joints could be produced for less, the FRP jacket production costs are lower than the welded jacket production costs.

The costs are calculated in collaboration with Jan Krielaart of Hillebrand (ASK Romein). The procedure takes into account the actual weld volume for tubular-tubular connections under an angle. It includes costs of steel material, welding and cutting. Welding costs include welding material, labour and non-destructive testing. Cutting costs include tapering, bevelling and shaping. The calculation excludes costs of welds around and below bottom Y-joint and steel elements below bottom Y-joint (e.g. mud brace). It also excludes welds around and above top Y-joint and steel elements above top Y-joint (e.g. transition piece) (see Fig. 5.2). Finally, it excludes handling, painting and other costs similar for the welded and wrapped FRP jointed structures. As a result, the cost can be used for comparison only and do not indicate the total jacket structure costs.

For the welded structure, welding and cutting costs of 12 multiplanar K-joints, 16 X-joints and 136 circumferential can-member welds are included. For the wrapped FRP structure, welding costs for 16 circumferential welds in legs are included, as well as cutting costs for both leg and brace elements.

The results from the cost calculation can be seen in Tab. 5.4. For the welded structure, welding and cutting have a share of around 25% of the total costs. The remainder of the costs is tubular steel material. For case 3a, excluding the costs of wrapping, the total costs are 65% lower than for case 1. Like mass, the steel costs are reduced by 57%. The welding and cutting costs are reduced by more than 85%. As the total costs are reduced by €726 088, this is the budget for wrapped FRP joints. Per joint (12 multiplanar K-joints and 16 X-joints), the maximum allowable wrapping costs are $\frac{€\ 726\,088}{28}$ = € 25 932.

From the difference between case 3a and case 3b, it can be seen that there is no economic advantage from using high strength steel. The cost of S690 steel is more than 40% higher than of S355, while the steel weight reduction is less than 6%.

Table 5.4: Costs of welded jacket structure (case 1) and FRP wrapped jacket structures (case 3a and 3b). The costs include steel, welding and cutting, but exclude FRP wrapping costs. Steel above top Y-joint and below bottom Y-joint is excluded, just like corresponding welds. For case 1, it includes 12 multiplanar K-joints, 16 X-joints and 136 circumferential can-member joints. For case 2, it includes 16 circumferential leg welds and cutting cost for both leg and brace elements.

	Cost for steel welded and wrapped FRP jacket		
	Case 1	Case 3a	Case 3b
Input			
Steel mass [t]	462.8	198.2	186.8
Steel costs [€/t]	1 750	1 750	2 500
Output			
Welding and cutting costs	€ 302 467	€ 39 429	€ 39 453
Steel costs	€ 809 900	€ 346 850	€ 467 000
Total costs (wrapping excluded)	**€ 1 112 367**	**€ 386 279**	**€ 506 453**

5.3. Additional results

Besides the answers to the research questions, it is relevant and interesting to dive into the results and draw additional conclusions. First, additional results regarding the FLS analysis are given for case 1, afterwards for the ULS analysis for case 2a. A comparison with the results of the UpWind jacket structure is made and can be seen in App. G.

5.3.1. Fatigue limit state

Detailed fatigue results are given for the optimised welded structure (case 1), as fatigue is governing dimensions for this case.

Influence of wind and waves seeds

As mentioned in the Sec. 4.1.2, minimum simulation time should be 60 minutes by either a single 60-minute simulation or six 10-minute simulations. The latter is done in this research, and different seeds should be chosen for different 10-minute simulations. Both the wind turbulence time series and the irregular wave time series depend on the seed number. If the number is unchanged, all six simulations give the same results. Changing the seed numbers generates *randomness* for the wind and wave load time series.

The influence of different wave and wind seeds to damage is large. For a single simulation, the damage for different wind/wave seeds can vary by a factor of over 2.5. Therefore, the IEC requirement for modelling different seeds for short simulations is substantiated [33].

Most harmful wind-wave scenario

App. G.1 gives the detailed quantitative results belonging to this section. Fatigue damage is assessed by summing together damage due to different wind-wave scenarios (see Tab 4.7). The occurrence percentage is taken into account when accumulating damage. During the majority of lifetime, the wind is relatively mild and the see calm (80% of time $V_{\text{wind}} < 15$ m/s and $H_s < 2.05$ m (see Fig. C.1 and Tab. 4.7)). These load conditions contribute to total damage to a minor extent (see Tab. 5.5). For legs, the average contribution is less than 15% and for braces, less than 25%. The scenario covering 15 m/s $< V_{\text{wind}} <$ 19 m/s, does significantly contribute. However, although the scenario for $V_{\text{wind}} = 22$ m/s only occurs 6% of lifetime, for all elements it is the most harmful scenario and damage is about 50% of total damage (see Tab. 5.5). The damage contribution of $V_{\text{wind}} = 28$ m/s is generally negligible. This is because the wind turbine is idling for $V_{\text{wind}} > 25$ m/s, meaning the blades are rotated out of the wind.

Governing joints, members and planes

App. G.1 gives detailed quantitative results belonging to this section. To limit the simulation time and to reduce the amount of data, time series of normal force and moments are recorded only for a part of the elements. All elements and joints in the front plane are analysed. Additionally, three K-joints (including the six corresponding brace members) in the side plane (facing West) are analysed. Below, interesting conclusions regarding governing joint can and member thickness are given:

Table 5.5: Contribution of five wind-wave scenarios to joint can (c) and member (m) fatigue damage unity check. Note, for brace members, both K- and X-member are mentioned. For those members, fatigue is evaluated at both K- and X-side of the element.

	Contribution of wind speed window to unity check [%]				
	1 - 9 m/s	9 - 15 m/s	15 - 19 m/s	19 - 25 m/s	25 - 31 m/s
Legs					
Level 1 (c + m)	8	7	38	46	1
Level 2 (c + m)	6	8	39	46	1
Level 3 (c + m)	4	10	39	47	1
Level 4 (c + m)	3	11	38	47	1
Average	**5**%	**9**%	**38**%	**46**%	**1**%
Braces					
Level 1 K (c + m)	10	5	33	50	2
Level 1 X (c + m)	26	1	19	51	2
Level 2 K (c + m)	12	7	33	47	1
Level 2 X (c + m)	36	2	20	40	2
Level 3 K (c + m)	11	8	34	46	1
Level 3 X (c + m)	28	4	22	44	2
Level 4 K (c + m)	8	9	33	49	1
Level 4 X (c + m)	12	8	29	50	1
Average	**18**%	**6**%	**28**%	**47**%	**2**%

- Can thickness X-joints:

  For the X-braces of the jacket structure, it is undefined which members are continuous and which members are discontinuous. Depending on the level of the X-joint, either configuration (see Fig. D.2) can be governing. In conclusion, there is no single preferred division of continuous and discontinuous members.

- Member thickness braces:

  For all braces, the thickness of members between X- and K-joints is governed by fatigue at the X-joint side.

- Can thickness K-joints:

  Depending on the level of the K-joint, either front plane, or side plane is governing brace can dimensions. Therefore, both planes should be analysed to obtain proper dimensioning of K-joint brace cans.

  Depending on the level of the leg, either the top or bottom element is governing leg can thickness.

- Member thickness legs:

  The leg thickness between K-joints is governed by the lower end.

Relative influence of normal force and moments

App. G.2 gives detailed quantitative results belonging to this section. Fatigue damage is assessed by a stress-based S-N approach. S-N curves are generally obtained from axial stress tests. For welded joints, these curves are widespread, accepted and verified by experiments. For the innovative wrapped FRP joints, it is unclear if the S-N curve, deducted from axial stress tests, is applicable. Possibly, the joint is more susceptible to stress generated by moments than stress generated by normal force. For this reason, the relative contribution of normal force N, in-plane bending moment M_{ip} and out-of-plane bending moment M_{op} is investigated. Main conclusions drawn are given below:

- General:

  Normal forces lead to stress at all hot spots, in-plane bending moments lead to stress at crown points only, while out-of-plane bending moments lead to stress at saddle points only. This makes sense as saddle and crown locations are separated by 90 degrees (see Fig. D.1).

Although the damage contribution of M_{ip} only and M_{op} only is (very) small compared to N, its cumulative contribution to respectively $N + M_{ip}$ and $N + M_{op}$ is considerable (see Tab. 5.6).

The values in the N only column and the reason why the combined damage adds to 100% (last column) of Tab. 5.6, are not easy to understand and interpret. This is because that fatigue damage is accumulated over 72 000 time steps, the loading of the complete joint influences the damage in a single element, and the normal force and moments are coupled by load-dependent stress concentration factors.

The values in the moment-only column are more in line with expectations. Larger damage due to moments for cans than members, larger damage due to moments for braces than legs, and larger damage due to in-plane moments (bending of jacket) than due to out-of-plane moments (hydrodynamic forces).

The influence of waves and currents can be seen when comparing braces below (X2), at (X3) and above (X4) sea level. The damage contribution of out-of-plane moments M_{op} is considerably larger at X3 level (see App. G.2).

Table 5.6: Contribution of normal force N, in-plane bending moment M_{ip} and out-of-plane bending moment M_{op} to fatigue damage unity check. Contribution of moments only is low, but contribution to combined unity check is large.

	Contribution to unity check [%]		
	N only	M_{ip} only	$N + M_{ip}$
Legs			
Members	76	0.0	100
Cans	31	0.4	100
Average	**54**%	**0**%	**100**%
Braces			
Members K	68	0.0	100
Members X	28	15.7	100
Cans K	27	5.5	100
Cans X	64	23.9	100
Average	**47**%	**11**%	**100**%

	Contribution to unity check [%]		
	N only	M_{op} only	$N + M_{op}$
Legs			
Members	61	0.0	100
Cans	100	1.3	100
Average	**81**%	**1**%	**100**%
Braces			
Members K	66	0.0	100
Members X	49	0.8	100
Cans K	96	0.5	100
Cans X	34	1.3	100
Average	**61**%	**1**%	**100**%

- Can thickness X-Joints:

  For all X-joints, the final can dimensions are governed by a combination of normal force N and out-of-plane bending moments M_{op}. In other words, the saddle locations are governing over crown locations.

- Member thickness braces:

  For all X-joints, the final member dimensions are governed by a combination of normal force N and in-plane bending moments M_{ip}.

- Can thickness K-Joints:

  For all K-joints, the final can dimensions are governed by a combination of normal force N and in-plane bending moments M_{ip}.

- Member thickness legs:

  For K-joint leg members, the final member dimensions are governed by a combination of normal force N and out-of-plane bending moments M_{op}.

5.3.2. Ultimate limit state

Detailed global buckling results are given for the unwelded jacket structure (case 2a), as global buckling is governing dimensions for this case.

Most harmful wind-wave scenario

App. G.3 gives detailed quantitative results belonging to this section. Three scenarios with the same wind and wave conditions, but with different directionalities are simulated (see Tab. 4.9 and Fig. 4.4). As a recap, scenario 1 has wind and waves co-directional and perpendicular to jacket structure, scenario 2 co-directional and diagonal to jacket structure and scenario 3 wind diagonal to jacket structure and waves 150 degrees misaligned.

The main conclusions are summarised in Tab. 5.7 and are commented on below:

- Scenario 1 is governing for 75% of leg elements and 50% of brace elements. The remaining legs and braces are governed by scenario 2.
- The average utilisation of all elements differs less than 10% for scenarios 1 and 2. However, for level 2 legs, level 1 braces and level 4 braces, the difference is significant.
- Although scenario 3 is most harmful to the lowest two front plane legs, it is not governing (see App. G.3). The thickness of these elements is governed by utilisation in the back plane for scenario 1. Therefore, scenario 3 does not influence jacket design.

Table 5.7: Difference in global buckling unity check for scenario 1 (waves and wind from 0 degrees) and scenario 2 (waves and wind from 45 degreees) (see Fig. 4.4). Positive values indicate scenario 1 is governing, negative values indicate scenario 2 is governing.

	Global buckling unity check difference between scenario 1 and 2 [%]
Legs	
Level 1	3
Level 2	15
Level 3	5
Level 4	-2
Average	**5**%
Braces	
Level 1	25
Level 2	-3
Level 3	-6
Level 4	18
Average	**9**%

Governing unity check and plane

App. F, G.3 and G.4 give the detailed quantitative results belonging to this section. The resistance against one in 50-year wind and waves is checked by evaluating both tension yielding, local buckling and global buckling. Similar to fatigue, time series of normal force and moment are recorded only for a part of the elements. Member buckling and tension yielding calculations are performed for 44 elements in back and side plane. Below, the main interesting conclusions are given:

- For all members, global buckling is governing member thickness;
- For all members, tension yielding has the lowest utilisation;
- For all brace members, the thickness is governed by the side plane;
- For all leg members except the top member, the thickness is governed by legs in the back plane.

Relative influence of normal force and moments

App. G.4 gives detailed quantitative results belonging to this section. For the same reason as mentioned in the corresponding section for fatigue, knowing the ratio between normal force and bending moments is relevant. The main conclusions are summarised in Tab. 5.8 and are commented on below:

- General:

  The global buckling unity check is a combination of normal force N, in-plane bending moment M_{ip} and out-of-plane bending moment M_{op}. On the contrary to fatigue, M_{ip} and M_{op} contribute to the same unity check.

  For both braces and legs, the contribution of normal force N reduces for higher levels.

- Member thickness braces:

  For all but the lowest level, in-plane bending moment M_{ip} has the largest contribution to damage. For the lowest level, normal force N has the largest contribution.

  Just like for fatigue of brace members, the presence and influence of waves can be seen for the braces around sea level (X3). The contribution of M_{op} is strongly increased, but still smaller than the contribution of M_{ip}.

  For all levels of braces, the contribution of $N + M_{ip}$ is larger than $N + M_{op}$.

- Member thickness legs:

  For all leg members, the contribution of normal force N is significantly larger than the contribution of bending moments M_{ip} and M_{op}.

  For leg members, the value of $N + M_{ip}$ is comparable to $N + M_{op}$. For all except the third level, the contribution of $N + M_{ip}$ is largest.

Table 5.8: Contribution of normal force N, in-plane bending moment M_{ip} and out-of-plane bending moment M_{op} to global buckling unity check. The global buckling unity check is a combination of both N, M_{ip}, M_{op}. The shown percentages in the first three columns are due to respectively N, M_{ip} and M_{op} only. Note, percentages do add to over 100% as contributions do not add linearly.

	Contribution to unity check [%]			
	N only	M_{ip} only	M_{op} only	$N + M_{ip} + M_{op}$
Legs				
Level 1	89	19	19	100
Level 2	91	9	10	100
Level 3	87	7	7	100
Level 4	81	13	10	100
Average	**87**%	**12**%	**12**	**100**%
Braces				
Level 1	60	43	15	100
Level 2	57	63	21	100
Level 3	44	75	35	100
Level 4	42	59	10	100
Average	**51**%	**60**%	**20**%	**100**%

Contribution of hydrodynamic force

App. G.5 gives detailed quantitative results belonging to this section. All results discussed so far, relate to structures exposed to both wind, waves and current. Jackets are said to be relatively transparent to waves and current [17]. This statement is checked for global buckling of both braces and legs. A comparison is made for perpendicular wind, and diagonal wind only. Results including wind, waves and current differ from main results, as only a single seed (10-minutes) is checked. The main conclusions are summarised in Tab. 5.9 and are commented on below:

- For 75% of leg elements, the wind only scenario is more harmful than the wind, waves and current scenario. With a maximum deviation of six per cent, the difference is small.
- Waves and current have more influence on braces than on legs.
- For the lowest three brace levels, the difference between the wind only scenario, and wind, waves and current scenario, is largest.

The results show that current and waves have a small influence on legs, but considerable influence on some of the brace levels. The results also indicate higher damage due to the wind only scenario, compared to the wind, waves and current scenario. This result is unexpected and questionable. Simulations are performed for a single wave and wind seed only. More simulations should be performed to give a more substantiated statement about the influence of waves and current.

Table 5.9: Contribution of hydrodynamic force for wind perpendicular (0 degrees) and wind diagonal (45 degrees) to the global buckling unity check. Positive values indicate waves and current add to unity check. Negative values indicate that wind only is more harmful than wind, waves and current. Values are based on a single 10-minute simulation with a single wind and wave seed.

	Contribution of hydrodynamic forces [%]	
	0 degrees direction	45 degrees direction
Legs		
Level 1	9	13
Level 2	-3	-3
Level 3	-6	-2
Level 4	-4	-1
Average	**-1**%	**2**%
Braces		
Level 1	71	39
Level 2	14	43
Level 3	15	7
Level 4	-4	0
Average	**24**%	**22**%

6

Discussion

The previous chapter discussed the potential benefit of replacing welds by innovative, wrapped FRP counterparts. This chapter lists the assumptions and modelling choices made and comments on their expected influence. Besides, it gives insight into the large steel weight reduction by investigating calculation and modelling sensitivities. The chapter ends with a short conclusion.

6.1. Assumptions, simplifications and modelling choices

Although the procedure and strategy to obtain the results are well-considered, the results should be handled with care. The model and calculations are based on assumptions and simplifications. Those influence the final results, and it is important to be aware of them. The main assumptions and simplifications are collected below. A clarification, including expected implication on results, is included in italic. From large to small, influence is indicates as *vital, large, significant, limited* or *negligible.*

Simulation model - Structural

- Simulations are performed for the OC4 jacket structure, while FLS and ULS calculations are performed for jacket structures with altered member thickness.
  The influence is significant and is discussed in Sec. 6.2.3 and Sec. 6.2.4. In these sections, the influence is quantified and explained.

- Local flexibility of joints is not taken into account in the simulation model. All joints are modelled as rigidly connected.
  The influence is expected to be small, as a sensitivity study performed in the UpWind project indicated minor influence [17]. Besides, depending on the wrapping thickness and length, FRP wrapped X-joints have a higher stiffness compared to welded X-joints (see Fig. 1.19). Higher stiffness of joints means better agreement with fixed joints in the simulation model.

- No secondary steel items (boat landing bumpers, anodes, J-tubes) are modelled.
  The influence is expected to be limited, but secondary steel items do influence dynamics, increase mass and increase hydrodynamic loading.

Simulation model - Load

- For the FLS analysis, wind and waves are assumed to originate from the North (perpendicular to jacket structure), to be co-directional and to come from the same direction for every load combination (see Tab. 4.6).
  The influence is expected to be significant as this scenario is not expected to be accurate or conservative for all hot spots. Unlike the extreme load scenario, the fatigue load should mimic the realistic load during lifetime as well as possible. For some hot spots, the modelled scenario will give conservative results as damage accumulates at the same location for all modelled scenarios. However, for other elements, non-perpendicular (e.g. 45 degrees) and misaligned wind and waves could govern fatigue damage.

- For the FLS analysis, the modelled amount of wind-wave scenarios is restricted.
  The influence is expected to be limited, as the modelled scenarios are chosen with care and are spread over the domain. In four of five scenarios, data from the middle of the domain is used (see Tab. 4.7). For the 9 - 15 m/s wind speed window, data for the wind speed with the highest trust force is chosen (V_{wind} = 11.4 m/s, see Fig. C.2). However, the accuracy of the results will improve if more scenarios are simulated.

- For the ULS analysis, a reduced number of wind-wave directional combinations is modelled.
  The influence is expected to be limited, as the three scenarios chosen are chosen with care. Different than the fatigue load scenario, the extreme load should mimic a potential storm scenario with one in 50-years wind and waves. Three scenarios are modelled (see Fig. 4.4). As expected, the perpendicular and diagonal co-directional wind-waves scenarios turned out to be governing. However, other combinations may be more harmful to some elements. Accuracy of and trust in results will increase if simulations are performed for more wind directions and wind-wave misalignment angles.

Simulation model - Data locations

- For the FLS analysis, time series of force and moments are obtained for the front plane and for K-joint elements in a single adjacent side plane, while resulting dimensions are used for all planes.
  The influence is expected to be significant, as for two of three K-joints, the side plane governs brace can section thickness. Additionally, the member thickness of braces, between K-joints and X-joints, is in most cases governed by fatigue at the X-joint side. However, no joint fatigue nor member fatigue of X-joints in the side plane is evaluated. It is expected that X-joint member and can thickness is governed by the side plane.

- For the ULS analysis, no time series of force and moment are obtained from the front plane, while resulting dimensions are used for this plane.
  The influence is expected to be limited, as elements in three of four planes are checked. The calculated unity check is expected to be representative for the remaining plane.

Calculations

- The lowest three X-joints are outside the validity range of the welded joint fatigue damage calculation [21]. For these braces, the value of $\alpha = 2L/D$ - in which L is the element length and D the element diameter - is above the upper limit of 40. From bottom to top X-brace, the value of α is respectively 54.2, 46.8, 40.5, and 35.
  The influence is expected to be limited, as it does influence the can thickness of three X-joints, but has a minimal influence on brace member thickness and no influence on the can and member thickness of legs. An increase of α gives a higher stress concentration factor, so the calculated can thickness of X-joints is expected to be insufficient.

- For ULS failure of welded tubular joints, the shear force is neglected.
  The influence is expected to be negligible, as shear forces turn out to be very low. The effect is investigated in a case study performed before this project.

- To determine the buckling unity check, a realistic estimate of the buckling length should be made. Joint cans are ignored when estimating buckling length and Eurocode procedure is used.
  The influence is expected to be significant, as doubling the buckling length gives an average increase of the global buckling unity check of 35%. The buckling length of legs and the in-plane buckling length of braces is chosen as the length between nodes, multiplied by 0.9 (according to EC1993-1-1 Annex BB.1.3 (1)B [51]). In reality, the buckling length (without correction factor) might be closer to the distance between the welds L_2, instead of the distance between the nodes $L_{\text{buc,EC}}$ (see Fig. 6.1). This especially influences the buckling length for leg members with gap K-joints. Research performed on this topic shows the Eurocode estimate is generally conservative [7]. When joint cans or wrapping is introduced, making an educated approximation of the buckling length is even trickier and the used value even more conservative.

- For local buckling, only meridional stress is checked and circumferential and shear stress are neglected.
  The influence of shear stress is expected to be negligible, as shear stress is low. The influence of circumferential stress is significant and is investigated in Sec. 6.2.5. Circumferential stress originates from external hydrostatic pressure and including it leads to increased minimum element thickness of braces. From bottom to top, brace thickness should be increased by respectively 2.5, 3 and 1.5 mm for the mild steel unwelded and wrapped FRP structure.

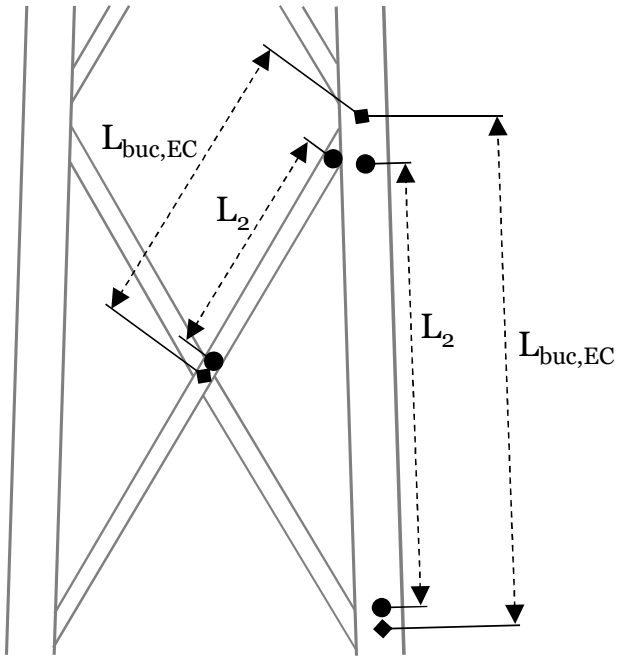

Figure 6.1: In plane buckling lengths to determine buckling utilisation in jacket structure. Length L_2 shows the distance between welds. In this report, according to EC1993-1-1 Annex BB, $L_{\text{buc}} = 0.9 \cdot L_{\text{buc,EC}}$ is used. However, this could be conservative, especially if joint cans or wrapping are introduced.

- For global buckling, secondary bending moments are not taken into account.
  The influence is expected to be limited, as the element deflection is likely to be small. Apart from wave and current loading, no forces are exerted along with the element.

- Mistakes or typos in data processing and calculation procedure can not be ruled out, although great care is taken.
  The influence could be large but is expected to be negligible. Data processing is done step by step, and intermediate results of calculations are checked. Moreover, calculation results are compared with the UpWind reference project, and results show a great resemblance (see App. A).

Wrapped FRP joints

- Wrapped FRP joints are assumed to be able to withstand ULS and FLS forces and moments. Even if immersed in seawater for 20 years.
  This assumption is vital for successful application of the wrapped FRP structure but does not influence the results of the unwelded structure. The joints should be able to cope with large compression forces, tension forces and bending moments. They should still function after long-time exposure to the harmful sea environment. As mentioned in Ch. 1, degradation is foreseeable, but can only be quantified by experiments.

- Wrapping thickness is based on a limited amount of experiments.
  The influence is expected to be large for the calculated wrapping thickness and the costs of wrapped FRP joints. The main uncertainties are enumerated below:

  - *Thickness effect of FRP wrapping thickness;*
  - *Size effect of steel member diameter;*
  - *Geometry effect of joint type (K-joint, X-joint, member angle);*
  - *Presence of transition point, usually present in fatigue curves;*
  - *(Long term) degradation of wrapped FRP joint properties in seawater;*
  - *Effect of bending moments on fatigue resistance. The current experimental results are obtained for axial load only.*

- *Correctness of wrapping thickness procedure. Currently, wrapping thickness is based on brace stress only.*
- *Influence of multiplanarity of K-joints. For welded joints, multiplanarity can be excluded [21], but this might not be the case for wrapped joints.*

6.2. Explanation of results

In this section, further explanation is given to gain insight into the main results of this report. First, the influence of stress concentration and fatigue curves on fatigue damage is given. Next, the sensitivity and minimum element thickness to resist buckling are given. Subsequently, the influence of member thickness on simulation results is investigated. After that, the limited influence of element thickness on eigenfrequency is explained. Finally, the minimum element thickness to resist local buckling due to uneven hydrostatic pressure is elaborated on.

6.2.1. Sensitivity of fatigue to stress range and fatigue curve

The strong enhancement of fatigue performance enables large steel weight reduction. In this section, the influence of stress concentration caused by a thickness transition is investigated. The thickness transition is present between can sections and members. A can section is present in the region around the joint and has increased thickness. Besides, the influence of the fatigue curve is evaluated for both a welded connection, unwelded mild steel and unwelded high strength steel base material.

The individual influence is investigated for the top brace of the bottom K-joint (K1, see Fig. 4.1). The results are shown in Fig. 6.2 and Fig. 6.3 and are summarized in Tab. 6.1.

The absence of a 10 mm thickness transition, reduces the stress range by 1.83 and the damage by more than 20 (situation 1 to 2). The absence of a weld gives an additional damage reduction factor of more than 7 (situation 2 to 3). If high strength steel instead of mild steel is used, the damage is reduced by an additional factor of 162 (situation 3 to 4).

The following relation explains the damage reduction for a reduced stress range:

$$D = \frac{n}{N}$$
$$N = 10^{\log(a) - m\log(\Delta\sigma)}$$

With

$$\begin{aligned} D &= \text{Damage} \\ n &= \text{Number of cycles of stress range } \Delta\sigma \\ N &= \text{Number of cycles of stress range } \Delta\sigma \text{ to failure} \\ \log(a) &= \text{Intercept of log N axis} \\ m &= \text{Negative inverse slope of the S - N curve} \\ \Delta\sigma &= \text{Stress range} \end{aligned}$$

By rewriting these equations, the damage reduction can be found. As all stress ranges are below 10^2 MPa, only the right part of the curve (slope m_2) is of interest. Note, as the thickness of the member is unchanged, the thickness effect is not shown.

$$\frac{N_{\text{sit2}}}{N_{\text{sit1}}} = 10^{m_2 \log_{10}\left(\frac{\Delta\sigma_{\text{sit1}}}{\Delta\sigma_{\text{sit2}}}\right)} = 10^{5\log_{10}(1.83)} = 20.5$$
$$\frac{D_{\text{sit2}}}{D_{\text{sit1}}} = \frac{N_{\text{sit1}}}{N_{\text{sit2}}} = \frac{1}{20.5}$$

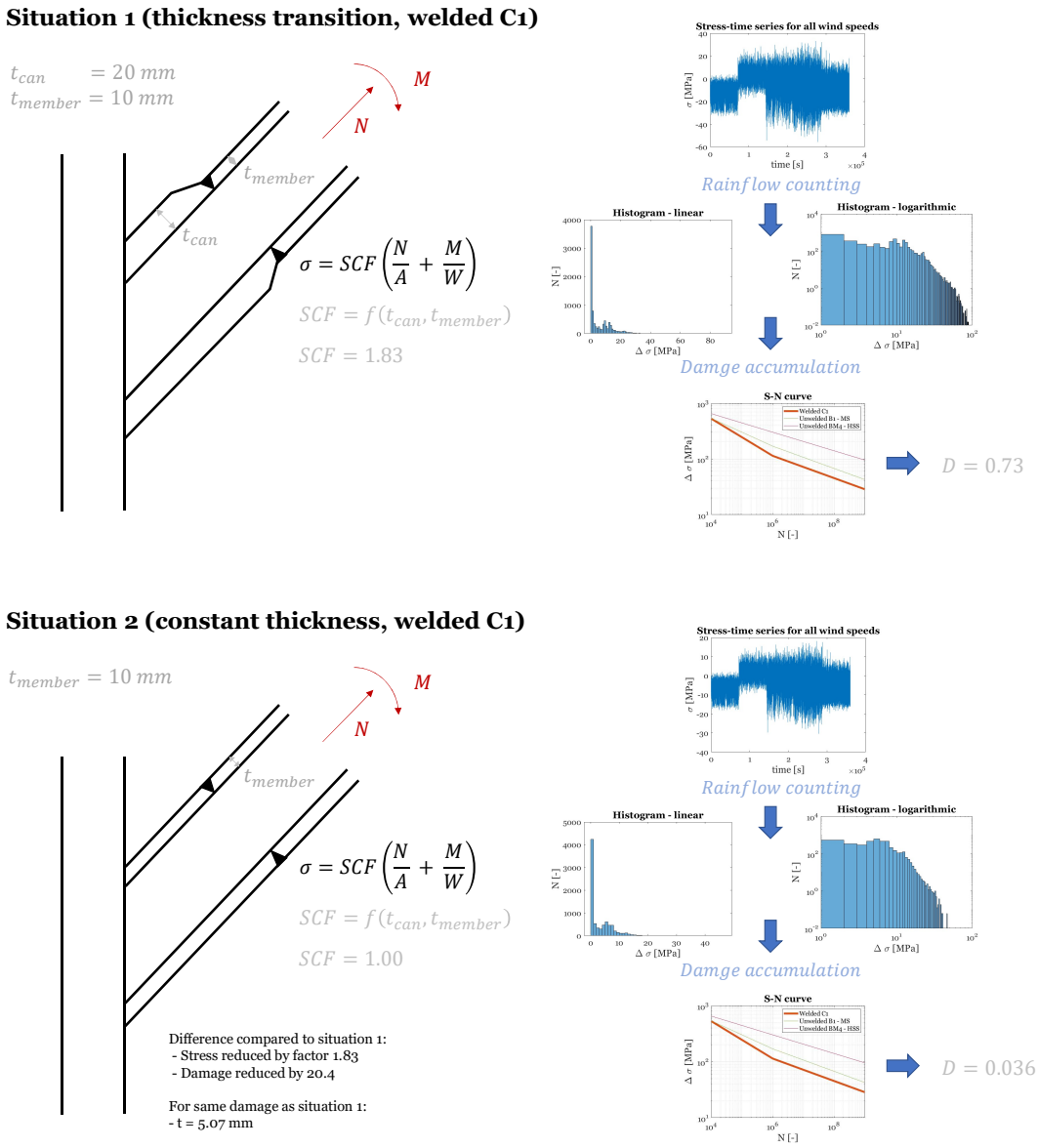

Figure 6.2: Fatigue damage calculation to show the influence of stress concentration due to a thickness transition. Although the stress is raised by a factor less than 2, the damage is raised by more than 20.

According to Fig. 6.2 and Fig. 6.3, the element thickness can be reduced by a factor of $\frac{10\text{ mm}}{1.83\text{ mm}} = 5.5$, if no thickness transition is present and high strength steel is used instead of mild steel. However, the thickness reduction between the welded (case 1) and unwelded structure (case 2b) is much less. This is mainly due to the limited buckling resistance of slender members. As a result, buckling instead of fatigue is governing dimensions for the unwelded structure. Next section compares the minimum element thickness for jackets checked for fatigue only, and buckling only.

Table 6.1: Reduction of fatigue damage and potential thickness reduction for situations shown in Fig. 6.2 and Fig. 6.3. MS = mild steel, HSS = high strength steel.

	Damage reduction [-]	Potential thickness reduction [-]
Sit 1 - Sit 2: Stress reduction of 1.83	20.4	1.97
Sit 2 - Sit 3: Unwelded MS vs. welded MS	7.4	1.40
Sit 3 - Sit 4: Unwelded HSS vs. unwelded MS	162.1	1.98

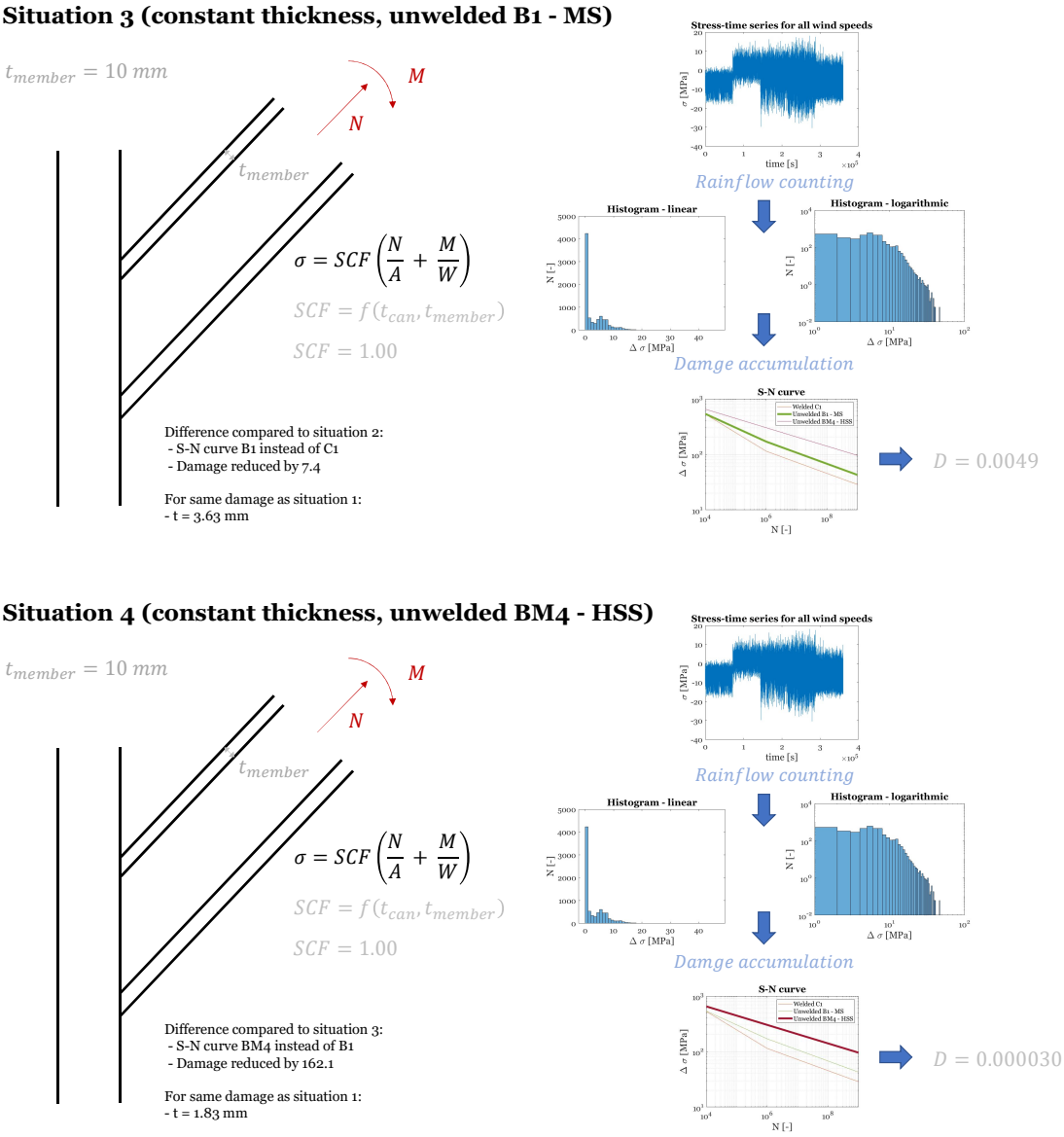

Figure 6.3: Fatigue damage calculation to show the influence of a weld compared to mild or high strength steel base material. The exclusion of a weld, reduces the damage by a factor of 7.4. The use of high strength steel instead of mild steel, reduces the damage by a factor of 162.1.

6.2.2. Sensitivity of global buckling to member thickness

Two mild steel unwelded jacket structures are designed to indicate when buckling governs element thickness. The left structure of Fig. 6.4 gives the minimum thickness if element fatigue is checked only, the right structure if buckling is checked only. The latter structure is equal to case 2a. It can be seen that for all members, the minimum thickness to resist buckling is larger than the minimum thickness to resist element fatigue. It illustrates that, for an unwelded structure, the governing unity check shifts from fatigue to buckling.

The sensitivity of global buckling to member thickness is investigated. In the equation, factors equal to unity are removed. Also, as a circular member has no strong and weak axis, no distinction between resistance around $y-$ and $z-$axis is made. The following equation describes the global buckling unity check [51]:

$$\mathrm{UC_{GB}} = \frac{N_{\mathrm{Ed}}}{\chi N_{\mathrm{Rk}}/\gamma_{M1}} + k_{\mathrm{yy}}\frac{M_{\mathrm{y,Ed}}}{M_{\mathrm{Rk}}/\gamma_{M1}} + k_{\mathrm{yz}}\frac{M_{\mathrm{z,Ed}}}{M_{\mathrm{Rk}}/\gamma_{M1}} \tag{6.1}$$

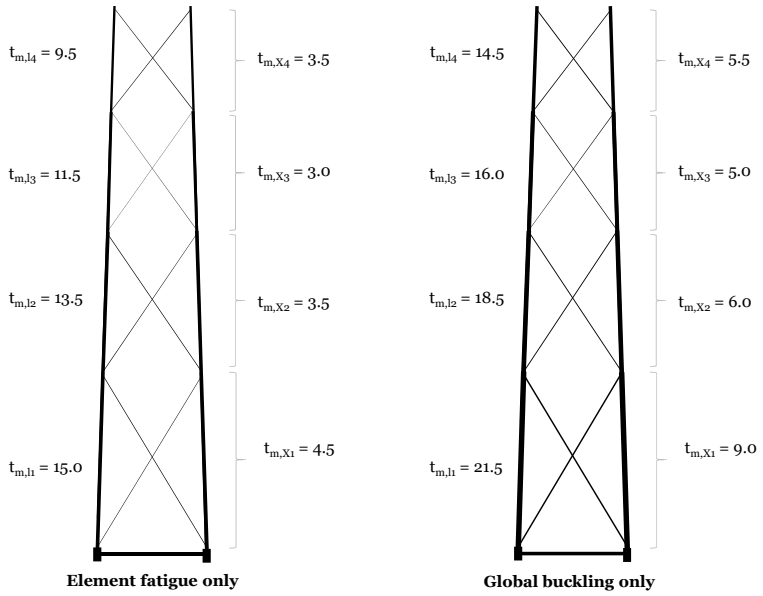

Figure 6.4: Comparison of minimum element thickness for mild strength steel jacket structure. Left structure indicates minimum thickness if element fatigue is calculated only. Right structure indicates thickness if global buckling is calculated only. Subscript l indicates legs, subscript X indicates braces. As can be seen, buckling is governing for all members in an unwelded structure.

With

$N_{\text{Ed}}, M_{\text{y,Ed}}$ and $M_{\text{z,Ed}}$ = Design values of the compression force and the maximum moments about the y- and z-axis along the member, respectively

χ = Reduction factor taking into account effective area for local buckling

N_{Rk} and M_{Rk} = Characteristic normal force and moment resistance of the critical cross section, respectively

γ_{M1} = Partial factor for resistance of members to instability

$k_{\text{yz}}, k_{\text{yy}}$ = Interaction factors

The sensitivity of global buckling to element thickness is graphically shown in Fig. 6.5. The element thickness of the right structure of Fig. 6.4 is taken as reference. The thickness of elements is altered and the average global buckling unity check for all members is shown. As buckling is a stability phenomenon, the sensitivity is larger for smaller element thickness.

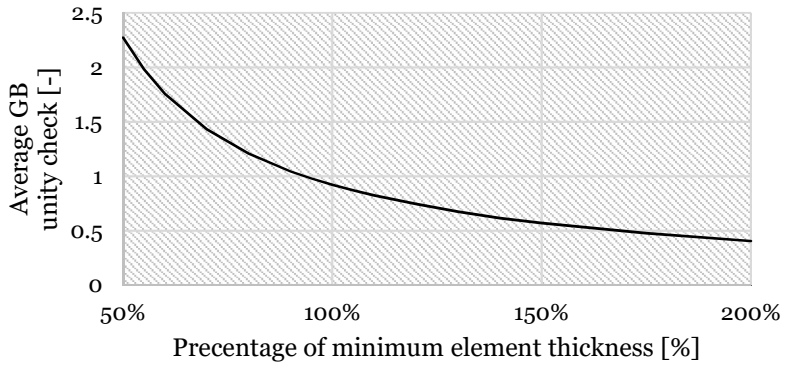

Figure 6.5: Relation between element thickness and average global buckling unity check. Element thickness at 100% corresponds to minimum element thickness to prevent buckling; the right structure in Fig. 6.4. Unity check of all elements is averaged, and thickness of all elements is changed by the same percentage. Unity check at 100% is unequal to unity, as multiple elements of a single type are checked, of which only one is governing. Besides, the thickness of Fig. 6.4 was optimised in steps of 0.5 mm.

6.2.3. Sensitivity of simulation results to member thickness

The manual thickness optimisation procedure applied is shown in Fig. 6.6. FLS and ULS simulations are performed for the reference (OC4) jacket structure, and time series of both axial forces and moments (in-plane and out-of-plane) are recorded for a selection of elements (step 1, 2 and 3). Next, the unity checks are calculated for both FLS and ULS (step 4). If the maximum unity checks are unequal to unity, the member thickness is altered and the unity check optimised (step 5 and 6).

To save simulation and calculation time, no simulations are performed for the optimised jacket. All force and moment time series originate from reference jacket simulations. An updated member thickness entails a new stiffness (distribution) and hence, different time series of forces and moments. As a result, the obtained unity checks are not exact. Accuracy of results can be increased if new simulations are performed and time series are updated. This is done in this section, and the influence is shown.

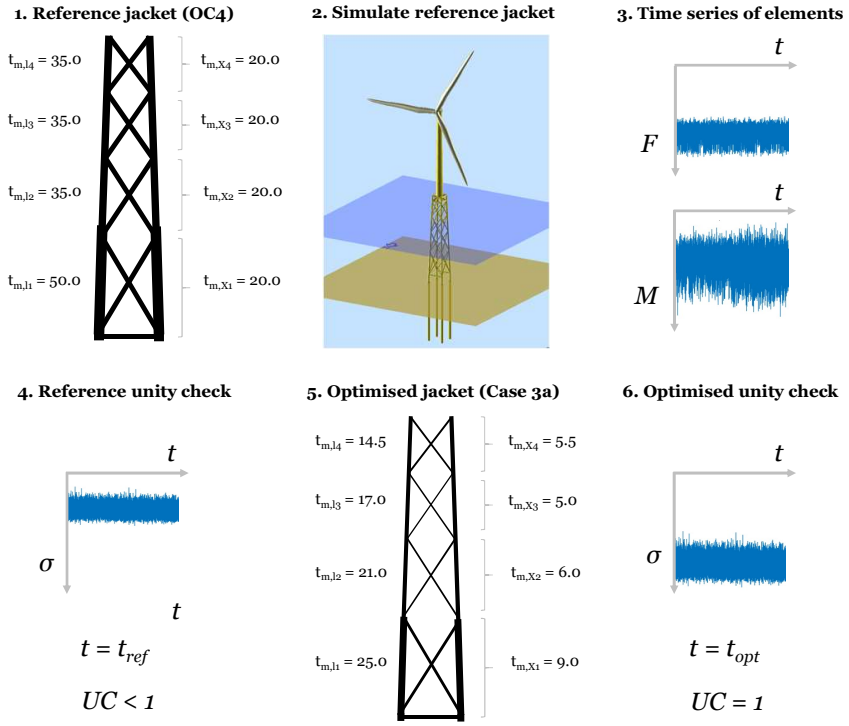

Figure 6.6: Visualisation of the manual member thickness optimisation procedure. Due to the time, no new simulations are performed for the optimised structure. Force, moment and stress time series illustrate global buckling check. Thickness is indicated in millimetres.

ULS simulations are performed for a single seed of scenario 1 (see Fig. 4.4), as this situation governs bottom leg thickness. This simulation is performed for a jacket with OC4 member thickness and a jacket with case 3a member thickness (see Fig. 6.6). The force and moment time series of both simulations are translated to global buckling unity checks for four legs and four brace elements. The results can be seen in Tab. 6.2.

For all elements, the unity check is reduced if updated time series of force and moments are used. This could be explained by a number of reasons.

The reduction of self weight is expected to have the most significant impact. The reference jacket is more than two times as heavy as the optimised jacket. As the normal force contributes to the global buckling unity check for respectively 87% and 51% for legs and braces, this has a large effect (see Tab. 5.8). As a change of jacket weight is more reflected in lower levels, this explains the increased effect for lower leg levels.

The change of eigenfrequency effects the unity check as well. The frequency is reduced from f_{OC4} = 0.272 Hz to f_{Case3a} = 0.240 Hz. It moves away from the 3P domain and gets closer to the 1P frequency range domain. Besides, the eigenfrequency gets closer to the forcing frequencies of waves (see Fig. 4.2).

Table 6.2: Dependency of global buckling unity check on member thickness of simulated jacket. First and second column show unity check for respectively OC4 and case 3a force and moment time series. Note, for both unity check calculations, case 3a member thickness is used. The last column gives the reduction of the unity check when case 3a time series are used. For all members the unity check is reduced.

	UC t_{OC4} time series [-]	UC t_{Case3a} time series [-]	Reduction of UC [%]
Legs			
Level 1	0.84	0.65	23
Level 2	0.84	0.70	16
Level 3	0.92	0.80	13
Level 4	0.97	0.89	8
Braces			
Level 1	0.69	0.58	17
Level 2	0.93	0.56	40
Level 3	0.88	0.53	40
Level 4	0.92	0.63	32
Average			**24**%

Note, the influence is checked for global buckling, a single case and a single seed only. If simulations would be performed for another seed, the unity check reduction might be different. For fatigue, it is not known if the damage will reduce, as not the maximum stress, but the stress range is of importance.

6.2.4. Sensitivity of eigenfrequency to member thickness

The eigenfrequency of the complete structure is an important variable for the load and resulting load effects. The complete structure consists of piles (including soil-structure interaction by non-linear springs), a jacket support structure, a transition piece, a tubular tower and a rotor-nacelle assembly (see Fig. 4.3).

The ratio between the total mass m_{tot} and the total stiffness k_{tot} influences the eigenfrequency by the following familiar equation:

$$f_{\text{tot}} = \frac{1}{2\pi}\sqrt{\frac{k_{\text{tot}}}{m_{\text{tot}}}} \qquad \text{[Hz]} \tag{6.2}$$

When jacket member thickness is changed, both the mass and stiffness are altered. As a result, it is not straightforward to predict the degree of eigenfrequency change. The shape of the first mode, shown in Fig. 6.7, will remain virtually unchanged for a moderate thickness change.

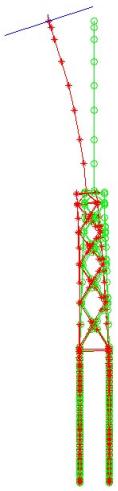

Figure 6.7: Mode shape of lowest eigenfrequency. From bottom to top: piles, jacket support structure, transition piece, tubular wind tower, rotor-nacelle assembly.

The total eigenfrequency change is analysed for the modelled OC4 structure, and a structure with jacket member thickness reduced by 30%. The jacket mass is lowered by about 30%, the total mass is reduced by about 7% and the eigenfrequency drops by about 6%. As the jacket mass comprises only about 25% of the total mass (partly due to the heavy concrete transition piece of 666 t), the change of jacket mass has a minor influence on the eigenfrequency.

Besides mass and stiffness, the eigenfrequency is influenced by the distribution of mass and stiffness and the contribution of those to the mode of interest. The mode corresponding to the lowest eigenfrequency is shown in Fig. 6.7. For this mode, the mass at the top (rotor-nacelle assembly; 350 t) has a larger displacement and a larger influence on the eigenfrequency than the mass of the jacket structure.

The stiffness of the jacket structure is rather large compared to the stiffness of the tubular wind tower. This is due to the large distance between the jacket legs. As a result, the structural stiffness of the tubular tower has a larger contribution to the total stiffness and a larger contribution to the eigenfrequency. Therefore, the eigenfrequency is less sensitive to jacket member thickness.

6.2.5. Sensitivity of local buckling to external hydrostatic pressure

For jacket structures, legs are normally flooded, while braces are not. For braces, a pressure difference exists between external hydrostatic pressure and internal atmospheric pressure. The hydrostatic pressure increases 1 bar for 10 meters water depth, resulting in a pressure difference of 0.5 $\mathrm{N\,mm^{-2}}$ at 50 m water depth.

Local buckling is calculated according to EN1993-1-6 [50]. In the local buckling results mentioned so far (see App. F), only stress induced by normal force and bending moments are taken into account (so-called meridional stress). Due to ring effects, a pressure difference induces circumferential stress. Meridional and circumferential stress interact and results for case 3a (mild steel wrapped FRP structure) are shown in Fig. 6.8. The three lowest brace levels have maximum water depths of respectively 45, 25 and 10 meters below MSL. Level four braces are located above sea level.

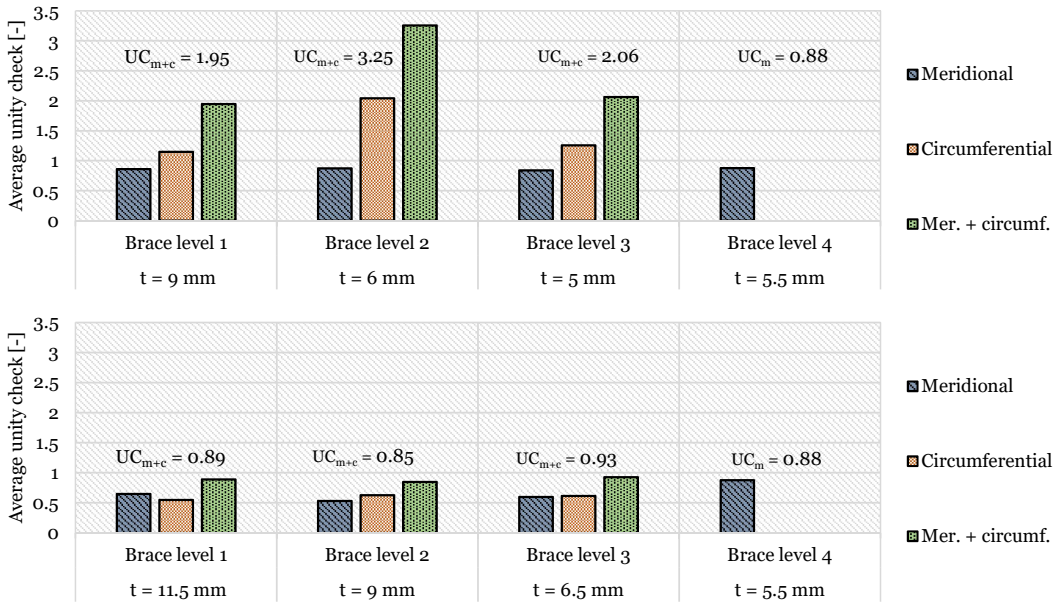

Figure 6.8: Graph showing the brace thickness and the local unity check for meridional stress (normal force + bending moment), circumferential stress (pressure difference) and their combination. Water depth from bottom to the top level is respectively 45, 25, 10 and 0 meters. The bottom graph shows the minimum thickness (in steps of 0.5 mm) to obtain a unity check below 1. A single bar is shown for level four, as the brace is above MSL.

For the three lowest brace levels, the resistance is insufficient. From bottom to top, the thickness should be increased by 2.5, 3 and 1.5 mm. This would yield a mass increase of the wrapped FRP structure of 17.5 t. For this structure, the total jacket weight would be 215.7t. This gives a weight reduction of 53% compared to the welded structure (see Tab. 5.1).

The sensitivity of meridional and circumferential buckling to element thickness can be seen when comparing the top and bottom graph of Fig. 6.8. The circumferential buckling unity check reduces more strongly.

High strength steel has increased buckling resistance. If high strength steel is used instead of mild steel, the minimum brace thickness from level 1 to level 3 is respectively 10.5, 8.5 and 6 mm.

Increasing the brace thickness to resist buckling due to meridional and circumferential stress, can be avoided if brace members would be flooded. However, this also influences the eigenfrequency and corrosion resistance and may not be the preferred option.

6.3. Conclusion

The modelling choices, assumptions and simplifications influence the results of this report. The results of the welded and unwelded structure are quite strong, as some main uncertainties are quantified. These were related to the sensitivity of force and moment time series to member thickness, and the susceptibility of members to local buckling due to hydrostatic pressure. The remaining main doubts can be eliminated if the number of FLS and ULS simulations is increased, and if time series are recorded for all elements.

Due to the novelty of the joints, the uncertainty for the wrapped FRP structure is larger. This is typical for innovations, and future experiments will provide additional insight. These uncertainties however, have no implications on the maximum potential benefit of the innovative joints. The main uncertainty is the capability of the joints to handle high forces and moments, even after long time exposure to harsh offshore conditions. Besides, the procedure to calculate wrapping thickness should be validated by additional experiments.

7

Conclusions and recommendations

The final chapter of this report gives a short overview of the adopted approach, answers the research questions and gives the overall conclusion. Additionally, recommendations are given whereby results can be strengthened and uncertainties eliminated. Also, future work is formulated for which this research forms the starting point. Future work aims to bring the application of wrapped FRP joints in the offshore wind one step closer.

7.1. Conclusions

The main goal of this research is to investigate the potential reduction of steel weight in offshore wind turbine jacket structures. The weight reduction should be enabled by innovative and fatigue resistant wrapped FRP joints. As fatigue is said to govern the design of welded jackets, significant weight reduction is to be expected.

A jacket model is built, simulations are performed, and detailed calculations are made. Simulations and calculations are performed for both fatigue and ultimate limit state. Fatigue limit state utilisation is checked for the strength of both joints and elements. Ultimate limit state utilisation is checked for the strength of joints, as well as the strength and stability of members. As input data is based on the UpWind report, results are compared to gain confidence and to eliminate errors.

Manual thickness optimisation is performed, and three material-efficient jacket structures are designed. Those are the welded, unwelded and wrapped FRP jointed structure. Conclusions per research question, as stated in Ch. 3, and an overall conclusion, are given below:

Potential steel weight reduction
The main research question referred to the possible reduction of steel weight if innovative wrapped FRP joints replace conventional welded joints. With 57% for mild steel and 60% for high strength steel, the weight reduction is large. If local buckling due to hydrostatic pressure is included, the reduction is still above 50%.

Governing unity check
The hypothesis that fatigue of welds governs member thickness for welded jackets, served as the basis of this research. Wrapped joints show superior fatigue performance which could only be exploited if fatigue governs current jacket design. This hypothesis is confirmed.

For the welded structure, the fatigue life of welds determines both the member thickness and the thickness of joint can sections. For the unwelded structure, the thickness of all members is governed by global buckling. For the wrapped FRP structure, both buckling and fatigue govern design. Due to the limited production length of tubular steel elements, (splice) welds are applied in the legs. The fatigue resistance of these welds governs leg member thickness. Braces, however, are unwelded, and therefore governed by global buckling. If local buckling due to hydrostatic pressure is included, local buckling governs thickness of the three lowest brace levels for the unwelded and wrapped FRP structure. The fatigue resistance of joints is tailored by increasing the FRP wrapping thickness.

Benefit of high strength steel
High strength steel is not commonly used in fatigue loaded welded structures, as the fatigue strength of welds is independent of the yield strength of the base material. Consequently, there is no benefit of high strength steel for the welded jacket structure. For the unwelded structure, the weight of the jacket could be reduced by 25% if high strength steel is used instead of mild steel. For the wrapped FRP structure, the benefit is negligible, as only the brace thickness can be reduced.

Potential cost reduction
The market potential of wrapped FRP joints depends to a large extent on the costs of production, transport, installation and maintenance. If the total costs of a wrapped FRP jacket structure are higher than of a conventional welded structure, future prospects are limited.

The costs of production for the welded and wrapped FRP structure are compared and include costs of steel, cutting and welding. It includes all members and welds between the bottom and top Y-joints. If the production costs of wrapped FRP joints are excluded, the difference for a mild steel jacket is more than 725 thousand Euro. Per multiplanar K-joint or uniplanar X-joint, the available budget for wrapping is about 25 thousand Euro. If production costs are less than 25 thousand Euro, economic benefits are made. Additional advantages of weight reduction, like the ease of handling and transportation, are not taken into account. The use of high strength steel is economically not attractive, as the total steel costs increase.

Overall conclusion
In short, wrapped FRP joints have great potential as the steel weight of jackets can be more than halved. Buckling governs the design, the use of high strength steel is not economical, and the cost reduction depends on wrapping costs. Experiments should reveal joint limitations, degradation in seawater, and correct procedure to calculate wrapping thickness. These outcomes will determine the viability of wrapped FRP joints for offshore wind jacket support structures.

7.2. Recommendations and future work

The uncertainties, weaknesses, and modelling choices mentioned in the discussion of Ch. 6, form the basis for the recommendations and future work. Additionally, thoughts are given on follow-up projects for which this report forms the starting point.

Obtain additional experimental results for wrapped FRP joints
The main recommendation relates to the novelty of wrapped FRP joints. The steel and the FRP thickness of the wrapped structure are based on the assumption that sufficient fatigue resistance of joints could be achieved, and that this could be achieved by increasing wrapping thickness only. Additionally, the wrapping thickness is determined by a relation based on a limited set of experiments. Experiments are performed for limited type, size and number of joints only. The thickness effect of FRP wrapping, the size effect of member diameter, the effect of joint geometry, the resistance to moments and the long term degradation in seawater are unknown. More experiments should be performed to gain insight into the required wrapping thickness and limitations of the joints.

Increase modelling and calculation accuracy
The second recommendation relates to the detail of modelling and calculation. In this report, the number of simulated load scenarios is limited. Increasing the number will generate better agreement with reality. Secondly, the amount of data points is limited. The data points are the locations where force and moment time series are obtained. If data would be recorded for all members, the certainty of the calculated member thickness is improved. Thirdly, the influence of the wrapping on the realistic buckling length could be included. The wrapping locally stiffens the member, and as a result, the realistic buckling length will reduce. Hence, the member thickness could be reduced. Finally, simulations should be performed for jackets with updated member thickness. As mentioned in the discussion of Ch. 6, this has a significant impact on the buckling unity check. The influence on the fatigue damage is yet unknown but worth investigating. For a significant member thickness change, the simulation and calculation procedure should be performed iteratively.

Optimise for complete structural layout
Another recommendation is to broaden the optimisation procedure to more variables than the element thickness t only. In this report, thickness t is chosen, as it is most simple, does not give element connectivity issues, and does not change the hydrodynamic force impact area. Further weight-saving may be achieved if the diameter D and the ratio D/t are optimised. Additionally, the global layout of the structure can be altered by changing the base width, top width, number of legs and number of brace levels.

Design supporting structure for larger turbine
The final recommendation is the design of a jacket support structure for a larger wind turbine. In this report, a jacket design is made for a relatively small 5 MW turbine, while current turbines have capacities of over 10 MW. Larger turbines have increased height, increased top mass, decreased operating frequencies and a smaller frequency range between the 1P and 3P domain. Those factors have a large influence on jacket design. For this follow-up, the INNWIND project could be used as a starting point [70].

Bibliography

[1] Maria Araceli Abanilla, Yan Li, and Vistasp M Karbhari. Durability characterization of wet layup graphite/epoxy composites used in external strengthening. *Composites Part B: Engineering*, 37(2-3): 200–212, 2005.

[2] Cristina Alia, María V Biezma, Paz Pinilla, José M Arenas, and Juan C Suárez. Degradation in seawater of structural adhesives for hybrid fibre-metal laminated materials. *Advances in Materials Science and Engineering*, 2013, 2013.

[3] Andrew. What does the capacity factor of wind mean?, September 2014. URL `http://energynumbers.info/capacity-factor-of-wind`. Consulted on: 12-04-2019.

[4] L Ascione, E Guttierez, S Dimova, A Pinto, and S Denton. Prospect for new guidance in the design of frp. *Support to the implementation, harmonization and future development of the Eurocodes. JRC Report EUR*, 27666, 2016.

[5] F Bellucci. Galvanic corrosion between nonmetallic composites and metals: I effect of metal and of temperature. *Corrosion*, 47(10):808–819, 1991.

[6] F Bellucci. Galvanic corrosion between nonmetallic composites and metals ii. effect of area ratio and environmental degradation. *Corrosion*, 48(4):281–291, 1992.

[7] HD Harm Boel. Buckling length factors of hollow section members in lattice girders. 2010.

[8] Amélie Boisseau and Catherine Peyrac. Long term durability of composites in marine environment: Comparative study of fatigue behavior. *Procedia Engineering*, 133:535–544, 2015.

[9] Amélie Boisseau, Peter Davies, and Frédéric Thiebaud. Fatigue behaviour of glass fibre reinforced composites for ocean energy conversion systems. *Applied Composite Materials*, 20(2):145–155, 2013.

[10] Djillali Amar Bouzid, Subhamoy Bhattacharya, and Lalahoum Otsmane. Assessment of natural frequency of installed offshore wind turbines using nonlinear finite element model considering soil-monopile interaction. *Journal of Rock Mechanics and Geotechnical Engineering*, 10(2):333–346, 2018.

[11] DM Brewis, J Comyn, AK Raval, and AJ Kinloch. The effect of humidity on the durability of aluminium-epoxide joints. *International Journal of Adhesion and Adhesives*, 10(4):247–253, 1990.

[12] A.R.G. Brown. The corrosion of cfrp-to-metal couples in saline environments. *Proceedings of the 2nd International Conference of Carbon Fibers*, pages 18–20, 1974. cited By 3.

[13] Flake C Campbell. *Structural composite materials*. ASM international, 2010.

[14] M Dawood. Durability of steel components strengthened with fiber-reinforced polymer (frp) composites. In *Rehabilitation of Metallic Civil Infrastructure Using Fiber Reinforced Polymer (FRP) Composites*, pages 96–114. Elsevier, 2014.

[15] Mina Dawood and Sami Rizkalla. Environmental durability of a cfrp system for strengthening steel structures. *Construction and Building Materials*, 24(9):1682–1689, 2010.

[16] Matthew Dawson, Peter Davies, Paul Harper, and Simon Wilkinson. Composite materials in tidal energy blades. In *Durability of Composites in a Marine Environment 2*, pages 173–194. Springer, 2018.

[17] WE De Vries, Naveen Kumar Vemula, Patrik Passon, Tim Fischer, Daniel Kaufer, Denis Matha, Bjrn Schmidt, and Fabian Vorpahl. Final report wp 4.2: support structure concepts for deep water sites: deliverable d4. 2.8 (wp4: offshore foundations and support structures). 2011.

[18] DNV. *Classification notes No 30.4, Foundations*, February 1992.

[19] DNVGL. *Support structures for wind turbines (DNVGL-ST-0126)*, April 2016.

[20] DNVGL. *Loads and site conditions for wind turbines (DNVGL-ST-0437)*, April 2016.

[21] DNVGL. *Fatigue design of offshore steel structures (DNVGL-RP-C203)*, November 2016.

[22] DNVGL. *Composite components (DNVGL-ST-C501)*, August 2017.

[23] M Efthymiou and S Durkin. Stress concentrations in t/y and gap/overlap k-joints. 1985.

[24] Yuan Fang, Kai Wang, David Hui, Fujun Xu, Weiqing Liu, Shulan Yang, and Lu Wang. Monitoring of sea-water immersion degradation in glass fibre reinforced polymer composites using quantum dots. *Composites Part B: Engineering*, 112:93–102, 2017.

[25] FiberCore-Europe. Architectural maintenance-free bridges in fibre reinforced polymers (frp) now standard technology, 2013. URL `https://www.fibercore-europe.com/en/first-34-frp-bridges-for-rotterdam/`. Consulted on: 2019-02-26.

[26] Michelle Fourse. Offshore wind industry heading out to deeper water, July 2018. URL `https://www.windpowerengineering.com/business-news-projects/offshore-wind-industry-heading-out-to-deeper-water/`. Consulted on: 2019-04-08.

[27] Yuguang Fu, Lewei Tong, Lang He, and Xiao-Ling Zhao. Experimental and numerical investigation on behavior of cfrp-strengthened circular hollow section gap k-joints. *Thin-Walled Structures*, 102:80–97, 2016.

[28] JD Garcia-Espinel, D Castro-Fresno, P Parbole Gayo, and F Ballester-Muñoz. Effects of sea water environment on glass fiber reinforced plastic materials used for marine civil engineering constructions. *Materials & Design (1980-2015)*, 66:46–50, 2015.

[29] AG Gibson. *The cost effective use of fibre reinforced composites offshore*. HSE Books Norwich, UK, 2003.

[30] RA Gledhill, AJ Kinloch, and SJ Shaw. A model for predicting joint durability. *The journal of Adhesion*, 11 (1):3–15, 1980.

[31] Mohsen Heshmati, Reza Haghani, and Mohammad Al-Emrani. Environmental durability of adhesively bonded frp/steel joints in civil engineering applications: state of the art. *Composites Part B: Engineering*, 81:259–275, 2015.

[32] Matt Hickman. Rotterdam is on a plastic bridge-building spree, March 2016. URL `https://www.mnn.com/green-tech/research-innovations/blogs/rotterdam-plastic-bridge-building-campaign`. Consulted on: 2019-02-26.

[33] IEC. *Wind turbines - Part 1: Design requirements (IEC-61400-1)*, August 2006.

[34] IEC. *Wind turbines - Part 3: Design requirements for offshore wind turbines (IEC61400-3)*, March 2015.

[35] J Jonkman, S Butterfield, W Musail, and G Scott. Definition of a 5-mw reference wind turbine for offshore system development. Technical report, NREL, 2009.

[36] Christoph W Kensche. Fatigue of composites for wind turbines. *International journal of fatigue*, 28(10): 1363–1374, 2006.

[37] Ivan Komusanac, Daniel Fraile, and Guy Brindley. Wind energy in europe in 2018 - trends and statistics. Technical report, WindEurope, 2019.

[38] A Kootsookos and AP Mouritz. Seawater durability of glass-and carbon-polymer composites. *Composites Science and Technology*, 64(10-11):1503–1511, 2004.

[39] Bhavesh G Kumar, Raman P Singh, and Toshio Nakamura. Degradation of carbon fiber-reinforced epoxy composites by ultraviolet radiation and condensation. *Journal of Composite materials*, 36(24):2713–2733, 2002.

[40] S Larbi, R Bensaada, A Bilek, and S Djebali. Hygrothermal ageing effect on mechanical properties of frp laminates. In *AIP Conference Proceedings*, volume 1653, page 020066. AIP Publishing, 2015.

[41] M Lesani, MR Bahaari, and MM Shokrieh. Numerical investigation of frp-strengthened tubular t-joints under axial compressive loads. *Composite structures*, 100:71–78, 2013.

[42] M Lesani, MR Bahaari, and MM Shokrieh. Experimental investigation of frp-strengthened tubular t-joints under axial compressive loads. *Construction and building materials*, 53:243–252, 2014.

[43] M Lesani, MR Bahaari, and MM Shokrieh. Frp wrapping for the rehabilitation of circular hollow section (chs) tubular steel connections. *Thin-Walled Structures*, 90:216–234, 2015.

[44] Shan Li, Hui Tao Ren, Yi Yan Lu, and Mu Huan Shi. Environmental degradation of carbon fiber reinforced polymer (cfrp) and steel bond subjected to hygrothermal aging and loading. In *Materials Science Forum*, volume 675, pages 559–562. Trans Tech Publ, 2011.

[45] Naumes J Linghoff D. D6.2.4: Appendix b, strengthening metallic structures using advanced composites - backround document for research and development. 2006.

[46] Martin Alberto Masuelli. Introduction of fibre-reinforced polymers- polymers and composites: Concepts, properties and processes. In *Fiber Reinforced Polymers-The Technology Applied for Concrete Repair*. IntechOpen, 2013.

[47] Pablo Castillo Meseguer. Structures for offshore wind turbines. fatigue analysis of a jacket support, comparison between welded and cast connections. Master's thesis, Lulea University of Technology, Sweden, February 2015.

[48] Abdel-Hamid I Mourad, Beckry Mohamed Abdel-Magid, Tamer El-Maaddawy, and Maryam E Grami. Effect of seawater and warm environment on glass/epoxy and glass/polyurethane composites. *Applied Composite Materials*, 17(5):557–573, 2010.

[49] NEN-EN. *Eurocode 3: Design of steel structures - Part 1-8: Design of joints (EN 1993-1-8)*, January 2006.

[50] NEN-EN. *Eurocode 3: Design of steel structures - Part 1-6: General - Strength and Stability of Shell Structures (EN 1993-1-6)*, March 2007.

[51] NEN-EN. *Eurocode 3: Design of steel structures - Part 1-1: General rules and rules for buildings (EN 1993-1-1)*, December 2016.

[52] N Norsok. 004: Design of steel structures. *Standards Norway, Rev*, 2, 2004.

[53] Tim Palucka and Bernadette Bensaude-Vincent. Composites overview. *History of Recent Science and Technology*, 2002.

[54] Dipak Kumar Patel and Shubhonil Banerjee. A comparative study of effects on characteristic properties of frp composites when exposed to distilled water, nacl-water solution and sea water separately. *Bachelor thesis. Department of Metallurgical and Materials Engineering National Institute of Technology, Rourkela, India*, 2008.

[55] Marko Pavlovic, Milan Veljkovic, and Michail Liatzouras. Wrapped frp joints of steel hollow sections. In *Thin-Walled Structures - ICTWS 2018*, 2018.

[56] Beetle Plastics. Resins in frp, 2018. URL `https://beetleplastics.com/custom-frp-fabrications/about-fiberglass/resins-in-frp/`. Consulted on: 2019-02-20.

[57] E Poodts, G Minak, and A Zucchelli. Impact of sea-water on the quasi static and fatigue flexural properties of gfrp. *Composite Structures*, 97:222–230, 2013.

[58] Seb Rae, Karen Thyssen Raaberg, and Julian Das. Offshore wind foundations - a european overview. *Renewables Consulting Group (RCG)*, 2017.

[59] G Sala. Composite degradation due to fluid absorption. *Composites Part B: Engineering*, 31(5):357–373, 2000.

[60] Florian Selot, Daniel Fraile, and Guy Brindley. Offshore wind in europe - key trends and statistics 2018. Technical report, WindEurope, 2019.

[61] Md Shamsuddoha, Md Mainul Islam, Thiru Aravinthan, Allan Manalo, and Kin-tak Lau. Effectiveness of using fibre-reinforced polymer composites for underwater steel pipeline repairs. *Composite Structures*, 100:40–54, 2013.

[62] Ying Shan and Kin Liao. Environmental fatigue behavior and life prediction of unidirectional glass–carbon/epoxy hybrid composites. *International journal of fatigue*, 24(8):847–859, 2002.

[63] Glen Eugene Smith et al. Bond characteristics and qualifications of adhesives for marine applications and steel pipe repair. 2005.

[64] Robert Sonnenschein, Katarina Gajdosova, and Ivan Holly. Frp composites and their using in the construction of bridges. *Procedia engineering*, 161:477–482, 2016.

[65] Robert Henry Stewart. *Introduction to physical oceanography*. Texas A & M University College Station, 2008.

[66] Mohammadreza Tavakkolizadeh and Hamid Saadatmanesh. Galvanic corrosion of carbon and steel in aggressive environments. *Journal of Composites for Construction*, 5(3):200–210, 2001.

[67] Thewindpower.net. Bard offshore 1 (germany), November 2018. URL `https://www.thewindpower.net/windfarm_en_7105_bard-offshore-1.php`. Consulted on: 2019-05-07.

[68] Lelli Van Den Einde, Lei Zhao, and Frieder Seible. Use of frp composites in civil structural applications. *Construction and building materials*, 17(6-7):389–403, 2003.

[69] Anastasios P Vassilopoulos and Thomas Keller. *Fatigue of fiber-reinforced composites*. Springer Science & Business Media, 2011.

[70] T Von Borstel. Innwind. eu deliverable 4.3. 1–design report–reference jacket, 2013.

[71] F Vorpahl and W Popko. Description of the load cases and output sensors to be simulated in the oc4 project under iea wind annex 30. Technical report, Fraunhofer IWES, 2013.

[72] F Vorpahl, W Popko, and D Kaufer. Description of the basic model of the 'upwind reference jacket' for code comparison in the oc4 project under iea wind annex 30. Technical report, Fraunhofer IWES, 2013.

[73] Patricia A Wagner, Brenda J Little, Kevin R Hart, and Richard I Ray. Biodegradation of composite materials. *International biodeterioration & biodegradation*, 38(2):125–132, 1996.

[74] Michael Walsh. *Coastal Engineering Manual – Part II*. US Army Corps of Engineers, September 2015.

[75] Arthouros Zervos. Renewables 2019 global status report. Technical report, REN21, 2019.

[76] Serge Zhandarov and Edith Mäder. Characterization of fiber/matrix interface strength: applicability of different tests, approaches and parameters. *Composites Science and Technology*, 65(1):149–160, 2005.

[77] Jianhua Zhang, Issa Fowai, and Ke Sun. A glance at offshore wind turbine foundation structures. *Brodogradnja: Teorija i praksa brodogradnje i pomorske tehnike*, 67(2):101–113, 2016.

A

Comparison with UpWind project

A.1. Model

The modelled jacket structure is based on the UpWind reference project. Due to various motives, both structure, load and soil are not an exact copy of the UpWind project. Consequently, the structural results like fatigue life and ultimate resistance are not expected to match the UpWind report results exactly. The main model changes with respect the UpWind are aggregated and given below:

Structural:

- In UpWind, member thickness is locally increased around joints. So-called cans are not modelled in GH bladed in this MSc thesis. The modelled jacket is an exact match of the OC4 structure.
- In UpWind, the structural damping is 0.5%, while in this MSc thesis, a value of 1% is taken. This value is equal to the OC4 damping value.
- In UpWind, local joint flexibility is taken into account. In this MSc thesis, all joints are modelled as rigidly connected in GH Bladed.
- In UpWind, also secondary steel such as boat landing bumpers, anodes and J-tubes are modelled. In this MSc thesis, this is not the case. This influences both structural mass and load.

Load:

- In UpWind, the jacket structure is analysed with fatigue loading from different directional combinations of wind and waves. In this MSc thesis, wind and waves are coming from the same direction for every wind-wave combination.
- In UpWind, a high amount of different wind-wave scenarios is modelled for the analysis. In this MSc thesis, the number of fatigue scenarios is reduced to five and the number of extreme scenarios to three.
- In UpWind, wind and wave load is applied in separate analyses. Afterwards, load effects are superimposed. In this MSc thesis, wind and waves load is applied in a single simulation for both the fatigue and extreme load.

Soil:

- In UpWind, the layered sandy soil profile has a maximum friction angle of 42.5 degrees. In this MSc thesis, the layered sandy soil has a maximum friction angle of 40 degrees. The higher the friction angle, the more rigid the soil.

The structural and soil modifications are reflected in the eigenfrequency of the complete structure. In the UpWind project, the lowest eigenfrequency is 0.290 Hz, while in this MSc thesis, the first modal frequency is equal to 0.272 Hz. Note, in UpWind the eigenfrequency is given, while in the GH Bladed software used for this MSc thesis, the modal frequency is given. For the lowest eigenfrequency, this difference is expected to be small.

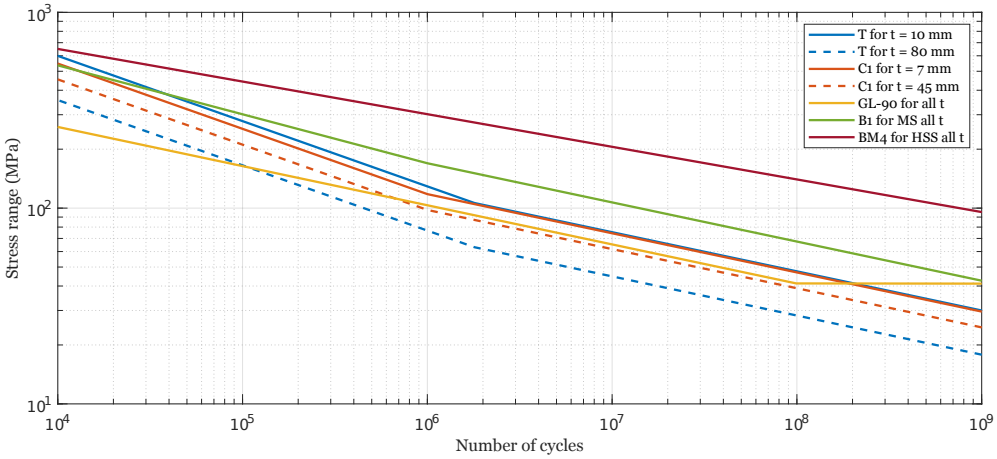

Figure A.1: S-N curves for welded joints and for unwelded base material. Curve GL-90 is applied in the UpWind project for both tubular joints and circumferential welds and is independent on both thickness and steel base material. Curve T (tubular joints) and C1 (circumferential welds) are used in this MSc thesis (case 1) and are thickness dependent and independent of steel base material. Curve B1 and BM4 show thickness independent curves for unwelded base material for respectively mild S355 steel and high strength S690 steel, used for case 2 of this MSc thesis.

A.2. Results

The jacket design in this MSc thesis is based on the structural, foundation and load properties of the UpWind project. However, the model is not an exact copy. Calculations of this MSc thesis are also not exactly equal to UpWind. A few differences are given below:

- In UpWind, buckling checks are performed according to NORSOK standard N-004 [52], while in this MSc thesis, global buckling checks are performed according to Eurocode 1993-1-1 Annex A [51].
- In Upwind, corrosion allowance is applied at the splash zone, while in this MSc thesis, corrosion is not included. The corrosion allowance is 6 mm and is present around the third level of braces (X3).
- In UpWind, fatigue damage for all joints is calculated with S-N curve GL-90, while in this MSc thesis curve T and curve C1 are used (see Fig. A.1). The S-N curve in UpWind is independent on element thickness, while this has a large influence on resistance for S-N curve T and C1. Depending on the stress range and element thickness, either the UpWind GL-90 curve or the MSc curves are more strict.
- In Upwind, the procedure to calculate fatigue stress might be approximated, while in this MSc thesis, an extensive procedure is applied. Different SCFs are applied for different hot spots, different kind of loading (normal force/in-plane moment/out-of-plane moment) and different loading conditions (balanced/unbalanced).
- In UpWind, the manufacturability is taken into account, while the structure in this MSc thesis is academical. All braces in Upwind are given the same thickness, and all element thicknesses are multiples of 5 mm. In this MSc thesis, member thicknesses are multiples of 0.5 mm.

Despite all differences, the structures are compared and shown in Fig. A.2. Clear similarities and dissimilarities are mentioned and commented on:

- General:

  In UpWind, the leg members are quite similar, and the brace members are generally thicker compared to this MSc thesis. In UpWind, the K-joint cans are smaller or absent, and the X-joint cans are quite similar. In both structures, the leg and brace members at the bottom are largest and at level three smallest.

- Can thickness X-joints:

  The dimensioning of X-joint cans are very similar to UpWind. The maximum thickness deviation is 4.5 mm.

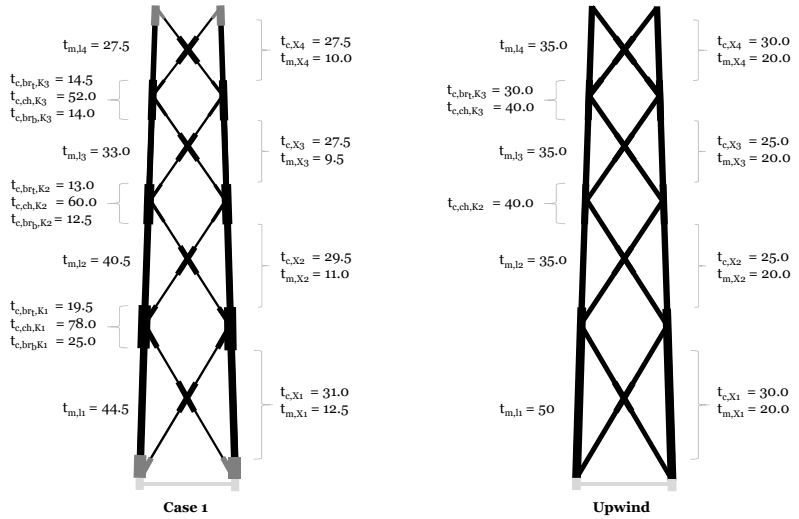

Figure A.2: Comparison between welded structure in MSc thesis (case 1) and UpWind structure.

- Member thickness braces:

  The member thickness is significantly different. The UpWind members are almost twice as thick.

- Can thickness K-joints:

  The can thickness in Upwind is less. The largest deviation compared to UpWind is visible at chord cans. In UpWind, the bottom K-joint has a chord thickness of 50 mm, while in the optimised steel welded structure $t_{\text{can}} = 78$ mm.

  Additional comment: Excluding the thickness effect in this MSc thesis (damage accumulation with S-N curve for $t_{\text{can}} = t_{\text{ref}} = 16$ mm), gives a can thickness reduction from 78 to 54 mm.

- Member thickness legs and K-side of braces:

  The member thickness of leg members in UpWind is comparable to the member thickness in this MSc thesis. The thickness in UpWind is slightly larger for the lowest chord members, slightly smaller for the second level and slightly larger for the third and fourth level from the bottom.

B

Model input GH Bladed

In this section, screenshots of the GH Bladed input are shown. Input is used for the ultimate limit state analysis.

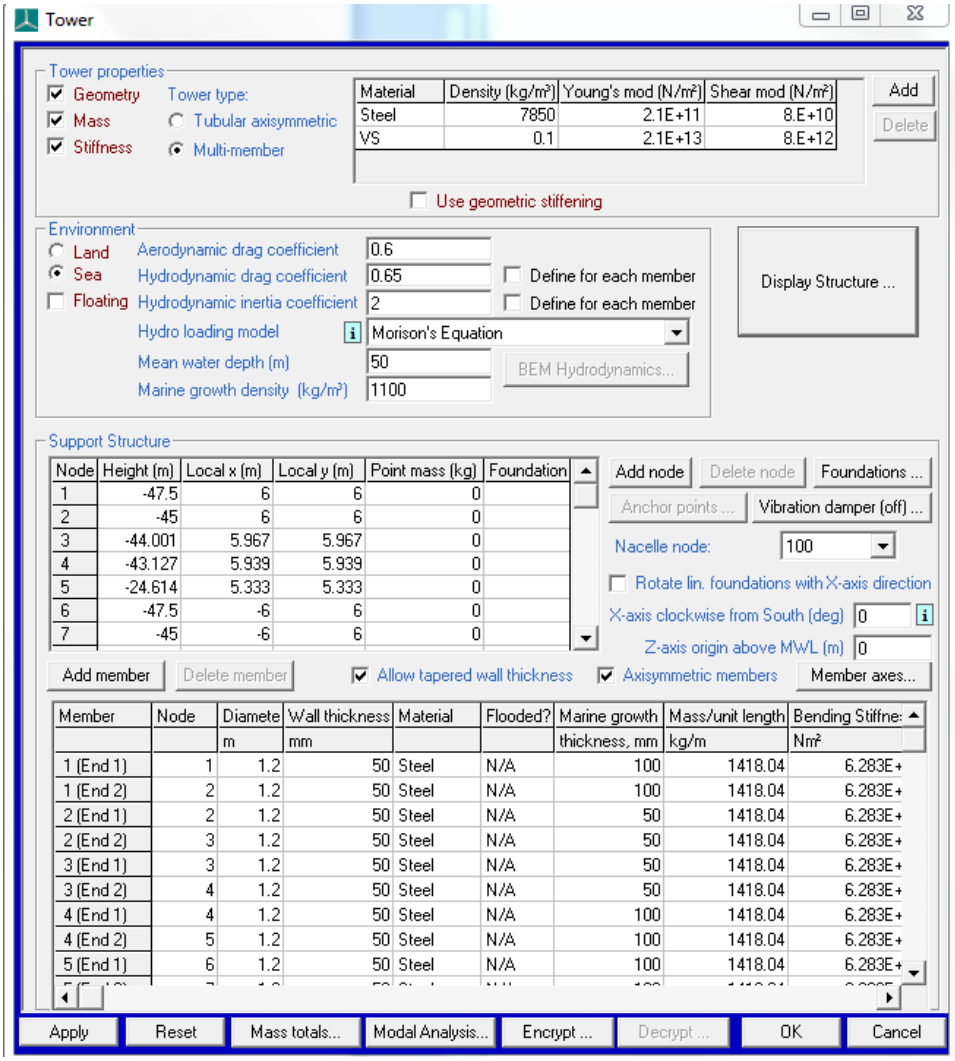

Figure B.1: Screenshot of GH Bladed showing input settings related to structure.

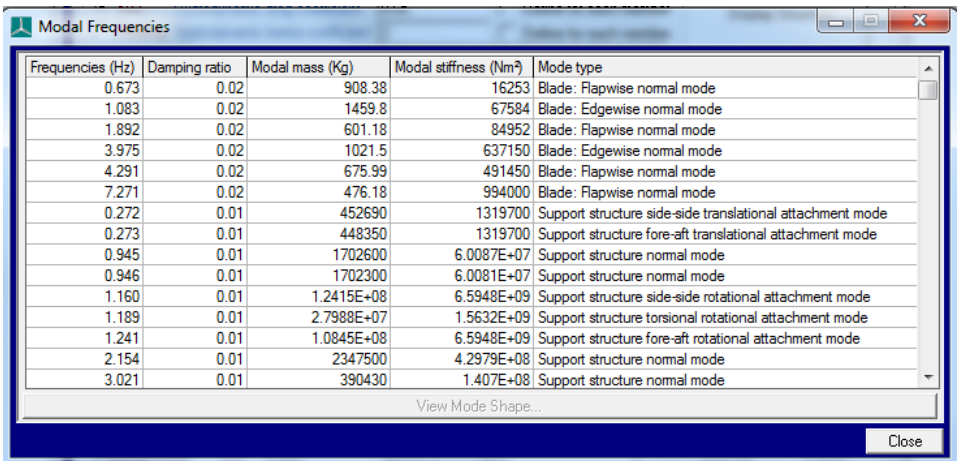

Figure B.2: Screenshot of GH Bladed showing model frequencies of modelled OC4 structure.

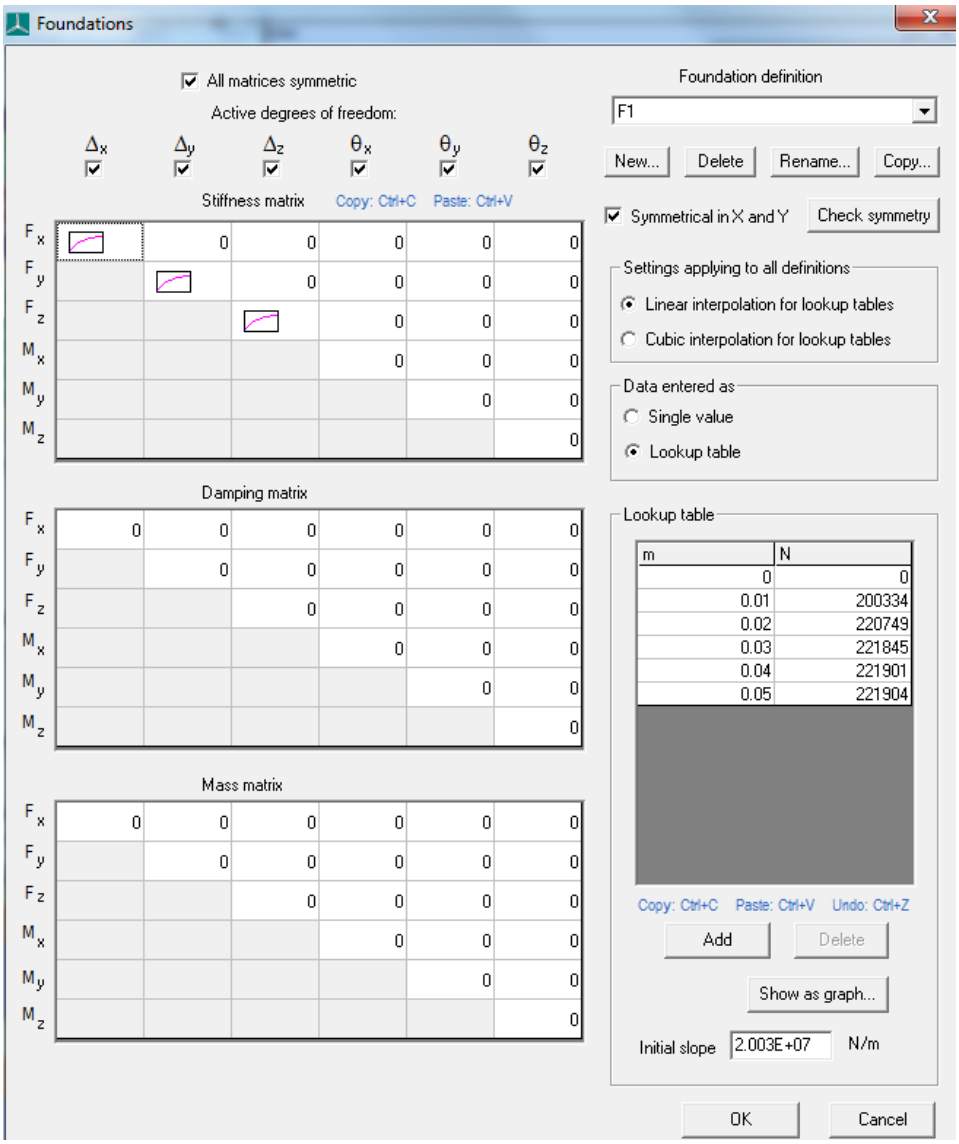

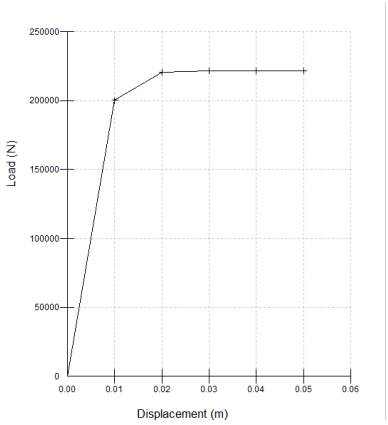

(a) Soil stiffness in x- and y-direction

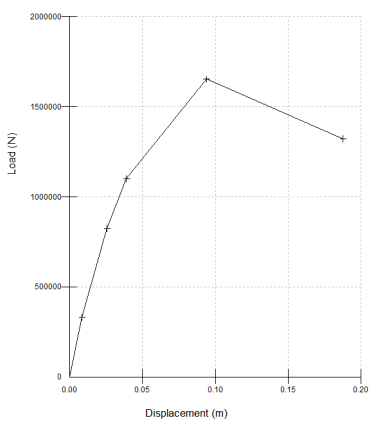

(b) Soil stiffness in z-direction

Figure B.3: Screenshot of GH Bladed showing input settings and soil stiffness relation for foundation at 1 m depth.

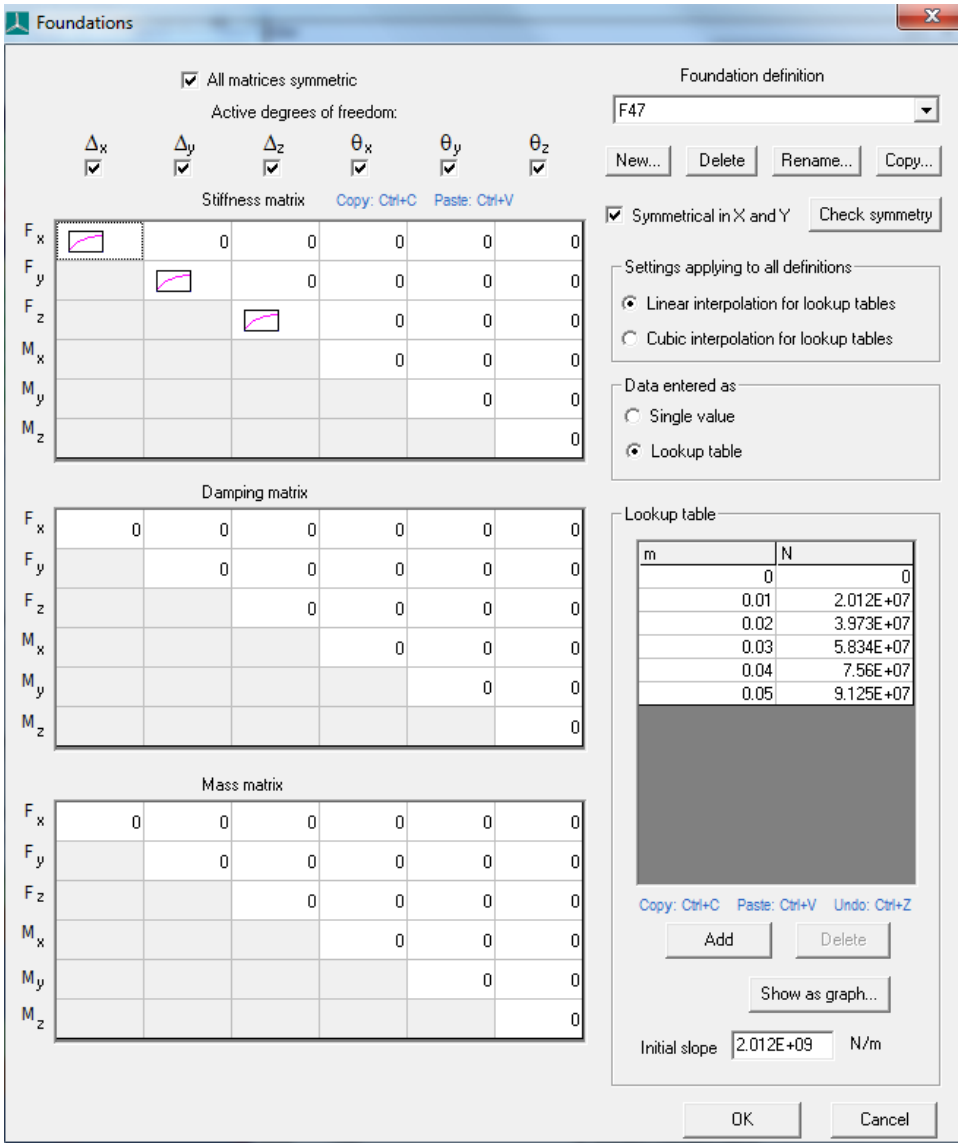

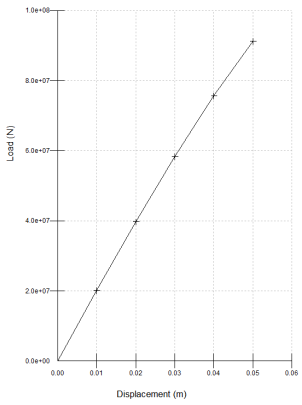

(a) Soil stiffness in x- and y-direction

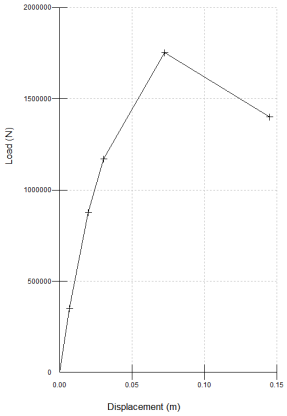

(b) Soil stiffness in z-direction

Figure B.4: Screenshot of GH Bladed showing input settings and soil stiffness relation for foundation at 47 m depth.

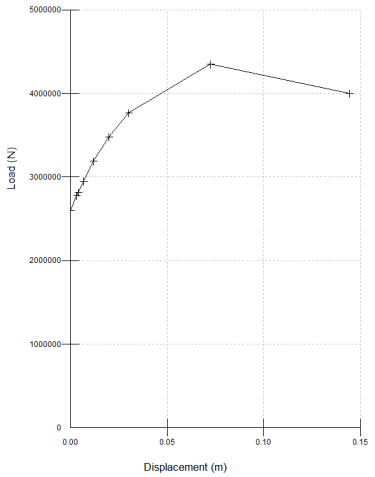

Figure B.5: Screenshot of GH Bladed showing soil stiffness relation in z-direction, including pile tip resistance, for foundation at 48 m depth.

3D Turbulent Wind Files

h:\my documents\documenten_afstuderen\extreme\wind files\w42s1.wnd Change...

Turbulence characteristics

Spectrum Type	Kaimal (General)	
Number of Components	3	-
Width of field	250	m
Number of points across	7	-
Height of field	250	m
Number of points in height	7	-
Length of field	43755.5	m
Alongwind spacing	0.667656	m
Turbulence Seed	1	-
Mean wind speed	42.73	m/s
Height above ground		m
Roughness length		m
Latitude		deg
Scale parameter (IEC-2)		m
Coherency scale param.	340	m
Coherence decay const.	12	-
Scale length		m
Shear parameter (gamma)		-
Max. lateral/vertical wavelength		m
FFT points		points

Approximate simulation times:
1021 s at 42.73 m/s
1021 s at 42.73 m/s

Turbulence Length Scales		Component of turbulence: Longitudinal	Lateral	Vertical
Along X (Longitudinal)	m	340.2	113.4	27.72
Along Y (Lateral)	m	0	0	0
Along Z (Vertical)	m	0	0	0

OK Cancel

Figure B.6: Screenshot of GH Bladed showing input settings related to turbulent wind file (Ultimate load scenario 1).

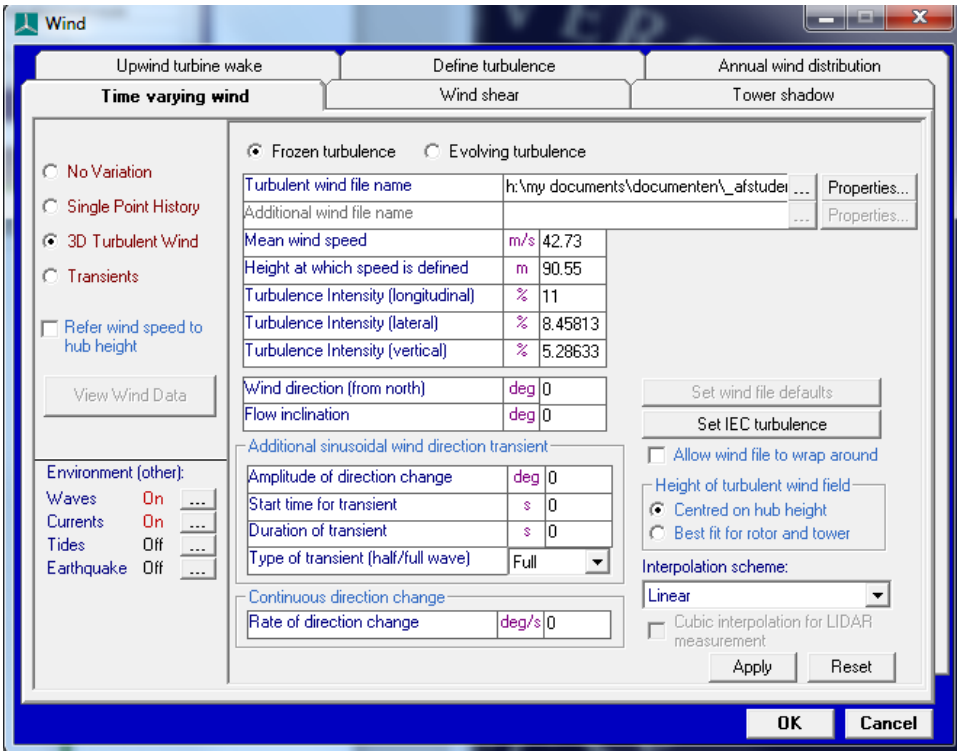

Figure B.7: Screenshot of GH Bladed showing input settings related to wind (Ultimate load scenario 1).

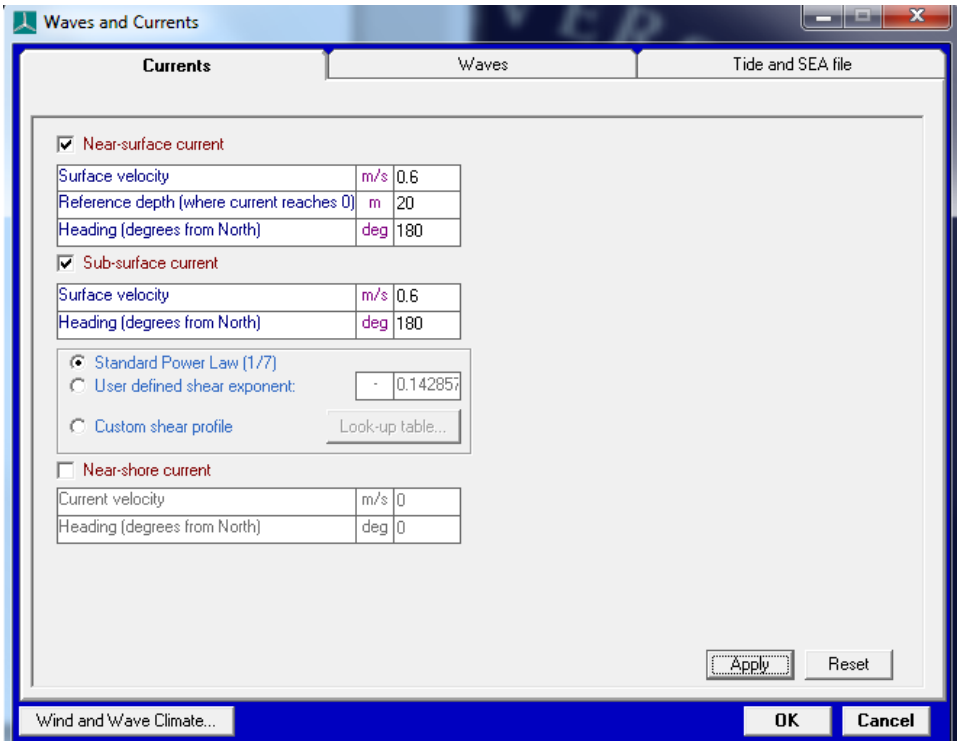

Figure B.8: Screenshot of GH Bladed showing input settings related to waves (Ultimate load scenario 1).

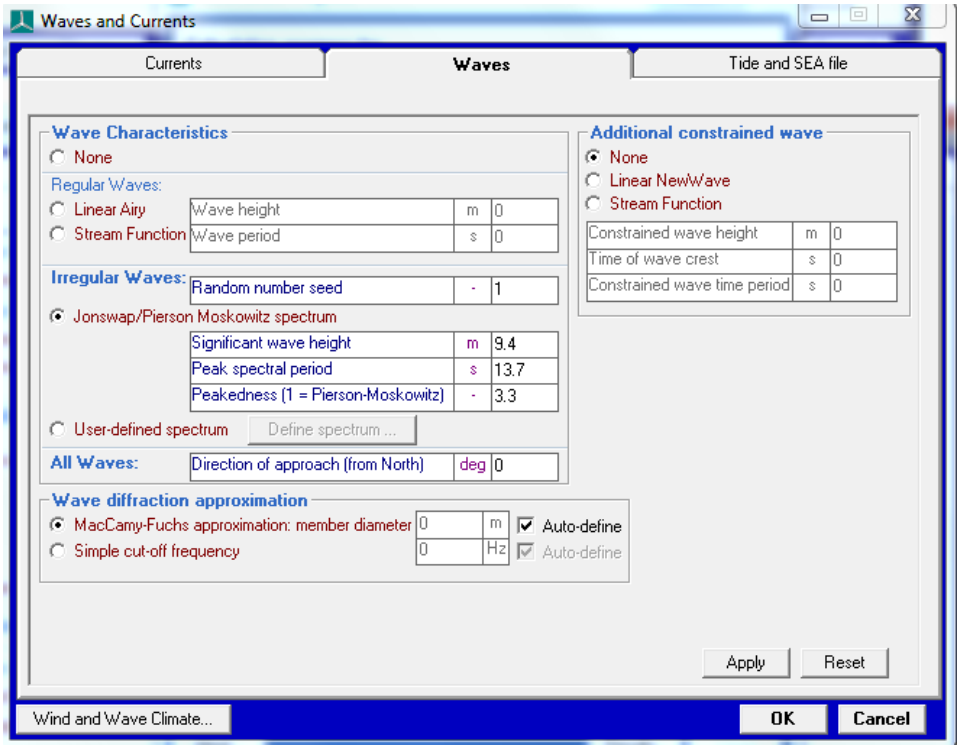

Figure B.9: Screenshot of GH Bladed showing input settings related to current (Ultimate load scenario 1).

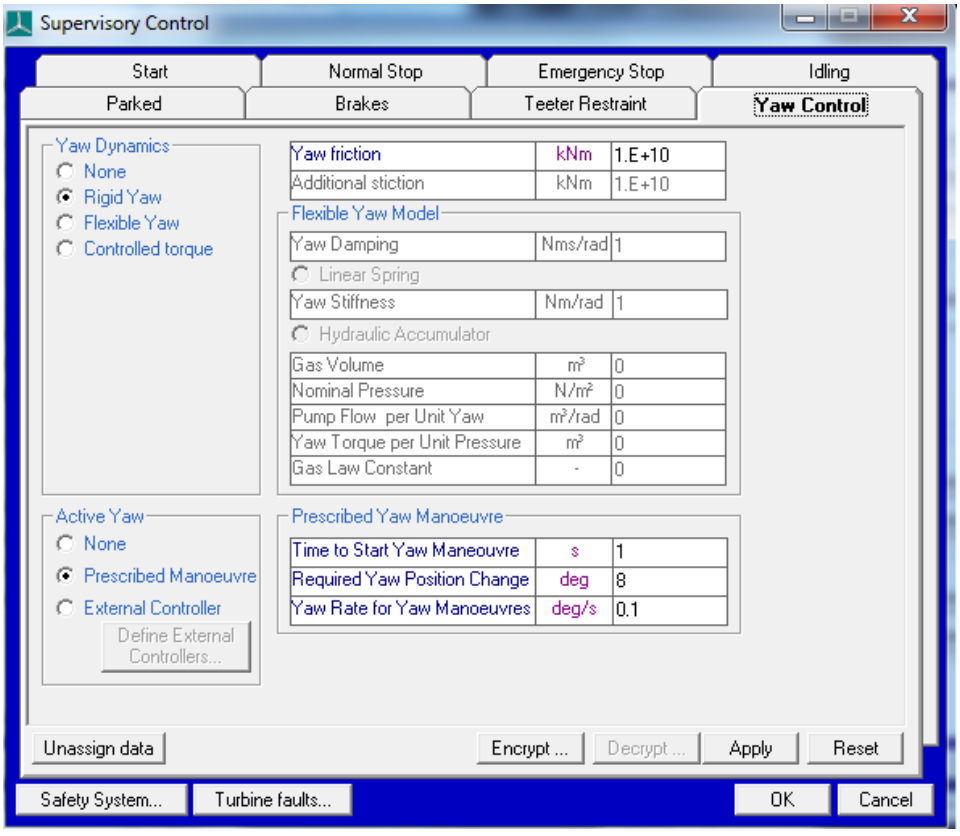

Figure B.10: Screenshot of GH Bladed showing input settings related to yaw misalignment (Ultimate load scenario 1).

C

Load

In this section, both FLS and ULS load are elaborated on in-depth.

C.1. Fatigue limit state

Loads are based on the UpWind report and to reduce modelling time, simplifications are made. The seventeen scenarios of Fig. C.1 are reduced to the five scenarios of Tab. C.1. For each of five scenarios, six analysis are performed with different wind turbulence and wave seeds. In this way, dependency on the chosen seed is reduced. The load considers both power production ($3 \leq V_{wind} \leq 25$ m/s) and idling ($V_{wind} > 25$) (see Fig. C.2). Waves and wind are taken uni-directional and similar directions are used for all simulations.

Force and moment time series of elements are obtained for the front plane and adjacent brace elements in the side plane (pointing West). Data is obtained at both nodes of elements. Directly at and at a certain distance away from the joint. For the legs, this distance is $0.5D_{leg}$ from the weld and for the braces $1.5D_{brace}$ from the weld. This results in a distance from 1.8 to 3.2 meters from the joint node.

Total simulation time of 800 s is conforming codes and time step is 0.05 s [33, 34]. First 200 seconds of the simulation are not recorded to remove start-up effects. The six different analyses per winds speed, in total 1 hour, will be used to extrapolate the 60-minutes of simulation to 20 years lifetime of a wind turbine. Occurrence per year will be taken into account (see Tab. C.1).

The current for all fatigue simulations is 0.6 m/s and consist of near-surface current only. At 20 meters below sea level, the current is zero. Note that unlike wind and wave direction, the current direction is defined as the direction that the current is flowing to, and not to the direction that the current is coming from.

The damping is equal to 1%. Marine growth is present according to Tab. C.2 and members are not flooded.

Table C.1: Load combinations used for fatigue load analysis. Binned wind speeds including the simulated wind speed, turbulence intensity, significant wave height, peak wave period and occurrence percentage. Numbers are based on UpWind project [17].

Wind speed window [m/s]	Wind speed [m/s]	Turbulence intensity [%]	H_s [m]	T_p [s]	Occurrence in lifetime [%]
1 - 9	5	18.95	1.14	5.82	43
9 - 15	11.4	14.78	1.63	5.84	37.5
15 - 19	17	13.75	2.33	6.54	12.5
19 - 25	22	13.30	3.09	7.4	6
25 - 31	28	11.9	4.17	8.49	1

V [ms]	TI[%]		Hs [m]	Tp [m]	Peakness [-]		f [%]	occ./year [hrs]
	normal	extreme			Fatigue	Extreme		
2	29,2	99,3	1,07	6,03	1	3,3	0,06071	531,8
4	20,4	53,1	1,1	5,88	1	3,3	0,08911	780,6
6	17,5	37,1	1,18	5,76	1	3,3	0,14048	1230,6
8	16	30	1,31	5,67	1	3,3	0,13923	1219,7
10	15,2	25,4	1,48	5,74	1	3,3	0,14440	1264,9
12	14,6	22,3	1,7	5,88	1	3,3	0,12806	1121,8
14	14,2	20,1	1,91	6,07	1	3,3	0,10061	881,3
16	13,9	18,5	2,19	6,37	1	3,3	0,07554	661,7
18	13,6	17,2	2,47	6,71	1	3,3	0,04878	427,3
20	13,4	16,1	2,76	6,99	1	3,3	0,03151	276,1
22	13,3	15,3	3,09	7,4	1	3,3	0,01924	168,6
24	13,1	14,6	3,42	7,8	1	3,3	0,00977	85,6
26	12	14	3,76	8,14	1	3,3	0,00474	41,6
28	11,9	13,5	4,17	8,49	1	3,3	0,00243	21,3
30	11,8	13,1	4,46	8,86	1	3,3	0,00093	8,2
32	11,8	12,7	4,79	9,12	1	3,3	0,00053	4,6
34-42	11,7	12,3	4,9	9,43	1	3,3	0,00019	1,6

Figure C.1: Lumped scatter diagram for reference site used for fatigue load. The coloured boxes indicate the five grouped load scenarios used in this MSc thesis. Adapted from [Fischer et al., 2010].

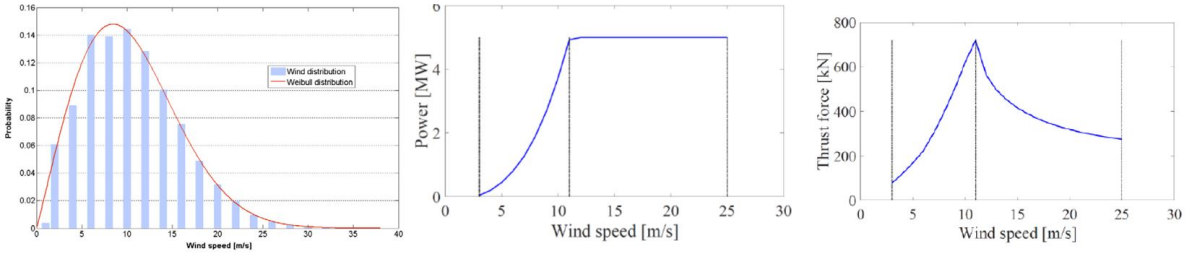

Figure C.2: Wind speed data, turbine power curve and turbine trust curve used to determine simulated wind speeds [Fischer et al., 2010].

Comments:

- Trust force influences jacket load, so smaller intervals are taken for $V_{wind} < 19$ m/s (see Fig. C.2). As an expected conservative approximation, $V_{rated} = 11.4$ m/s is simulated instead of $V_{wind} = 11$ (which is in middle of wind speed domain). Occurrence percentages are based on probability of lumped scatter diagram. Significant wave height H_s, peak period T_p and turbulence intensity are approximated by interpolation if needed (see Tab. C.1).
- Damage expected at $V_{wind} > 25$ m/s relevant for out-of-plane loading of braces by waves.
- Jackets are relatively transparent to waves. Most damage is induced by wind [17].
- No start-up and shut-down events modelled, as damage contribution is expected to be low [47].

Table C.2: Marine growth thickness [mm] as function of water depth and location [DNVGL, 2016].

Depth below MWL [m]	Central and Northern North Sea (56° to 59° N)	Norwegian Sea (59° to 72° N)
-2 to 40	100	60
> 40	50	30

C.2. Ultimate limit state

Loads are based on the UpWind report, but simplifications are made. All simulations consider idling of turbine in storm conditions (see Tab. C.3). In the UpWind report, all possible wind-wave directions and misalignment are simulated (in steps of 30 degrees), while in this MSc report only three wind/wave directionalities are simulated (see Fig. C.3). Scenario 1 considers co-directional wind and waves perpendicular to jacket side, scenario 2 co-directional wind and waves in a diagonal direction and scenario 3 wind diagonal to jacket side and waves 150 degrees misaligned. The latter scenario is governing for most elements, according to UpWind [17]. All scenarios are simulated with six different wind turbulence and wave seeds.

Force and moment time series of elements are obtained for the back plane and the side plane (pointing East), including adjacent three legs (North-East, South-East and East-West). Data is obtained at both nodes of elements. All nodes correspond with either X- or K-joints in structure. Additionally, force and moment time series are recorded at the K1-joint of the front plane.

Total simulation time is 700 s, and the time step is 0.05 s. First 100 s are removed, as the yaw error is introduced in this time window.

The current for all extreme simulations is 1.2 m/s and consist of 0.6 m/s near-surface current (zero at 20 m below sea level) and of 0.6 m/s subsurface current. Note that unlike wind and wave direction, the current direction is defined as the direction that the current is flowing to, and not to the direction that the current is coming from.

The damping, marine growth and flooding characteristics are similar to the fatigue analysis.

Table C.3: Extreme load properties used for all simulated ultimate limit state simulations. Numbers based on UpWind project [17].

Wind speed [m/s]	Turbulence intensity [%]	Current speed [m/s]	H_s [m]	T_p [s]	Yaw error [deg]
42.73	11.00	1.2	9.40	13.70	8

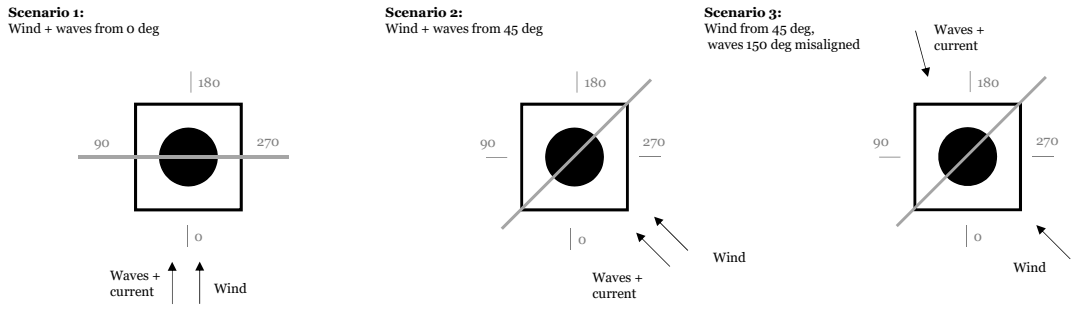

Figure C.3: Modelled wave-wind scenarios to simulate extreme load scenarios. Zero degrees corresponds to the North.

D

Analyses

In this section, both FLS and ULS load analyses are elaborated on in-depth. Procedures are given in step-by-step format.

D.1. Fatigue limit state

1. Run simulation in GH Bladed for five different scenarios with corresponding wind and wave conditions (see Tab. C.1). Six simulations are performed per scenario with different wind turbulence and wave seeds.

   (a) Obtain normal force and bending moment time series at nodes around joints. For member fatigue, also record normal force and bending moment time series at a distance from the joint (for clarity and compactness, not treated in the procedure below).

      i. 3x K-joint:
         Front plane: 4x $N-t$, 4x $M_{\text{ip}}-t$, 4x $M_{\text{op}}-t$ per joint.
         Side plane: 4x $N-t$, 4x $M_{\text{ip}}-t$, 4x $M_{\text{op}}-t$ per joint.

      ii. 4x X-joint:
         Front plane: 4x $N-t$, 4x $M_{\text{ip}}-t$, 4x $M_{\text{op}}-t$ per joint.

   (b) Calculate hot spot stress at every time step.
      Four locations per member (crown toe, crown heel, saddle side 1, saddle side 2 (see Fig. D.1)).

   (c) Create time series of hot spot stress for t = 200-800 s.

   (d) Apply rainflow counting on stress time series.

   (e) Apply safety factor γ_{Mf} = 1.25 to stress range.

   (f) Apply Palmgren-Miner rule to calculate damage at hot spot locations (S-N material curves in App. E, Fig. E.2).

   (g) Redo (a) - (f) for remaining five wind turbulence and wave seeds.

   (h) Accumulate damage of all six 10-minute simulations to one hour. Extrapolate one hour to 20-years lifetime, based on occurrence in lifetime. (see Tab. C.1).

   (i) Redo (a)-(h) for remaining four wind-wave scenarios. Accumulate damage to obtain total damage per hot spot location.

Comments:

- X-joint: Damage for X-joints will be evaluated for two cases, which differ by continuous and discontinuous member allocation (see Fig. D.2).
- Both joints: Both in-plane and out-of-plane moments taken into account (according to DNVGL-RP-C203 [21]).
- Both joints: Both saddle and crown locations (toe and heel) along the circumference of a weld are checked.

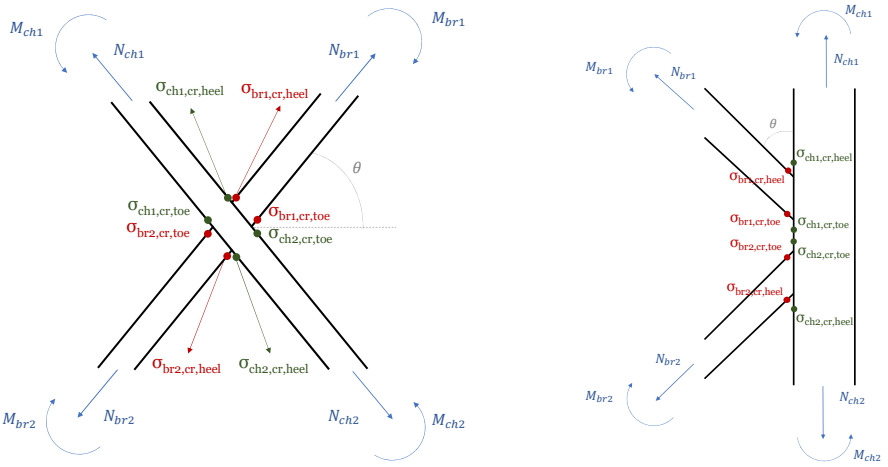

(a) Schematic of X-Joint. (b) Schematic of K-Joint.

Figure D.1: Schematic picture of joints including hot spot stress points. The saddle points are not shown.

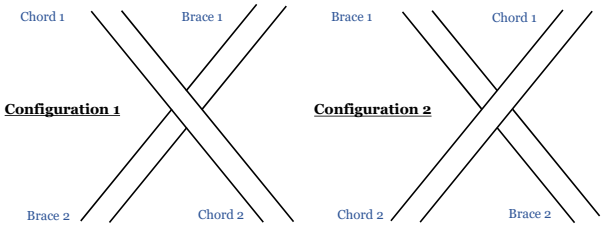

Figure D.2: Schematic indicating discontinuous and continuous member configuration for two analysed configurations. The distinction between chord 1 and chord 2 is for calculation only, as in reality this member is continuous.

D.2. Ultimate limit state

1. Run simulation for 3 different scenarios with corresponding extreme wind and wave conditions (see Tab. C.3 and Fig. C.3). Six simulations are performed per scenario with different wind turbulence and wave seeds.
   (a) Obtain normal force and bending moment time series at elements in back and side plane. All nodes of elements are located at either K- or X-joints. For K1-joint in the front plane, only a single node is located at the joint (for clarity and compactness, not treated in the procedure below).
      i. 44 elements :
         2x $N-t$, 2x $M_{\text{ip}}-t$, 2x $M_{\text{op}}-t$ per element.
   (b) Perform ULS check for joint punching shear and chord face failure [49].
   (c) Perform ULS check for tension yielding and local and global member buckling [50, 51].
   (d) Redo (a) - (c) for remaining five wind turbulence and wave seeds.
   (e) Redo (a) - (d) for remaining two wind-wave scenarios.

Comments:

- Joints: Shear in a gap of a joint is neglected as force is expected to be negligible.
- Elements: For local buckling, only meridional stress is checked as circumferential and shear stress unity checks are expected to be negligible. Circumferential stress is checked in the discussion of Ch. 6.
- Elements: For buckling, the system length is equal to the length between the nodes and joint cans are ignored. This is a conservative assumption.
- Elements: For global buckling, secondary moments are ignored as the influence is expected to be small.

E

S-N curves

In this section, the S-N curves used for fatigue calculations are presented. Curves are valid for steel structures in seawater with cathodic protection [21].

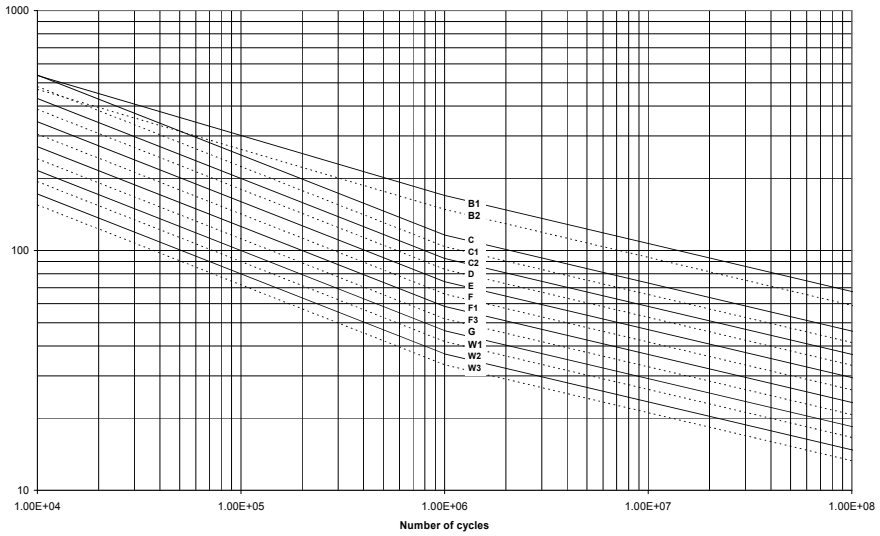

S-N curve	$N \leq 10^6$ cycles		$N > 10^6$ cycles	Fatigue limit at 10^7 cycles (MPa) *)	Thickness exponent k	Structural stress concentration embedded in the detail (S-N class), see also equation (2.3.2)
	m_1	$\log \bar{a}_1$	$\log \bar{a}_2$ $m_2 = 5.0$			
B1	4.0	14.917	17.146	106.97	0	
B2	4.0	14.685	16.856	93.59	0	
C	3.0	12.192	16.320	73.10	0.05	
C1	3.0	12.049	16.081	65.50	0.10	
C2	3.0	11.901	15.835	58.48	0.15	
D	3.0	11.764	15.606	52.63	0.20	1.00
E	3.0	11.610	15.350	46.78	0.20	1.13
F	3.0	11.455	15.091	41.52	0.25	1.27
F1	3.0	11.299	14.832	36.84	0.25	1.43
F3	3.0	11.146	14.576	32.75	0.25	1.61
G	3.0	10.998	14.330	29.24	0.25	1.80
W1	3.0	10.861	14.101	26.32	0.25	2.00
W2	3.0	10.707	13.845	23.39	0.25	2.25
W3	3.0	10.570	13.617	21.05	0.25	2.50
*) see also [2.11]						

Figure E.1: S-N curve for mild strength steel base material (B1), and circumferential butt weld (C1) for steel in seawater with cathodic protection [DNVGL-ST-C203, 2016].

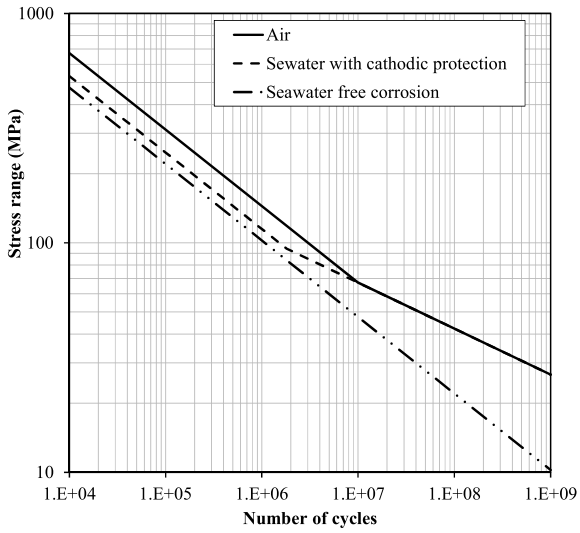

Environment	m_1	$\log \bar{a}_1$	m_2	$\log \bar{a}_2$	*Fatigue limit at 10^7 cycles (MPa)*)*	*Thickness exponent k*
Air	N ≤ 10^7 cycles		N > 10^7 cycles			
	3.0	12.48	5.0	16.13	67.09	0.25
Seawater with cathodic protection	N ≤ $1.8 \cdot 10^6$ cycles		N > $1.8 \cdot 10^6$ cycles			
	3.0	12.18	5.0	16.13	67.09	0.25
Seawater free corrosion	3.0	12.03	3.0	12.03	0	0.25
*) see also [2.11]						

Figure E.2: S-N curves for steel tubular joints in seawater with cathodic protection [DNVGL-ST-C203, 2016].

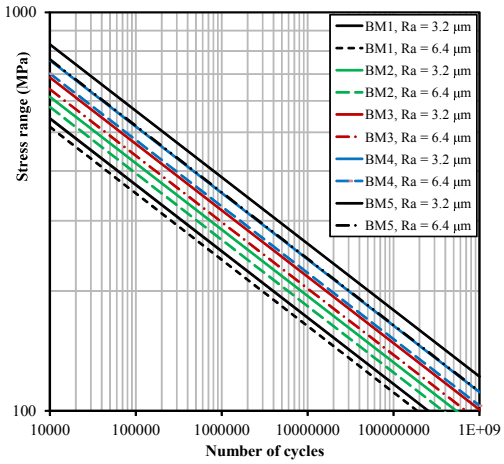

S-N curve	*Tensile strength in MPa (ksi)*	*Typical yield strength for the given tensile strength in MPa (ksi)*	$\log \bar{a}$ $m = 6.0$	
			Ra ≤ 3.2 µm	*Ra ≤ 6.4 µm*
BM1	Including and above 517 (75) Up to 586 (85)	448 (65) and below	20.002	19.875
BM2	Including and above 586 (85) Up to 655 (95)	448 (65) - 586 (85)	20.328	20.176
BM3	Including and above 655 (95) Up to 724 (105)	552 (80) - 665 (95)	20.618	20.442
BM4	Including and above 724 (105) Up to 793 (115)	586 (85) - 689 (100)	20.879	20.678

Figure E.3: S-N curves for steel base material for high strength steel [DNVGL-ST-C203, 2016].

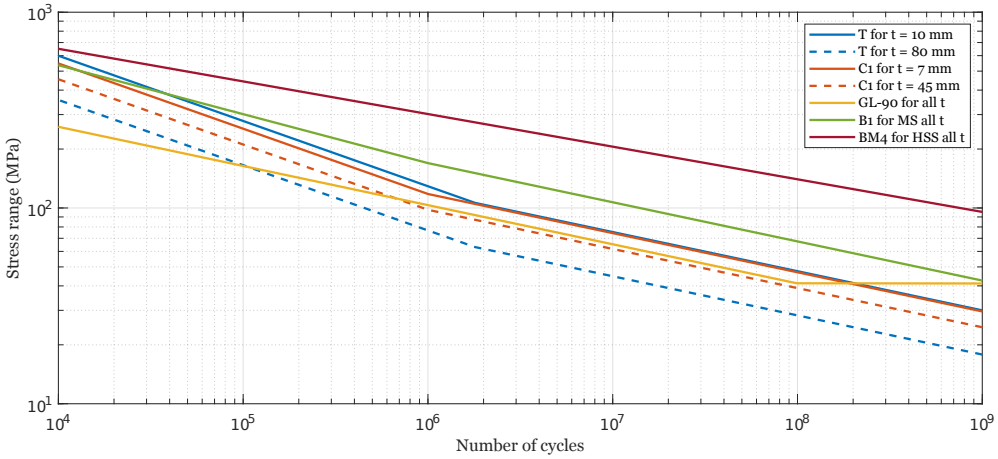

Figure E.4: S-N curves for welded joints and base material. Curve GL-90 is applied in the UpWind project for both tubular joints and circumferential welds and is independent on both thickness and steel base material. Curve T (tubular joints) and C1 (circumferential welds) are used in this MSc thesis (case 1) and are thickness dependent and independent of steel base material. Curve B1 and BM4 show thickness independent curves for unwelded base material for respectively mild S355 steel and high strength S690 steel, used for case 2 of this MSc thesis.

F

Main results

In this section, the main results for case 1, case 2 and case 3 are given (see Tab. 4.11). Both joint FLS, element FLS, joint ULS and member ULS unity checks are indicated. For case 3, the wrapping thickness is indicated. For all structures, the total steel weight of the jacket structure is given. Note, the weight excludes the mudbrace and elements below bottom Y-joint (see Fig. 4.1 and Fig. 5.1).

Case 1a: Optimised welded structure (Mild steel)

Fatigue S-N curve:
Joints: T *Members: C1*

Yield strength: 355 MPa

Jacket mass

	Steel mass [t]
Legs	309.7
Braces	153.1
Total	462.8

Joint fatigue

Joint description				*Steel thickness [mm]*	*Unity check*
K-joint	K1	Brace	Top	19.5	0.96
			Bottom	25	0.98
		Leg	Top	78	0.92
			Bottom	78	1.00
	K2	Brace	Top	13	0.99
			Bottom	12.5	0.95
		Leg	Top	60	1.00
			Bottom	60	0.32
	K3	Brace	Top	14.5	0.99
			Bottom	14	0.91
		Leg	Top	52	0.91
			Bottom	52	0.96
X-joint	X1			31	0.95
	X2			29.5	0.95
	X3			27.5	0.99
	X4			27.5	0.90
				Average	**0.92**

Element fatigue

Element description			*Steel thickness [mm]*		*Unity check*
			Can	*Member*	
Legs	Level 1	Member - top can	78	44.5	0.99
	Level 2	Bottom can - member	78	40.5	0.99
		Member - top can	60	40.5	0.49
	Level 3	Bottom can - member	60	33	0.96
		Member - top can	52	33	0.59
	Level 4	Bottom can - member	52	27.5	0.93
Braces	Level 1	Member - X-joint can	31	12.5	0.90
		Member - top K-joint can	25	12.5	0.68
	Level 2	Bottom K-joint can - member	19.5	11	0.34
		Member - X-joint can	29.5	11	0.76
		Member - top K-joint can	12.5	11	0.03
	Level 3	Bottom K-joint can - member	13	9.5	0.12
		Member - X-joint can	27.5	9.5	0.81
		Member - top K-joint can	14	9.5	0.14
	Level 4	Bottom K-joint can - member	14.5	10	0.07
		Member - X-joint can	27.5	10	0.95
				Average	**0.61**

Notes:
Thickness of both element and cans is altered in steps of 0.5 mm.
Element thickness constant for both a single leg and a single brace.
To avoid extra welding and extra stress concentration, leg can thickness for elements within a single joint equal.
Low utilisation ratio's of certain elements/joints are due to element thickness governed by other side of same element.
No benefit of using high strength steel as weld fatigue curves are not dependent on yield strength of base material.

Joint extreme:

Joint description				*Steel thickness [mm]*	*Unity check*
K-Joints	K1	Front	Bottom brace	25	0.05
			Top brace	19.5	0.03
		Side	Bottom brace	25	0.06
			Top brace	19.5	0.05
		Back	Bottom brace	25	0.05
			Top brace	19.5	0.04
	K2	Side	Bottom brace	12.5	0.07
			Top brace	13	0.06
		Back	Bottom brace	12.5	0.06
			Top brace	13	0.06
	K3	Side	Bottom brace	14	0.06
			Top brace	14.5	0.07
		Back	Bottom brace	14	0.06
			Top brace	14.5	0.05
X-Joints	X1	Side		31	0.31
		Back		31	0.26
	X2	Side		29.5	0.21
		Back		29.5	0.16
	X3	Side		27.5	0.17
		Back		27.5	0.16
	X4	Side		27.5	0.18
		Back		27.5	0.14
			Average		**0.11**

Member extreme:

Element description			*Steel thickness [mm]*	*Unity check*		
				Tension yielding	*Local buckling*	*Global buckling*
Legs	Level 1	Front	44.5	0.09	0.36	0.39
		Back	44.5	0.12	0.40	0.45
	Level 2	Front	40.5	0.03	0.33	0.37
		Back	40.5	0.09	0.37	0.41
	Level 3	Front	33	0.02	0.37	0.40
		Back	33	0.10	0.39	0.42
	Level 4	Front	27.5	0.02	0.43	0.46
		Back	27.5	0.12	0.42	0.45
Braces	Level 1	Side	12.5	0.41	0.59	0.66
		Back	12.5	0.31	0.45	0.49
	Level 2	Side	11	0.35	0.42	0.47
		Back	11	0.28	0.38	0.40
	Level 3	Side	9.5	0.38	0.38	0.45
		Back	9.5	0.30	0.33	0.40
	Level 4	Side	10	0.19	0.42	0.48
		Back	10	0.18	0.37	0.42
		Average		**0.19**	**0.40**	**0.44**

Case 1b: Optimised welded structure (High strength steel)

Fatigue S-N curve:
Joints: T *Members: C1*

Yield strength: 690 MPa

Jacket mass

	Steel mass [t]
Legs	309.7
Braces	153.1
Total	462.8

Joint fatigue

Joint description				*Steel thickness [mm]*	*Unity check*
K-joint	K1	Brace	Top	19.5	0.96
			Bottom	25	0.98
		Leg	Top	78	0.92
			Bottom	78	1.00
	K2	Brace	Top	13	0.99
			Bottom	12.5	0.95
		Leg	Top	60	1.00
			Bottom	60	0.32
	K3	Brace	Top	14.5	0.99
			Bottom	14	0.91
		Leg	Top	52	0.91
			Bottom	52	0.96
X-joint	X1			31	0.95
	X2			29.5	0.95
	X3			27.5	0.99
	X4			27.5	0.90
				Average	**0.92**

Element fatigue

Element description			*Steel thickness [mm]*		*Unity check*
			Can	*Member*	
Legs	Level 1	Member - top can	78	44.5	0.99
	Level 2	Bottom can - member	78	40.5	0.99
		Member - top can	60	40.5	0.49
	Level 3	Bottom can - member	60	33	0.96
		Member - top can	52	33	0.59
	Level 4	Bottom can - member	52	27.5	0.93
Braces	Level 1	Member - X-joint can	31	12.5	0.90
		Member - top K-joint can	25	12.5	0.68
	Level 2	Bottom K-joint can - member	19.5	11	0.34
		Member - X-joint can	29.5	11	0.76
		Member - top K-joint can	12.5	11	0.03
	Level 3	Bottom K-joint can - member	13	9.5	0.12
		Member - X-joint can	27.5	9.5	0.81
		Member - top K-joint can	14	9.5	0.14
	Level 4	Bottom K-joint can - member	14.5	10	0.07
		Member - X-joint can	27.5	10	0.95
				Average	**0.61**

Notes:
Thickness of both element and cans is altered in steps of 0.5 mm.
Element thickness constant for both a single leg and a single brace.
To avoid extra welding and extra stress concentration, leg can thickness for elements within a single joint equal.
Low utilisation ratio's of certain elements/joints are due to element thickness governed by other side of same element.
No benefit of using high strength steel as weld fatigue curves are not dependent on yield strength of base material.

Joint extreme:

Joint description				*Steel thickness [mm]*	*Unity check*
K-Joints	K1	Front	Bottom brace	25	0.03
			Top brace	19.5	0.01
		Side	Bottom brace	25	0.03
			Top brace	19.5	0.02
		Back	Bottom brace	25	0.03
			Top brace	19.5	0.02
	K2	Side	Bottom brace	12.5	0.03
			Top brace	13	0.03
		Back	Bottom brace	12.5	0.03
			Top brace	13	0.03
	K3	Side	Bottom brace	14	0.03
			Top brace	14.5	0.03
		Back	Bottom brace	14	0.03
			Top brace	14.5	0.03
X-Joints	X1	Side		31	0.16
		Back		31	0.13
	X2	Side		29.5	0.11
		Back		29.5	0.08
	X3	Side		27.5	0.09
		Back		27.5	0.08
	X4	Side		27.5	0.09
		Back		27.5	0.07
			Average		**0.05**

Member extreme:

Element description			*Steel thickness [mm]*	*Unity check*		
				Tension yielding	*Local buckling*	*Global buckling*
Legs	Level 1	Front	44.5	0.05	0.20	0.26
		Back	44.5	0.06	0.22	0.30
	Level 2	Front	40.5	0.02	0.18	0.24
		Back	40.5	0.05	0.20	0.27
	Level 3	Front	33	0.01	0.21	0.26
		Back	33	0.05	0.22	0.27
	Level 4	Front	27.5	0.01	0.24	0.29
		Back	27.5	0.06	0.24	0.28
Braces	Level 1	Side	12.5	0.21	0.34	0.41
		Back	12.5	0.16	0.26	0.31
	Level 2	Side	11	0.18	0.25	0.29
		Back	11	0.15	0.22	0.24
	Level 3	Side	9.5	0.19	0.22	0.27
		Back	9.5	0.15	0.19	0.25
	Level 4	Side	10	0.10	0.25	0.31
		Back	10	0.09	0.22	0.27
		Average		**0.10**	**0.23**	**0.28**

Case 2a: Wrapped FRP structure - Idealistic (Mild steel)

Fatigue S-N curve:
Joints: Inf *Members: B1*

Yield strength: 355 MPa

Jacket mass

	Steel mass [t]
Legs	124.2
Braces	60.6
Total	184.8

Joint fatigue

Joints assumed not governing for design. This is an idealistic boundary case.

Element fatigue

Element description			*Steel thickness [mm]* *Member*	*Unity check*
Legs	Level 1	Top	21.5	0.17
	Level 2	Bottom	18.5	0.18
		Top	18.5	0.19
	Level 3	Bottom	16	0.17
		Top	16	0.16
	Level 4	Bottom	14.5	0.11
Braces	Level 1	Around X-joint	9	0.02
		Top	9	0.02
	Level 2	Bottom	6	0.06
		Around X-joint	6	0.05
		Top	6	0.04
	Level 3	Bottom	5	0.06
		Around X-joint	5	0.07
		Top	5	0.06
	Level 4	Bottom	5.5	0.02
		Around X-joint	5.5	0.06
			Average	**0.09**

Joint extreme:

Procedure of steel joint failure (chord face failure and punching shear failure) not applicable to wrapped FRP joints. Joint extreme resistance is checked by tension yielding of elements (see table below).

Average UC Joints: **0.32**

Joint and member extreme:

Element description			*Steel thickness [mm]*	*Unity check* *Tension yielding*	*Local buckling*	*Global buckling*
Legs	Level 1	Front	21.5	0.17	0.74	0.86
		Back	21.5	0.22	0.83	0.99
	Level 2	Front	18.5	0.06	0.74	0.87
		Back	18.5	0.18	0.83	0.97
	Level 3	Front	16	0.04	0.83	0.94
		Back	16	0.21	0.87	0.99
	Level 4	Front	14.5	0.04	0.88	0.99
		Back	14.5	0.22	0.87	0.97
Braces	Level 1	Side	9	0.56	0.86	0.95
		Back	9	0.43	0.66	0.71
	Level 2	Side	6	0.64	0.87	0.96
		Back	6	0.51	0.78	0.81
	Level 3	Side	5	0.70	0.84	0.98
		Back	5	0.56	0.72	0.88
	Level 4	Side	5.5	0.35	0.88	0.99
		Back	5.5	0.31	0.77	0.87
			Average	**0.32**	**0.81**	**0.92**

Case 2b: Wrapped FRP structure - Idealistic (High strength steel)

Fatigue S-N curve:
Joints: Inf *Members: BM4*

Yield strength: 690 MPa

Jacket mass

	Steel mass [t]
Legs	89.3
Braces	49.2
Total	138.5

Joint fatigue

Joints assumed not governing for design. This is an idealistic boundary case.

Element fatigue

Element description			*Steel thickness [mm]*	*Unity check*
			Member	
Legs	Level 1	Top	15.5	0.01
	Level 2	Bottom	13	0.02
		Top	13	0.02
	Level 3	Bottom	11.5	0.02
		Top	11.5	0.02
	Level 4	Bottom	10.5	0.01
Braces	Level 1	Around X-joint	6.5	0.00
		Top	6.5	0.00
	Level 2	Bottom	5	0.00
		Around X-joint	5	0.00
		Top	5	0.00
	Level 3	Bottom	4.5	0.00
		Around X-joint	4.5	0.00
		Top	4.5	0.00
	Level 4	Bottom	5	0.00
		Around X-joint	5	0.00
			Average	**0.01**

Joint extreme:

Procedure of steel joint failure (chord face failure and punching shear failure) not applicable to wrapped FRP joints. Joint extreme resistance is checked by tension yielding of elements (see table below).

Average UC Joints: **0.21**

Joint and member extreme:

Element description			*Steel thickness [mm]*	*Unity check*		
				Tension yielding	*Local buckling*	*Global buckling*
Legs	Level 1	Front	15.5	0.12	0.63	0.85
		Back	15.5	0.16	0.71	0.97
	Level 2	Front	13	0.04	0.68	0.88
		Back	13	0.13	0.75	0.98
	Level 3	Front	11.5	0.03	0.76	0.92
		Back	11.5	0.15	0.79	0.97
	Level 4	Front	10.5	0.03	0.81	0.96
		Back	10.5	0.16	0.80	0.94
Braces	Level 1	Side	6.5	0.39	0.81	0.95
		Back	6.5	0.30	0.62	0.72
	Level 2	Side	5	0.39	0.75	0.85
		Back	5	0.32	0.68	0.73
	Level 3	Side	4.5	0.40	0.68	0.81
		Back	4.5	0.32	0.59	0.74
	Level 4	Side	5	0.20	0.67	0.84
		Back	5	0.18	0.59	0.72
			Average	**0.21**	**0.71**	**0.87**

Case 3a: Wrapped FRP structure - Realistic (Mild steel)

Fatigue S-N curve:
Joints: Inf *Leg members: C1* *Brace members: B1*

Yield strength: 355 MPa

Jacket mass

	Steel mass [t]
Legs	137.6
Braces	60.6
Total	198.2

Joint fatigue

Joint description				*FRP Wrapping thickness [mm]*	*Wrapping length [mm]*	*Unity check*
K-joint	K1	Brace	Top	22.5	1200	0.78
			Bottom	25.5	1200	0.93
	K2	Brace	Top	18	1200	0.68
			Bottom	18	1200	0.67
	K3	Brace	Top	19.5	1200	0.96
			Bottom	19.5	1200	0.83
X-joint	X1			25.5	1200	1.00
	X2			22.5	1200	0.78
	X3			19.5	1200	0.88
	X4			22.5	1200	0.78
				Average		**0.83**

Element fatigue

Element description			*Steel thickness [mm]* *Member*	*Unity check*
Legs	Level 1	Top	25	0.95
	Level 2	Middle	21	0.92
	Level 3	Middle	17	0.88
	Level 4	Bottom	14.5	0.94
Braces	Level 1	Around X-joint	9	0.02
		Top	9	0.02
	Level 2	Bottom	6	0.06
		Around X-joint	6	0.05
		Top	6	0.04
	Level 3	Bottom	5	0.06
		Around X-joint	5	0.07
		Top	5	0.06
	Level 4	Bottom	5.5	0.02
		Around X-joint	5.5	0.06
			Average	**0.30**

Notes
Thickness of FRP wrapping is changed in steps of 1.5 mm.
Wrapping length measured from weld heel.
Thickness of steel is changed in steps of 0.5 mm.

Joint extreme:

Procedure of steel joint failure (chord face failure and punching shear failure) not applicable to wrapped FRP joints. Joint extreme resistance is checked by tension yielding of elements (see table below).

Average UC Joints: **0.32**

Joint and member extreme:

Element description			*Steel thickness [mm]*	*Unity check*		
				Tension yielding	*Local buckling*	*Global buckling*
Legs	Level 1	Front	25	0.15	0.63	0.73
		Back	25	0.19	0.71	0.84
	Level 2	Front	21	0.05	0.64	0.76
		Back	21	0.16	0.72	0.84
	Level 3	Front	17	0.03	0.77	0.88
		Back	17	0.20	0.81	0.92
	Level 4	Front	14.5	0.04	0.88	0.99
		Back	14.5	0.22	0.87	0.97
Braces	Level 1	Side	9	0.56	0.86	0.95
		Back	9	0.43	0.66	0.71
	Level 2	Side	6	0.64	0.87	0.96
		Back	6	0.51	0.78	0.81
	Level 3	Side	5	0.70	0.84	0.98
		Back	5	0.56	0.72	0.88
	Level 4	Side	5.5	0.35	0.88	0.99
		Back	5.5	0.31	0.77	0.87
			Average	**0.32**	**0.78**	**0.88**

Case 3b: Wrapped FRP structure - Realistic (High strength steel)

Fatigue S-N curve:
Joints: Inf *Leg members: C1* *Brace members: BM4*

Yield strength: 355 MPa

Jacket mass

	Steel mass [t]
Legs	137.6
Braces	49.2
Total	186.8

Joint fatigue

Joint description				*FRP Wrapping thickness [mm]*	*Wrapping length [mm]*	*Unity check*
K-joint	K1	Brace	Top	22.5	1200	0.78
			Bottom	25.5	1200	0.93
	K2	Brace	Top	18	1200	0.68
			Bottom	18	1200	0.67
	K3	Brace	Top	19.5	1200	0.96
			Bottom	19.5	1200	0.83
X-joint	X1			25.5	1200	1.00
	X2			22.5	1200	0.78
	X3			19.5	1200	0.88
	X4			22.5	1200	0.78
			Average			**0.83**

Element fatigue

Element description			*Steel thickness [mm]*	*Unity check*
			Member	
Legs	Level 1	Top	25	0.95
	Level 2	Middle	21	0.92
	Level 3	Middle	17	0.88
	Level 4	Bottom	14.5	0.94
Braces	Level 1	Around X-joint	6.5	0.00
		Top	6.5	0.00
	Level 2	Bottom	5	0.00
		Around X-joint	5	0.00
		Top	5	0.00
	Level 3	Bottom	4.5	0.00
		Around X-joint	4.5	0.00
		Top	4.5	0.00
	Level 4	Bottom	5	0.00
		Around X-joint	5	0.00
		Average		**0.26**

Notes
Thickness of FRP wrapping is changed in steps of 1.5 mm.
Thickness of FRP wrapping equal to case 3a.
Wrapping length measured from weld heel.
Thickness of steel is changed in steps of 0.5 mm.

Joint extreme:

Procedure of steel joint failure (chord face failure and punching shear failure) not applicable to wrapped FRP joints. Joint extreme resistance is checked by tension yielding of elements (see table below).

Average UC Joints: **0.19**

Joint and member extreme:

Element description			*Steel thickness [mm]*	*Unity check*		
				Tension yielding	*Local buckling*	*Global buckling*
Legs	Level 1	Front	25	0.08	0.35	0.48
		Back	25	0.10	0.40	0.55
	Level 2	Front	21	0.03	0.37	0.48
		Back	21	0.08	0.41	0.54
	Level 3	Front	17	0.02	0.45	0.56
		Back	17	0.10	0.47	0.58
	Level 4	Front	14.5	0.02	0.52	0.62
		Back	14.5	0.11	0.51	0.61
Braces	Level 1	Side	6.5	0.39	0.81	0.95
		Back	6.5	0.30	0.62	0.72
	Level 2	Side	5	0.39	0.75	0.85
		Back	5	0.32	0.68	0.73
	Level 3	Side	4.5	0.40	0.68	0.81
		Back	4.5	0.32	0.59	0.74
	Level 4	Side	5	0.20	0.67	0.84
		Back	5	0.18	0.59	0.72
			Average	**0.19**	**0.56**	**0.67**

G

Detailed results

G.1. FLS welded structure: Utilisation tables per scenario

In this section, detailed fatigue utilisation factors are given for the steel welded structure (case 1). Damage due to individual wind-wave scenarios can be seen. S-N curves and SCFs applied can be seen in Tab. 4.11.

Important and maximum values are highlighted.

Highlighted in red: In extensive tables, maximum total damage values per element. In summary tables, damage values above 0.9.

Highlighted in yellow: In extensive tables, damage belonging to wind-wave scenario causing most damage to hot spot location. In summary sheet, damage belonging the wind-wave scenario causing most damage to member.

In final table, colours indicate harmfulness of scenario. The darker the red, the more harmful. The darker the green, the less harmful.

Case 1a: X-Joint - cans

X1 case 1 (t_{br} = 31mm, t_{ch} = 31mm)

	Brace 1 (top)				Brace 2 (bottom)				Chord 1 (top)				Chord 2 (bottom)			
V_{wind}	Cr toe	Cr heel	Sa si1	Sa si2	Cr toe	Cr heel	Sa si1	Sa si2	Cr toe	Cr heel	Sa si1	Sa si2	Cr toe	Cr heel	Sa si1	Sa si2
1 - 9	0.037	0.005	0.002	0.024	0.070	0.000	0.009	0.011	0.039	0.053	0.020	0.306	0.005	0.000	0.092	0.112
9 - 15	0.004	0.008	0.001	0.001	0.004	0.000	0.001	0.001	0.001	0.075	0.011	0.015	0.001	0.000	0.012	0.012
15 - 19	0.056	0.037	0.013	0.015	0.078	0.001	0.012	0.016	0.046	0.350	0.151	0.172	0.012	0.002	0.117	0.154
19 - 25	0.135	0.045	0.032	0.039	0.264	0.002	0.031	0.050	0.172	0.394	0.358	0.432	0.024	0.005	0.279	0.482
25 - 31	0.005	0.000	0.001	0.002	0.010	0.000	0.001	0.002	0.008	0.003	0.009	0.026	0.001	0.000	0.011	0.016
Total	0.236	0.095	0.049	0.082	0.426	0.002	0.055	0.079	0.266	0.876	0.550	0.951	0.043	0.007	0.512	0.776

X1 case 2 (t_{br} = 31mm, t_{ch} = 31mm)

	Brace 1 (top)				Brace 2 (bottom)				Chord 1 (top)				Chord 2 (bottom)			
V_{wind}	Cr toe	Cr heel	Sa si1	Sa si2	Cr toe	Cr heel	Sa si1	Sa si2	Cr toe	Cr heel	Sa si1	Sa si2	Cr toe	Cr heel	Sa si1	Sa si2
1 - 9	0.039	0.005	0.025	0.003	0.070	0.000	0.009	0.011	0.040	0.050	0.310	0.030	0.006	0.000	0.090	0.115
9 - 15	0.005	0.007	0.001	0.001	0.003	0.000	0.001	0.001	0.002	0.077	0.011	0.009	0.001	0.000	0.009	0.010
15 - 19	0.067	0.033	0.014	0.009	0.072	0.001	0.017	0.010	0.045	0.356	0.162	0.105	0.015	0.002	0.170	0.098
19 - 25	0.182	0.041	0.033	0.029	0.227	0.001	0.045	0.028	0.164	0.406	0.373	0.324	0.035	0.004	0.444	0.255
25 - 31	0.005	0.000	0.002	0.001	0.011	0.000	0.002	0.001	0.008	0.003	0.030	0.007	0.001	0.000	0.020	0.010
Total	0.297	0.086	0.076	0.042	0.384	0.002	0.074	0.051	0.259	0.891	0.886	0.475	0.059	0.007	0.733	0.487

X2 case 1 (t_{br} = 29.5mm, t_{ch} = 29.5mm)

	Brace 1 (top)				Brace 2 (bottom)				Chord 1 (top)				Chord 2 (bottom)			
V_{wind}	Cr toe	Cr heel	Sa si1	Sa si2	Cr toe	Cr heel	Sa si1	Sa si2	Cr toe	Cr heel	Sa si1	Sa si2	Cr toe	Cr heel	Sa si1	Sa si2
1 - 9	0.013	0.001	0.010	0.008	0.023	0.005	0.031	0.002	0.010	0.002	0.107	0.079	0.003	0.048	0.382	0.015
9 - 15	0.001	0.002	0.001	0.000	0.007	0.007	0.001	0.000	0.004	0.008	0.009	0.002	0.000	0.062	0.010	0.002
15 - 19	0.013	0.006	0.006	0.002	0.053	0.031	0.010	0.002	0.027	0.028	0.067	0.024	0.001	0.287	0.125	0.016
19 - 25	0.020	0.009	0.014	0.006	0.082	0.041	0.024	0.004	0.040	0.037	0.157	0.059	0.002	0.327	0.292	0.041
25 - 31	0.001	0.000	0.001	0.000	0.001	0.000	0.002	0.000	0.001	0.000	0.008	0.005	0.000	0.004	0.026	0.002
Total	0.048	0.018	0.031	0.017	0.166	0.084	0.068	0.008	0.080	0.075	0.348	0.169	0.007	0.728	0.835	0.076

X2 case 2 (t_{br} = 29.5mm, t_{ch} = 29.5mm)

	Brace 1 (top)				Brace 2 (bottom)				Chord 1 (top)				Chord 2 (bottom)			
V_{wind}	Cr toe	Cr heel	Sa si1	Sa si2	Cr toe	Cr heel	Sa si1	Sa si2	Cr toe	Cr heel	Sa si1	Sa si2	Cr toe	Cr heel	Sa si1	Sa si2
1 - 9	0.014	0.001	0.007	0.010	0.020	0.006	0.002	0.033	0.009	0.002	0.073	0.113	0.003	0.052	0.014	0.411
9 - 15	0.002	0.002	0.000	0.001	0.006	0.008	0.000	0.001	0.004	0.010	0.002	0.010	0.000	0.078	0.002	0.011
15 - 19	0.016	0.006	0.002	0.006	0.047	0.037	0.002	0.012	0.029	0.034	0.020	0.065	0.002	0.338	0.015	0.150
19 - 25	0.028	0.010	0.005	0.014	0.060	0.048	0.004	0.029	0.033	0.045	0.052	0.156	0.003	0.395	0.036	0.348
25 - 31	0.001	0.000	0.000	0.001	0.002	0.001	0.000	0.002	0.001	0.000	0.005	0.008	0.000	0.004	0.002	0.027
Total	0.062	0.019	0.015	0.032	0.135	0.100	0.008	0.077	0.075	0.091	0.152	0.352	0.009	0.867	0.068	0.947

Case 1a: X-Joint - cans (continued)

X3 case 1 (t_{br} = 27.5mm, t_{ch} = 27.5mm)

	Brace 1 (top)				Brace 2 (bottom)				Chord 1 (top)				Chord 2 (bottom)			
V_{wind}	Cr toe	Cr heel	Sa si1	Sa si2	Cr toe	Cr heel	Sa si1	Sa si2	Cr toe	Cr heel	Sa si1	Sa si2	Cr toe	Cr heel	Sa si1	Sa si2
1 - 9	0.013	0.002	0.018	0.017	0.018	0.001	0.024	0.019	0.014	0.012	0.223	0.219	0.006	0.005	0.298	0.231
9 - 15	0.006	0.006	0.003	0.002	0.003	0.002	0.003	0.002	0.001	0.054	0.048	0.029	0.005	0.011	0.047	0.026
15 - 19	0.030	0.018	0.013	0.010	0.019	0.007	0.015	0.010	0.007	0.138	0.183	0.142	0.016	0.037	0.213	0.135
19 - 25	0.041	0.026	0.025	0.021	0.034	0.010	0.031	0.019	0.012	0.174	0.335	0.269	0.021	0.045	0.402	0.237
25 - 31	0.001	0.000	0.002	0.002	0.001	0.000	0.002	0.002	0.001	0.001	0.023	0.029	0.001	0.001	0.029	0.024
Total	0.091	0.052	0.061	0.053	0.075	0.020	0.076	0.051	0.035	0.379	0.812	0.689	0.048	0.099	0.989	0.652

X3 case 2 (t_{br} = 27.5mm, t_{ch} = 27.5mm)

	Brace 1 (top)				Brace 2 (bottom)				Chord 1 (top)				Chord 2 (bottom)			
V_{wind}	Cr toe	Cr heel	Sa si1	Sa si2	Cr toe	Cr heel	Sa si1	Sa si2	Cr toe	Cr heel	Sa si1	Sa si2	Cr toe	Cr heel	Sa si1	Sa si2
1 - 9	0.015	0.002	0.017	0.018	0.018	0.001	0.018	0.023	0.018	0.013	0.218	0.225	0.009	0.007	0.217	0.291
9 - 15	0.008	0.006	0.002	0.003	0.003	0.002	0.001	0.003	0.001	0.057	0.022	0.041	0.008	0.018	0.017	0.038
15 - 19	0.035	0.019	0.008	0.013	0.019	0.008	0.007	0.016	0.009	0.160	0.103	0.175	0.022	0.046	0.090	0.215
19 - 25	0.057	0.027	0.016	0.025	0.028	0.011	0.014	0.033	0.012	0.190	0.204	0.322	0.032	0.056	0.169	0.416
25 - 31	0.001	0.000	0.002	0.002	0.001	0.000	0.002	0.002	0.001	0.001	0.027	0.027	0.001	0.001	0.023	0.032
Total	0.116	0.053	0.044	0.060	0.068	0.023	0.041	0.077	0.041	0.421	0.574	0.789	0.071	0.127	0.515	0.992

X4 case 1 (t_{br} = 27.5mm, t_{ch} = 27.5mm)

	Brace 1 (top)				Brace 2 (bottom)				Chord 1 (top)				Chord 2 (bottom)			
V_{wind}	Cr toe	Cr heel	Sa si1	Sa si2	Cr toe	Cr heel	Sa si1	Sa si2	Cr toe	Cr heel	Sa si1	Sa si2	Cr toe	Cr heel	Sa si1	Sa si2
1 - 9	0.003	0.000	0.010	0.006	0.008	0.001	0.012	0.008	0.007	0.000	0.123	0.069	0.001	0.001	0.138	0.091
9 - 15	0.000	0.000	0.006	0.000	0.018	0.001	0.005	0.001	0.057	0.002	0.082	0.003	0.003	0.013	0.059	0.007
15 - 19	0.002	0.001	0.020	0.004	0.058	0.006	0.016	0.006	0.132	0.004	0.256	0.034	0.007	0.040	0.192	0.064
19 - 25	0.005	0.002	0.036	0.008	0.091	0.009	0.031	0.013	0.180	0.005	0.432	0.081	0.011	0.047	0.366	0.135
25 - 31	0.000	0.000	0.001	0.000	0.001	0.000	0.001	0.000	0.001	0.000	0.008	0.004	0.000	0.000	0.010	0.005
Total	0.010	0.005	0.073	0.019	0.176	0.017	0.064	0.028	0.377	0.012	0.900	0.192	0.022	0.101	0.766	0.303

X4 case 2 (t_{br} = 27.5mm, t_{ch} = 27.5mm)

	Brace 1 (top)				Brace 2 (bottom)				Chord 1 (top)				Chord 2 (bottom)			
V_{wind}	Cr toe	Cr heel	Sa si1	Sa si2	Cr toe	Cr heel	Sa si1	Sa si2	Cr toe	Cr heel	Sa si1	Sa si2	Cr toe	Cr heel	Sa si1	Sa si2
1 - 9	0.002	0.000	0.006	0.009	0.006	0.001	0.007	0.011	0.005	0.000	0.065	0.110	0.001	0.002	0.082	0.127
9 - 15	0.000	0.000	0.000	0.005	0.015	0.002	0.001	0.004	0.054	0.002	0.004	0.066	0.003	0.013	0.007	0.052
15 - 19	0.002	0.001	0.003	0.018	0.052	0.006	0.005	0.014	0.132	0.005	0.030	0.225	0.007	0.039	0.057	0.179
19 - 25	0.005	0.003	0.008	0.031	0.067	0.010	0.011	0.029	0.148	0.006	0.076	0.373	0.009	0.054	0.118	0.338
25 - 31	0.000	0.000	0.000	0.001	0.001	0.000	0.000	0.001	0.001	0.000	0.004	0.008	0.000	0.000	0.005	0.011
Total	0.010	0.005	0.018	0.064	0.140	0.019	0.025	0.059	0.340	0.014	0.180	0.782	0.020	0.107	0.269	0.706

Case 1a: X-Joint - cans (maximum values)

X1 (t_{br} = 31mm, t_{ch} = 31mm)

Case 1

V_{wind}	Brace 1 Max	Brace 2 Max	Chord 1 Max	Chord 2 Max
1 - 9	0.037	0.070	0.306	0.112
9 - 15	0.004	0.004	0.015	0.012
15 - 19	0.056	0.078	0.172	0.154
19 - 25	0.135	0.264	0.432	0.482
25 - 31	0.005	0.010	0.026	0.016
Total	0.236	0.426	0.951	0.776

Case 2

V_{wind}	Brace 1 Max	Brace 2 Max	Chord 1 Max	Chord 2 Max
1 - 9	0.039	0.070	0.050	0.090
9 - 15	0.005	0.003	0.077	0.009
15 - 19	0.067	0.072	0.356	0.170
19 - 25	0.182	0.227	0.406	0.444
25 - 31	0.005	0.011	0.003	0.020
Total	0.297	0.384	0.891	0.733

X2 (t_{br} = 29.5mm, t_{ch} = 29.5mm)

Case 1

V_{wind}	Brace 1 Max	Brace 2 Max	Chord 1 Max	Chord 2 Max
1 - 9	0.013	0.023	0.107	0.382
9 - 15	0.001	0.007	0.009	0.010
15 - 19	0.013	0.053	0.067	0.125
19 - 25	0.020	0.082	0.157	0.292
25 - 31	0.001	0.001	0.008	0.026
Total	0.048	0.166	0.348	0.835

Case 2

V_{wind}	Brace 1 Max	Brace 2 Max	Chord 1 Max	Chord 2 Max
1 - 9	0.014	0.020	0.113	0.411
9 - 15	0.002	0.006	0.010	0.011
15 - 19	0.016	0.047	0.065	0.150
19 - 25	0.028	0.060	0.156	0.348
25 - 31	0.001	0.002	0.008	0.027
Total	0.062	0.135	0.352	0.947

X3 (t_{br} = 27.5mm, t_{ch} = 27.5mm)

Case 1

V_{wind}	Brace 1 Max	Brace 2 Max	Chord 1 Max	Chord 2 Max
1 - 9	0.013	0.024	0.223	0.298
9 - 15	0.006	0.003	0.048	0.047
15 - 19	0.030	0.015	0.183	0.213
19 - 25	0.041	0.031	0.335	0.402
25 - 31	0.001	0.002	0.023	0.029
Total	0.091	0.076	0.812	0.989

Case 2

V_{wind}	Brace 1 Max	Brace 2 Max	Chord 1 Max	Chord 2 Max
1 - 9	0.015	0.023	0.225	0.291
9 - 15	0.008	0.003	0.041	0.038
15 - 19	0.035	0.016	0.175	0.215
19 - 25	0.057	0.033	0.322	0.416
25 - 31	0.001	0.002	0.027	0.032
Total	0.116	0.077	0.789	0.992

X4 (t_{br} = 27.5mm, t_{ch} = 27.5mm)

Case 1

V_{wind}	Brace 1 Max	Brace 2 Max	Chord 1 Max	Chord 2 Max
1 - 9	0.010	0.008	0.123	0.138
9 - 15	0.006	0.018	0.082	0.059
15 - 19	0.020	0.058	0.256	0.192
19 - 25	0.036	0.091	0.432	0.366
25 - 31	0.001	0.001	0.008	0.010
Total	0.073	0.176	0.900	0.766

Case 2

V_{wind}	Brace 1 Max	Brace 2 Max	Chord 1 Max	Chord 2 Max
1 - 9	0.009	0.006	0.110	0.127
9 - 15	0.005	0.015	0.066	0.052
15 - 19	0.018	0.052	0.225	0.179
19 - 25	0.031	0.067	0.373	0.338
25 - 31	0.001	0.001	0.008	0.011
Total	0.064	0.140	0.782	0.706

Case 1a: X-Joint - members

X1 case 1 (t_{br} = 12.5mm, t_{ch} = 12.5mm)

	Brace 1 (top)				Brace 2 (bottom)				Chord 1 (top)				Chord 2 (bottom)			
V_{wind}	Point 1	Point 2	Point 3	Point 4	Point 1	Point 2	Point 3	Point 4	Point 1	Point 2	Point 3	Point 4	Point 1	Point 2	Point 3	Point 4
1 - 9	0.016	0.184	0.096	0.024	0.009	0.177	0.102	0.053	0.014	0.192	0.027	0.086	0.009	0.177	0.058	0.088
9 - 15	0.022	0.009	0.007	0.006	0.003	0.011	0.006	0.013	0.019	0.010	0.005	0.006	0.003	0.009	0.011	0.005
15 - 19	0.127	0.144	0.101	0.081	0.029	0.174	0.133	0.153	0.101	0.156	0.061	0.100	0.027	0.154	0.115	0.141
19 - 25	0.211	0.414	0.301	0.205	0.084	0.514	0.431	0.384	0.161	0.473	0.183	0.247	0.075	0.424	0.349	0.354
25 - 31	0.002	0.020	0.012	0.006	0.001	0.019	0.016	0.011	0.002	0.019	0.005	0.014	0.002	0.020	0.009	0.020
Total	0.378	0.770	0.516	0.322	0.126	0.896	0.689	0.613	0.296	0.851	0.281	0.452	0.115	0.784	0.542	0.608

X2 case 1 (t_{br} = 11mm, t_{ch} = 11mm)

	Brace 1 (top)				Brace 2 (bottom)				Chord 1 (top)				Chord 2 (bottom)			
V_{wind}	Point 1	Point 2	Point 3	Point 4	Point 1	Point 2	Point 3	Point 4	Point 1	Point 2	Point 3	Point 4	Point 1	Point 2	Point 3	Point 4
1 - 9	0.020	0.153	0.037	0.096	0.027	0.211	0.034	0.130	0.019	0.157	0.096	0.037	0.030	0.198	0.131	0.033
9 - 15	0.007	0.006	0.001	0.009	0.017	0.019	0.002	0.008	0.006	0.008	0.009	0.001	0.020	0.015	0.009	0.001
15 - 19	0.033	0.070	0.015	0.053	0.095	0.182	0.016	0.060	0.030	0.082	0.062	0.012	0.116	0.153	0.073	0.013
19 - 25	0.065	0.138	0.034	0.125	0.149	0.335	0.038	0.145	0.060	0.171	0.141	0.031	0.181	0.251	0.168	0.033
25 - 31	0.001	0.009	0.003	0.007	0.003	0.012	0.002	0.009	0.001	0.009	0.007	0.002	0.003	0.013	0.009	0.002
Total	0.126	0.377	0.090	0.290	0.290	0.759	0.092	0.352	0.117	0.427	0.316	0.084	0.349	0.630	0.391	0.083

X3 case 1 (t_{br} = 9.5mm, t_{ch} = 9.5mm)

	Brace 1 (top)				Brace 2 (bottom)				Chord 1 (top)				Chord 2 (bottom)			
V_{wind}	Point 1	Point 2	Point 3	Point 4	Point 1	Point 2	Point 3	Point 4	Point 1	Point 2	Point 3	Point 4	Point 1	Point 2	Point 3	Point 4
1 - 9	0.046	0.214	0.115	0.133	0.069	0.230	0.136	0.187	0.042	0.223	0.128	0.109	0.067	0.215	0.183	0.132
9 - 15	0.019	0.024	0.014	0.035	0.015	0.019	0.018	0.042	0.016	0.029	0.035	0.013	0.016	0.016	0.044	0.017
15 - 19	0.094	0.155	0.065	0.115	0.078	0.154	0.089	0.149	0.083	0.182	0.125	0.051	0.083	0.136	0.177	0.071
19 - 25	0.165	0.305	0.128	0.229	0.154	0.322	0.168	0.298	0.150	0.367	0.238	0.103	0.157	0.271	0.337	0.136
25 - 31	0.003	0.014	0.012	0.012	0.004	0.014	0.017	0.020	0.003	0.013	0.013	0.010	0.004	0.015	0.023	0.015
Total	0.326	0.711	0.335	0.525	0.321	0.739	0.428	0.696	0.295	0.814	0.539	0.286	0.327	0.653	0.763	0.372

X4 case 1 (t_{br} = 10.0mm, t_{ch} = 10.0mm)

	Brace 1 (top)				Brace 2 (bottom)				Chord 1 (top)				Chord 2 (bottom)			
V_{wind}	Point 1	Point 2	Point 3	Point 4	Point 1	Point 2	Point 3	Point 4	Point 1	Point 2	Point 3	Point 4	Point 1	Point 2	Point 3	Point 4
1 - 9	0.032	0.053	0.031	0.056	0.032	0.093	0.036	0.067	0.031	0.048	0.050	0.030	0.032	0.077	0.061	0.034
9 - 15	0.010	0.009	0.003	0.024	0.005	0.071	0.003	0.023	0.009	0.008	0.020	0.003	0.005	0.056	0.019	0.003
15 - 19	0.044	0.049	0.019	0.095	0.027	0.286	0.024	0.092	0.040	0.042	0.078	0.018	0.029	0.241	0.078	0.021
19 - 25	0.086	0.106	0.042	0.186	0.059	0.488	0.049	0.191	0.082	0.091	0.152	0.040	0.061	0.365	0.165	0.045
25 - 31	0.002	0.003	0.002	0.004	0.002	0.006	0.002	0.004	0.002	0.004	0.004	0.002	0.002	0.008	0.005	0.002
Total	0.175	0.220	0.097	0.364	0.124	0.945	0.114	0.378	0.164	0.192	0.304	0.092	0.128	0.746	0.328	0.105

Case 1a: X-Joint - members (maximum values)

X1 case 1 (t_{br} = 12.5mm, t_{ch} = 12.5mm)

	Brace 1	Brace 2	Chord 1	Chord 2
V_{wind}	Max	Max	Max	Max
1 - 9	0.184	0.177	0.192	0.177
9 - 15	0.009	0.011	0.010	0.009
15 - 19	0.144	0.174	0.156	0.154
19 - 25	0.414	0.514	0.473	0.424
25 - 31	0.020	0.019	0.019	0.020
Total	0.770	0.896	0.851	0.784

X2 case 1 (t_{br} = 11mm, t_{ch} = 11mm)

	Brace 1	Brace 2	Chord 1	Chord 2
V_{wind}	Max	Max	Max	Max
1 - 9	0.153	0.211	0.157	0.198
9 - 15	0.006	0.019	0.008	0.015
15 - 19	0.070	0.182	0.082	0.153
19 - 25	0.138	0.335	0.171	0.251
25 - 31	0.009	0.012	0.009	0.013
Total	0.377	0.759	0.427	0.630

X3 case 1 (t_{br} = 9.5mm, t_{ch} = 9.5mm)

	Brace 1	Brace 2	Chord 1	Chord 2
V_{wind}	Max	Max	Max	Max
1 - 9	0.214	0.230	0.223	0.183
9 - 15	0.024	0.019	0.029	0.044
15 - 19	0.155	0.154	0.182	0.177
19 - 25	0.305	0.322	0.367	0.337
25 - 31	0.014	0.014	0.013	0.023
Total	0.711	0.739	0.814	0.763

X4 case 1 (t_{br} = 10.0mm, t_{ch} = 10.0mm)

	Brace 1	Brace 2	Chord 1	Chord 2
V_{wind}	Max	Max	Max	Max
1 - 9	0.056	0.093	0.050	0.077
9 - 15	0.024	0.071	0.020	0.056
15 - 19	0.095	0.286	0.078	0.241
19 - 25	0.186	0.488	0.152	0.365
25 - 31	0.004	0.006	0.004	0.008
Total	0.364	0.945	0.304	0.746

Case 1a: K-Joint - cans

K1 front plane (t_{br1} = 19.5mm, t_{ch1} = 78mm, t_{br2} = 25mm, t_{ch2} = 78mm)

	Brace 1 (top)				Brace 2 (bottom)				Chord 1 (top)				Chord 2 (bottom)			
V_{wind}	Cr toe	Cr heel	Sa si1	Sa si2	Cr toe	Cr heel	Sa si1	Sa si2	Cr toe	Cr heel	Sa si1	Sa si2	Cr toe	Cr heel	Sa si1	Sa si2
1 - 9	0.085	0.122	0.002	0.015	0.021	0.069	0.001	0.005	0.081	0.116	0.001	0.000	0.049	0.009	0.002	0.000
9 - 15	0.040	0.018	0.000	0.000	0.025	0.009	0.000	0.000	0.001	0.013	0.000	0.000	0.075	0.011	0.000	0.000
15 - 19	0.298	0.137	0.001	0.006	0.112	0.093	0.004	0.005	0.023	0.133	0.001	0.000	0.366	0.075	0.002	0.002
19 - 25	0.526	0.200	0.003	0.014	0.152	0.216	0.010	0.015	0.056	0.185	0.002	0.000	0.503	0.152	0.005	0.004
25 - 31	0.006	0.007	0.000	0.001	0.002	0.011	0.000	0.001	0.005	0.009	0.000	0.000	0.006	0.002	0.000	0.000
Total	0.956	0.484	0.006	0.036	0.313	0.397	0.016	0.026	0.166	0.457	0.004	0.001	0.997	0.250	0.010	0.006

K2 front plane (t_{br1} = 13mm, t_{ch1} = 60mm, t_{br2} = 12.5mm, t_{ch2} = 60mm)

	Brace 1 (top)				Brace 2 (bottom)				Chord 1 (top)				Chord 2 (bottom)			
V_{wind}	Cr toe	Cr heel	Sa si1	Sa si2	Cr toe	Cr heel	Sa si1	Sa si2	Cr toe	Cr heel	Sa si1	Sa si2	Cr toe	Cr heel	Sa si1	Sa si2
1 - 9	0.050	0.198	0.029	0.020	0.127	0.132	0.020	0.032	0.038	0.092	0.002	0.004	0.009	0.000	0.003	0.002
9 - 15	0.019	0.023	0.005	0.002	0.045	0.024	0.001	0.002	0.003	0.030	0.001	0.001	0.030	0.001	0.000	0.000
15 - 19	0.084	0.163	0.020	0.014	0.243	0.186	0.009	0.019	0.028	0.211	0.003	0.004	0.113	0.004	0.002	0.001
19 - 25	0.154	0.294	0.039	0.028	0.410	0.277	0.022	0.042	0.052	0.295	0.005	0.007	0.163	0.007	0.005	0.003
25 - 31	0.003	0.013	0.003	0.002	0.008	0.009	0.002	0.002	0.003	0.011	0.001	0.001	0.002	0.000	0.000	0.000
Total	0.309	0.690	0.096	0.067	0.832	0.627	0.054	0.097	0.125	0.638	0.011	0.017	0.317	0.012	0.011	0.006

K3 front plane (t_{br1} = 14.5mm, t_{ch1} = 52mm, t_{br2} = 14mm, t_{ch2} = 52mm)

	Brace 1 (top)				Brace 2 (bottom)				Chord 1 (top)				Chord 2 (bottom)			
V_{wind}	Cr toe	Cr heel	Sa si1	Sa si2	Cr toe	Cr heel	Sa si1	Sa si2	Cr toe	Cr heel	Sa si1	Sa si2	Cr toe	Cr heel	Sa si1	Sa si2
1 - 9	0.013	0.063	0.014	0.011	0.069	0.081	0.030	0.041	0.016	0.050	0.004	0.005	0.022	0.002	0.016	0.011
9 - 15	0.008	0.086	0.004	0.001	0.077	0.070	0.004	0.013	0.002	0.083	0.000	0.002	0.120	0.001	0.010	0.003
15 - 19	0.035	0.345	0.017	0.007	0.304	0.303	0.016	0.048	0.014	0.335	0.002	0.007	0.352	0.005	0.032	0.009
19 - 25	0.060	0.489	0.034	0.018	0.457	0.401	0.031	0.090	0.029	0.436	0.006	0.014	0.468	0.009	0.054	0.016
25 - 31	0.001	0.006	0.001	0.001	0.004	0.006	0.004	0.007	0.002	0.009	0.000	0.000	0.003	0.000	0.005	0.003
Total	0.116	0.989	0.069	0.038	0.911	0.861	0.086	0.199	0.063	0.913	0.013	0.029	0.965	0.017	0.115	0.044

Case 1a: K-Joint - cans (continued)

K1 side plane (t_{br1} = 19.5mm, t_{ch1} = 78mm, t_{br2} = 25mm, t_{ch2} = 78mm)

	Brace 1 (top)				Brace 2 (bottom)				Chord 1 (top)				Chord 2 (bottom)			
V_{wind}	Cr toe	Cr heel	Sa si1	Sa si2	Cr toe	Cr heel	Sa si1	Sa si2	Cr toe	Cr heel	Sa si1	Sa si2	Cr toe	Cr heel	Sa si1	Sa si2
1 - 9	0.062	0.049	0.008	0.001	0.017	0.139	0.006	0.002	0.050	0.083	0.000	0.001	0.039	0.010	0.000	0.001
9 - 15	0.063	0.049	0.006	0.002	0.008	0.043	0.003	0.001	0.051	0.069	0.000	0.000	0.008	0.010	0.000	0.001
15 - 19	0.222	0.194	0.026	0.005	0.043	0.315	0.021	0.009	0.255	0.365	0.000	0.003	0.050	0.051	0.002	0.005
19 - 25	0.369	0.222	0.036	0.007	0.079	0.454	0.035	0.018	0.289	0.390	0.000	0.005	0.120	0.109	0.005	0.010
25 - 31	0.018	0.010	0.001	0.000	0.004	0.025	0.001	0.001	0.007	0.010	0.000	0.000	0.010	0.005	0.000	0.000
Total	0.734	0.524	0.076	0.014	0.151	0.976	0.067	0.032	0.652	0.917	0.001	0.009	0.226	0.184	0.008	0.018

K2 side plane (t_{br1} = 13mm, t_{ch1} = 60mm, t_{br2} = 12.5mm, t_{ch2} = 60mm)

	Brace 1 (top)				Brace 2 (bottom)				Chord 1 (top)				Chord 2 (bottom)			
V_{wind}	Cr toe	Cr heel	Sa si1	Sa si2	Cr toe	Cr heel	Sa si1	Sa si2	Cr toe	Cr heel	Sa si1	Sa si2	Cr toe	Cr heel	Sa si1	Sa si2
1 - 9	0.034	0.136	0.010	0.017	0.123	0.115	0.021	0.017	0.034	0.082	0.002	0.001	0.008	0.001	0.001	0.002
9 - 15	0.034	0.068	0.004	0.011	0.084	0.052	0.013	0.012	0.035	0.071	0.001	0.000	0.013	0.003	0.001	0.001
15 - 19	0.097	0.340	0.020	0.044	0.293	0.285	0.058	0.046	0.161	0.383	0.004	0.001	0.034	0.005	0.005	0.006
19 - 25	0.143	0.432	0.029	0.055	0.430	0.336	0.082	0.061	0.179	0.453	0.005	0.002	0.062	0.008	0.007	0.009
25 - 31	0.007	0.015	0.001	0.002	0.021	0.011	0.002	0.004	0.003	0.010	0.000	0.000	0.004	0.000	0.001	0.000
Total	0.316	0.992	0.063	0.127	0.951	0.798	0.176	0.140	0.411	0.999	0.012	0.005	0.121	0.017	0.015	0.017

K3 side plane (t_{br1} = 14.5mm, t_{ch1} = 52mm, t_{br2} = 14mm, t_{ch2} = 52mm)

	Brace 1 (top)				Brace 2 (bottom)				Chord 1 (top)				Chord 2 (bottom)			
V_{wind}	Cr toe	Cr heel	Sa si1	Sa si2	Cr toe	Cr heel	Sa si1	Sa si2	Cr toe	Cr heel	Sa si1	Sa si2	Cr toe	Cr heel	Sa si1	Sa si2
1 - 9	0.007	0.037	0.007	0.008	0.043	0.067	0.025	0.017	0.015	0.040	0.004	0.003	0.007	0.003	0.005	0.007
9 - 15	0.006	0.032	0.005	0.007	0.024	0.040	0.021	0.006	0.023	0.074	0.003	0.002	0.014	0.007	0.002	0.009
15 - 19	0.020	0.149	0.024	0.022	0.087	0.171	0.086	0.019	0.094	0.318	0.009	0.010	0.046	0.013	0.006	0.038
19 - 25	0.034	0.221	0.034	0.034	0.164	0.215	0.122	0.028	0.121	0.416	0.014	0.014	0.083	0.017	0.009	0.056
25 - 31	0.001	0.010	0.001	0.001	0.008	0.012	0.002	0.001	0.001	0.010	0.000	0.000	0.006	0.001	0.000	0.001
Total	0.068	0.449	0.071	0.072	0.326	0.505	0.256	0.071	0.255	0.857	0.030	0.030	0.156	0.040	0.022	0.111

Case 1a: K-Joint - cans (maximum values)

K1 (t_{br1} = 19.5mm, t_{ch1} = 78mm, t_{br2} = 25mm, t_{ch2} = 78mm)

Front plane

	Brace 1	Brace 2	Chord 1	Chord 2
V_{wind}	Max	Max	Max	Max
1 - 9	0.085	0.069	0.116	0.049
9 - 15	0.040	0.009	0.013	0.075
15 - 19	0.298	0.093	0.133	0.366
19 - 25	0.526	0.216	0.185	0.503
25 - 31	0.006	0.011	0.009	0.006
Total	0.956	0.397	0.457	0.997

Side plane

	Brace 1	Brace 2	Chord 1	Chord 2
V_{wind}	Max	Max	Max	Max
1 - 9	0.062	0.139	0.083	0.039
9 - 15	0.063	0.043	0.069	0.008
15 - 19	0.222	0.315	0.365	0.050
19 - 25	0.369	0.454	0.390	0.120
25 - 31	0.018	0.025	0.010	0.010
Total	0.734	0.976	0.917	0.226

K2 (t_{br1} = 13mm, t_{ch1} = 60mm, t_{br2} = 12.5mm, t_{ch2} = 60mm)

Front plane

	Brace 1	Brace 2	Chord 1	Chord 2
V_{wind}	Max	Max	Max	Max
1 - 9	0.198	0.127	0.092	0.009
9 - 15	0.023	0.045	0.030	0.030
15 - 19	0.163	0.243	0.211	0.113
19 - 25	0.294	0.410	0.295	0.163
25 - 31	0.013	0.008	0.011	0.002
Total	0.690	0.832	0.638	0.317

Side plane

	Brace 1	Brace 2	Chord 1	Chord 2
V_{wind}	Max	Max	Max	Max
1 - 9	0.136	0.123	0.082	0.008
9 - 15	0.068	0.084	0.071	0.013
15 - 19	0.340	0.293	0.383	0.034
19 - 25	0.432	0.430	0.453	0.062
25 - 31	0.015	0.021	0.010	0.004
Total	0.992	0.951	0.999	0.121

K3 (t_{br1} = 14.5mm, t_{ch1} = 52mm, t_{br2} = 14mm, t_{ch2} = 52mm)

Front plane

	Brace 1	Brace 2	Chord 1	Chord 2
V_{wind}	Max	Max	Max	Max
1 - 9	0.063	0.069	0.050	0.022
9 - 15	0.086	0.077	0.083	0.120
15 - 19	0.345	0.304	0.335	0.352
19 - 25	0.489	0.457	0.436	0.468
25 - 31	0.006	0.004	0.009	0.003
Total	0.989	0.911	0.913	0.965

Side plane

	Brace 1	Brace 2	Chord 1	Chord 2
V_{wind}	Max	Max	Max	Max
1 - 9	0.037	0.067	0.040	0.007
9 - 15	0.032	0.040	0.074	0.014
15 - 19	0.149	0.171	0.318	0.046
19 - 25	0.221	0.215	0.416	0.083
25 - 31	0.010	0.012	0.010	0.006
Total	0.449	0.505	0.857	0.156

Case 1a: K-Joint - members

K1 front plane (t_{br1} = 11mm, t_{ch1} = 40.5mm, t_{br2} = 12.5mm, t_{ch2} = 44.5mm)

	Brace 1 (top)				Brace 2 (bottom)				Chord 1 (top)				Chord 2 (bottom)			
V_{wind}	Point 1	Point 2	Point 3	Point 4	Point 1	Point 2	Point 3	Point 4	Point 1	Point 2	Point 3	Point 4	Point 1	Point 2	Point 3	Point 4
1 - 9	0.022	0.037	0.011	0.066	0.034	0.017	0.011	0.043	0.047	0.054	0.037	0.067	0.076	0.104	0.067	0.114
9 - 15	0.002	0.004	0.002	0.001	0.003	0.007	0.003	0.004	0.061	0.027	0.024	0.070	0.058	0.023	0.021	0.062
15 - 19	0.018	0.034	0.009	0.020	0.046	0.051	0.032	0.036	0.337	0.207	0.174	0.400	0.340	0.209	0.175	0.400
19 - 25	0.033	0.065	0.020	0.047	0.155	0.097	0.093	0.098	0.396	0.236	0.213	0.442	0.349	0.226	0.192	0.407
25 - 31	0.001	0.002	0.001	0.004	0.005	0.001	0.002	0.003	0.006	0.009	0.007	0.007	0.007	0.010	0.007	0.010
Total	0.076	0.142	0.042	0.138	0.243	0.174	0.141	0.183	0.847	0.533	0.455	0.987	0.830	0.572	0.463	0.992

K2 front plane (t_{br1} = 9.5mm, t_{ch1} = 33mm, t_{br2} = 11mm, t_{ch2} = 40.5mm)

	Brace 1 (top)				Brace 2 (bottom)				Chord 1 (top)				Chord 2 (bottom)			
V_{wind}	Point 1	Point 2	Point 3	Point 4	Point 1	Point 2	Point 3	Point 4	Point 1	Point 2	Point 3	Point 4	Point 1	Point 2	Point 3	Point 4
1 - 9	0.025	0.012	0.022	0.014	0.003	0.005	0.002	0.006	0.010	0.020	0.008	0.023	0.013	0.029	0.013	0.031
9 - 15	0.002	0.001	0.002	0.000	0.000	0.000	0.000	0.000	0.040	0.066	0.026	0.095	0.014	0.026	0.011	0.033
15 - 19	0.012	0.007	0.013	0.005	0.002	0.003	0.001	0.003	0.164	0.304	0.125	0.383	0.083	0.167	0.069	0.198
19 - 25	0.025	0.015	0.028	0.012	0.003	0.006	0.002	0.006	0.195	0.369	0.154	0.452	0.093	0.193	0.079	0.222
25 - 31	0.001	0.001	0.001	0.001	0.000	0.000	0.000	0.000	0.003	0.007	0.003	0.007	0.002	0.004	0.002	0.004
Total	0.065	0.035	0.066	0.031	0.008	0.014	0.006	0.015	0.411	0.766	0.316	0.960	0.205	0.419	0.172	0.488

K3 front plane (t_{br1} = 10mm, t_{ch1} = 27.5mm, t_{br2} = 9.5mm, t_{ch2} = 33mm)

	Brace 1 (top)				Brace 2 (bottom)				Chord 1 (top)				Chord 2 (bottom)			
V_{wind}	Point 1	Point 2	Point 3	Point 4	Point 1	Point 2	Point 3	Point 4	Point 1	Point 2	Point 3	Point 4	Point 1	Point 2	Point 3	Point 4
1 - 9	0.012	0.007	0.011	0.007	0.015	0.025	0.017	0.022	0.007	0.004	0.003	0.010	0.009	0.010	0.006	0.014
9 - 15	0.003	0.001	0.003	0.001	0.002	0.003	0.001	0.003	0.102	0.046	0.037	0.127	0.045	0.025	0.018	0.060
15 - 19	0.015	0.005	0.014	0.004	0.009	0.018	0.005	0.018	0.276	0.162	0.122	0.359	0.172	0.130	0.091	0.236
19 - 25	0.029	0.011	0.029	0.010	0.020	0.039	0.012	0.039	0.328	0.207	0.153	0.432	0.200	0.163	0.113	0.278
25 - 31	0.001	0.000	0.001	0.000	0.001	0.001	0.001	0.001	0.003	0.006	0.005	0.004	0.002	0.004	0.003	0.003
Total	0.060	0.023	0.058	0.023	0.046	0.087	0.036	0.083	0.715	0.425	0.320	0.931	0.428	0.332	0.231	0.591

Case 1a: K-Joint - members (continued)

K1 side plane (t_{br1} = 11mm, t_{ch1} = 40.5mm, t_{br2} = 12.5mm, t_{ch2} = 44.5mm)

	Brace 1 (top)				Brace 2 (bottom)				Chord 1 (top)				Chord 2 (bottom)			
V_{wind}	Point 1	Point 2	Point 3	Point 4	Point 1	Point 2	Point 3	Point 4	Point 1	Point 2	Point 3	Point 4	Point 1	Point 2	Point 3	Point 4
1 - 9	0.017	0.031	0.045	0.009	0.040	0.019	0.039	0.016	0.047	0.054	0.037	0.067	0.076	0.104	0.067	0.114
9 - 15	0.015	0.020	0.023	0.013	0.043	0.020	0.037	0.023	0.061	0.027	0.024	0.070	0.058	0.023	0.021	0.062
15 - 19	0.059	0.087	0.117	0.042	0.224	0.083	0.170	0.109	0.337	0.207	0.174	0.400	0.340	0.209	0.175	0.400
19 - 25	0.071	0.121	0.150	0.053	0.359	0.130	0.246	0.186	0.396	0.236	0.213	0.442	0.349	0.226	0.192	0.407
25 - 31	0.003	0.005	0.005	0.002	0.016	0.004	0.009	0.008	0.006	0.009	0.007	0.007	0.007	0.010	0.007	0.010
Total	0.164	0.264	0.340	0.119	0.681	0.257	0.501	0.342	0.847	0.533	0.455	0.987	0.830	0.572	0.463	0.992

K2 side plane (t_{br1} = 9.5mm, t_{ch1} = 33mm, t_{br2} = 11mm, t_{ch2} = 40.5mm)

	Brace 1 (top)				Brace 2 (bottom)				Chord 1 (top)				Chord 2 (bottom)			
V_{wind}	Point 1	Point 2	Point 3	Point 4	Point 1	Point 2	Point 3	Point 4	Point 1	Point 2	Point 3	Point 4	Point 1	Point 2	Point 3	Point 4
1 - 9	0.017	0.007	0.008	0.014	0.002	0.004	0.004	0.002	0.010	0.020	0.008	0.023	0.013	0.029	0.013	0.031
9 - 15	0.009	0.005	0.003	0.010	0.002	0.003	0.003	0.002	0.040	0.066	0.026	0.095	0.014	0.026	0.011	0.033
15 - 19	0.038	0.017	0.016	0.039	0.007	0.011	0.012	0.006	0.164	0.304	0.125	0.383	0.083	0.167	0.069	0.198
19 - 25	0.049	0.025	0.022	0.051	0.008	0.014	0.015	0.007	0.195	0.369	0.154	0.452	0.093	0.193	0.079	0.222
25 - 31	0.002	0.001	0.001	0.001	0.000	0.001	0.000	0.000	0.003	0.007	0.003	0.007	0.002	0.004	0.002	0.004
Total	0.114	0.055	0.050	0.115	0.019	0.033	0.034	0.017	0.411	0.766	0.316	0.960	0.205	0.419	0.172	0.488

K3 side plane (t_{br1} = 10mm, t_{ch1} = 27.5mm, t_{br2} = 9.5mm, t_{ch2} = 33mm)

	Brace 1 (top)				Brace 2 (bottom)				Chord 1 (top)				Chord 2 (bottom)			
V_{wind}	Point 1	Point 2	Point 3	Point 4	Point 1	Point 2	Point 3	Point 4	Point 1	Point 2	Point 3	Point 4	Point 1	Point 2	Point 3	Point 4
1 - 9	0.008	0.004	0.005	0.007	0.010	0.015	0.015	0.011	0.007	0.004	0.003	0.010	0.009	0.010	0.006	0.014
9 - 15	0.004	0.003	0.002	0.006	0.006	0.008	0.012	0.004	0.102	0.046	0.037	0.127	0.045	0.025	0.018	0.060
15 - 19	0.017	0.013	0.009	0.022	0.022	0.034	0.046	0.015	0.276	0.162	0.122	0.359	0.172	0.130	0.091	0.236
19 - 25	0.026	0.018	0.013	0.033	0.030	0.052	0.066	0.022	0.328	0.207	0.153	0.432	0.200	0.163	0.113	0.278
25 - 31	0.001	0.000	0.000	0.001	0.001	0.001	0.001	0.001	0.003	0.006	0.005	0.004	0.002	0.004	0.003	0.003
Total	0.057	0.038	0.029	0.069	0.069	0.111	0.140	0.052	0.715	0.425	0.320	0.931	0.428	0.332	0.231	0.591

Case 1a: K-Joint - members (maximum values)

K1 (t_{br1} = 11mm, t_{ch1} = 40.5mm, t_{br2} = 12.5mm, t_{ch2} = 44.5mm)

Front plane

	Brace 1	Brace 2	Chord 1	Chord 2
V_{wind}	Max	Max	Max	Max
1 - 9	0.037	0.034	0.067	0.114
9 - 15	0.004	0.003	0.070	0.062
15 - 19	0.034	0.046	0.400	0.400
19 - 25	0.065	0.155	0.442	0.407
25 - 31	0.002	0.005	0.007	0.010
Total	0.142	0.243	0.987	0.992

Side plane

	Brace 1	Brace 2	Chord 1	Chord 2
V_{wind}	Max	Max	Max	Max
1 - 9	0.045	0.040	0.067	0.114
9 - 15	0.023	0.043	0.070	0.062
15 - 19	0.117	0.224	0.400	0.400
19 - 25	0.150	0.359	0.442	0.407
25 - 31	0.005	0.016	0.007	0.010
Total	0.340	0.681	0.987	0.992

K2 (t_{br1} = 9.5mm, t_{ch1} = 33mm, t_{br2} = 11mm, t_{ch2} = 40.5mm)

Front plane

	Brace 1	Brace 2	Chord 1	Chord 2
V_{wind}	Max	Max	Max	Max
1 - 9	0.022	0.006	0.023	0.031
9 - 15	0.002	0.000	0.095	0.033
15 - 19	0.013	0.003	0.383	0.198
19 - 25	0.028	0.006	0.452	0.222
25 - 31	0.001	0.000	0.007	0.004
Total	0.066	0.015	0.960	0.488

Side plane

	Brace 1	Brace 2	Chord 1	Chord 2
V_{wind}	Max	Max	Max	Max
1 - 9	0.014	0.004	0.023	0.031
9 - 15	0.010	0.003	0.095	0.033
15 - 19	0.039	0.012	0.383	0.198
19 - 25	0.051	0.015	0.452	0.222
25 - 31	0.001	0.000	0.007	0.004
Total	0.115	0.034	0.960	0.488

K3 (t_{br1} = 10mm, t_{ch1} = 27.5mm, t_{br2} = 9.5mm, t_{ch2} = 33mm)

Front plane

	Brace 1	Brace 2	Chord 1	Chord 2
V_{wind}	Max	Max	Max	Max
1 - 9	0.012	0.025	0.010	0.014
9 - 15	0.003	0.003	0.127	0.060
15 - 19	0.015	0.018	0.359	0.236
19 - 25	0.029	0.039	0.432	0.278
25 - 31	0.001	0.001	0.004	0.003
Total	0.060	0.087	0.931	0.591

Side plane

	Brace 1	Brace 2	Chord 1	Chord 2
V_{wind}	Max	Max	Max	Max
1 - 9	0.007	0.015	0.010	0.014
9 - 15	0.006	0.012	0.127	0.060
15 - 19	0.022	0.046	0.359	0.236
19 - 25	0.033	0.066	0.432	0.278
25 - 31	0.001	0.001	0.004	0.003
Total	0.069	0.140	0.931	0.591

Case 1a: Average contribution of wind speed scenarios to unity check

Extensive table

Vwind	1 - 9	9 - 15	15 - 19	19 - 25	25 - 31	Total
Legs						
Level 1 c	5%	7%	37%	50%	1%	100%
Level 1 m	11%	6%	40%	41%	1%	100%
Level 2 c	6%	8%	38%	47%	1%	100%
Level 2 m	7%	7%	41%	45%	1%	100%
Level 3 c	5%	10%	37%	47%	1%	100%
Level 3 m	2%	10%	40%	47%	1%	100%
Level 4 c	5%	9%	37%	48%	1%	100%
Level 4 m	1%	14%	39%	46%	0%	100%
Average legs	**5%**	**9%**	**38%**	**46%**	**1%**	100%
Braces						
Level 1c K	14%	4%	32%	47%	3%	100%
Level 1m K	6%	6%	33%	53%	2%	100%
Level 1c X	32%	2%	18%	45%	3%	100%
Level 1m X	20%	1%	19%	57%	2%	100%
Level 2c K	11%	7%	31%	50%	1%	100%
Level 2m K	12%	8%	34%	44%	1%	100%
Level 2c X	43%	1%	16%	37%	3%	100%
Level 2m X	28%	2%	24%	44%	2%	100%
Level 3c K	11%	8%	34%	47%	1%	100%
Level 3m K	11%	9%	33%	46%	1%	100%
Level 3c X	29%	4%	22%	42%	3%	100%
Level 3m X	27%	4%	22%	45%	2%	100%
Level 4c K	6%	9%	35%	49%	1%	100%
Level 4m K	10%	9%	32%	48%	1%	100%
Level 4c X	14%	9%	28%	48%	1%	100%
Level 4m X	10%	8%	30%	52%	1%	100%
Average braces	**18%**	**6%**	**28%**	**47%**	**2%**	100%
Average	**17%**	**6%**	**29%**	**47%**	**2%**	**100%**

G.2. FLS welded structure: Relative contribution of normal force and bending moments

In this section, the relative contribution of normal force N, in-plane bending moment M_{ip} and out-of-plane bending moment M_{op} to the total fatigue damage of the steel welded structure (case 1) is given.

Important and maximum values are highlighted.

Highlighted in red: Value of N, M_{ip} or M_{op} with largest contribution to total damage.

Highlighted in yellow: Value of $N + M_{ip}$ or $N + M_{op}$ with largest damage contribution. Highlighted value of $N + M_{ip}$ indicates crown is governing, whereas highlighted value of $N + M_{op}$ indicates saddle location is governing.

In final table, the values highlighted in red indicate the value of N, M_{ip} or M_{op} with largest contribution to total damage $N + M_{ip}$ or $N + M_{op}$

Case 1a: X-Joint - cans - Damage contribution N, M_{ip}, M_{op}

X1 (t_{br} = 31mm, t_{ch} = 31mm)

Case 1

V_{wind}	Brace 1 Max	Brace 2 Max	Chord 1 Max	Chord 2 Max
N	0.032	0.054	0.286	0.408
M_{ip}	0.042	0.002	0.286	0.046
M_{op}	0.001	0.000	0.024	0.005
N + M_{ip}	0.236	0.426	0.876	0.408
N + M_{op}	0.082	0.079	0.951	0.776
Total	0.236	0.426	0.951	0.776

Case 2

V_{wind}	Brace 1 Max	Brace 2 Max	Chord 1 Max	Chord 2 Max
N	0.029	0.049	0.252	0.360
M_{ip}	0.053	0.002	0.326	0.055
M_{op}	0.001	0.000	0.022	0.005
N + M_{ip}	0.297	0.384	0.891	0.360
N + M_{op}	0.076	0.074	0.886	0.733
Total	0.297	0.384	0.891	0.733

X2 (t_{br} = 29.5mm, t_{ch} = 29.5mm)

Case 1

V_{wind}	Brace 1 Max	Brace 2 Max	Chord 1 Max	Chord 2 Max
N	0.018	0.020	0.177	0.193
M_{ip}	0.005	0.044	0.052	0.550
M_{op}	0.000	0.000	0.001	0.005
N + M_{ip}	0.048	0.166	0.177	0.728
N + M_{op}	0.031	0.068	0.348	0.835
Total	0.048	0.166	0.348	0.835

Case 2

V_{wind}	Brace 1 Max	Brace 2 Max	Chord 1 Max	Chord 2 Max
N	0.018	0.020	0.179	0.196
M_{ip}	0.005	0.038	0.057	0.510
M_{op}	0.000	0.000	0.001	0.006
N + M_{ip}	0.062	0.135	0.179	0.867
N + M_{op}	0.032	0.077	0.352	0.947
Total	0.062	0.135	0.352	0.947

X3 (t_{br} = 27.5mm, t_{ch} = 27.5mm)

Case 1

V_{wind}	Brace 1 Max	Brace 2 Max	Chord 1 Max	Chord 2 Max
N	0.031	0.036	0.339	0.385
M_{ip}	0.019	0.006	0.280	0.071
M_{op}	0.001	0.001	0.020	0.019
N + M_{ip}	0.091	0.075	0.379	0.385
N + M_{op}	0.061	0.076	0.812	0.989
Total	0.091	0.076	0.812	0.989

Case 2

V_{wind}	Brace 1 Max	Brace 2 Max	Chord 1 Max	Chord 2 Max
N	0.030	0.034	0.322	0.365
M_{ip}	0.021	0.005	0.291	0.068
M_{op}	0.001	0.001	0.018	0.017
N + M_{ip}	0.116	0.068	0.421	0.365
N + M_{op}	0.060	0.077	0.789	0.992
Total	0.116	0.077	0.789	0.992

X4 (t_{br} = 27.5mm, t_{ch} = 27.5mm)

Case 1

V_{wind}	Brace 1 Max	Brace 2 Max	Chord 1 Max	Chord 2 Max
N	0.036	0.039	0.401	0.425
M_{ip}	0.000	0.019	0.051	0.288
M_{op}	0.000	0.000	0.000	0.001
N + M_{ip}	0.036	0.176	0.401	0.425
N + M_{op}	0.073	0.064	0.900	0.766
Total	0.073	0.176	0.900	0.766

Case 2

V_{wind}	Brace 1 Max	Brace 2 Max	Chord 1 Max	Chord 2 Max
N	0.032	0.035	0.356	0.379
M_{ip}	0.000	0.017	0.047	0.271
M_{op}	0.000	0.000	0.000	0.001
N + M_{ip}	0.032	0.140	0.355	0.379
N + M_{op}	0.064	0.059	0.782	0.706
Total	0.064	0.140	0.782	0.706

Case 1a: X-Joint - members - Damage contribution N, M_{ip}, M_{op}

X1 (t_{br} = 31mm, t_{ch} = 31mm)

Case 1

	Brace 1	Brace 2	Chord 1	Chord 2
V_{wind} [m/s	Max	Max	Max	Max
N	0.224	0.350	0.198	0.310
M_{ip}	0.022	0.000	0.027	0.000
M_{op}	0.008	0.013	0.007	0.012
N + M_{ip}	0.770	0.896	0.851	0.784
N + M_{op}	0.516	0.688	0.452	0.608
Total	0.770	0.896	0.851	0.784

X2 (t_{br} = 29.5mm, t_{ch} = 29.5mm)

Case 1

	Brace 1	Brace 2	Chord 1	Chord 2
V_{wind} [m/s	Max	Max	Max	Max
N	0.141	0.157	0.144	0.161
M_{ip}	0.003	0.042	0.004	0.036
M_{op}	0.000	0.001	0.000	0.001
N + M_{ip}	0.377	0.759	0.427	0.630
N + M_{op}	0.290	0.352	0.316	0.391
Total	0.377	0.759	0.427	0.630

X3 (t_{br} = 27.5mm, t_{ch} = 27.5mm)

Case 1

	Brace 1	Brace 2	Chord 1	Chord 2
V_{wind} [m/s	Max	Max	Max	Max
N	0.265	0.312	0.256	0.301
M_{ip}	0.012	0.007	0.014	0.006
M_{op}	0.007	0.013	0.006	0.014
N + M_{ip}	0.711	0.739	0.814	0.653
N + M_{op}	0.525	0.696	0.539	0.763
Total	0.711	0.739	0.814	0.763

X4 (t_{br} = 27.5mm, t_{ch} = 27.5mm)

Case 1

	Brace 1	Brace 2	Chord 1	Chord 2
V_{wind} [m/s	Max	Max	Max	Max
N	0.186	0.201	0.166	0.181
M_{ip}	0.000	0.012	0.000	0.010
M_{op}	0.000	0.000	0.000	0.000
N + M_{ip}	0.220	0.945	0.192	0.746
N + M_{op}	0.364	0.378	0.304	0.328
Total	0.364	0.945	0.304	0.746

Case 1a: K-Joint - cans - Damage contribution N, M_{ip}, M_{op}

K1 (t_{br1} = 11mm, t_{ch1} = 40.5mm, t_{br2} = 12.5mm, t_{ch2} = 44.5mm)

Front plane

V_{wind} [m/s	Brace 1 Max	Brace 2 Max	Chord 1 Max	Chord 2 Max
N	0.157	0.088	0.185	0.242
M_{ip}	0.110	0.036	0.004	0.001
M_{op}	0.000	0.000	0.000	0.001
N + M_{ip}	0.956	0.397	0.456	0.997
N + M_{op}	0.157	0.088	0.185	0.242
Total	0.956	0.397	0.456	0.997

Side plane

V_{wind} [m/s	Brace 1 Max	Brace 2 Max	Chord 1 Max	Chord 2 Max
N	0.339	0.283	0.459	0.092
M_{ip}	0.016	0.006	0.001	0.001
M_{op}	0.000	0.001	0.000	0.001
N + M_{ip}	0.734	0.976	0.917	0.226
N + M_{op}	0.339	0.283	0.459	0.092
Total	0.734	0.976	0.917	0.226

K2 (t_{br1} = 9.5mm, t_{ch1} = 33mm, t_{br2} = 11mm, t_{ch2} = 40.5mm)

Front plane

V_{wind} [m/s	Brace 1 Max	Brace 2 Max	Chord 1 Max	Chord 2 Max
N	0.234	0.268	0.214	0.101
M_{ip}	0.017	0.053	0.001	0.002
M_{op}	0.001	0.000	0.002	0.000
N + M_{ip}	0.690	0.832	0.638	0.317
N + M_{op}	0.234	0.268	0.214	0.101
Total	0.690	0.832	0.638	0.317

Side plane

V_{wind} [m/s	Brace 1 Max	Brace 2 Max	Chord 1 Max	Chord 2 Max
N	0.413	0.614	0.447	0.058
M_{ip}	0.004	0.006	0.000	0.000
M_{op}	0.000	0.000	0.000	0.000
N + M_{ip}	0.992	0.951	0.999	0.121
N + M_{op}	0.413	0.614	0.447	0.058
Total	0.992	0.951	0.999	0.121

K3 (t_{br1} = 10mm, t_{ch1} = 27.5mm, t_{br2} = 9.5mm, t_{ch2} = 33mm)

Front plane

V_{wind} [m/s	Brace 1 Max	Brace 2 Max	Chord 1 Max	Chord 2 Max
N	0.095	0.129	0.264	0.113
M_{ip}	0.053	0.181	0.005	0.010
M_{op}	0.000	0.006	0.000	0.011
N + M_{ip}	0.989	0.911	0.913	0.965
N + M_{op}	0.095	0.199	0.264	0.115
Total	0.989	0.911	0.913	0.965

Side plane

V_{wind} [m/s	Brace 1 Max	Brace 2 Max	Chord 1 Max	Chord 2 Max
N	0.118	0.210	0.311	0.067
M_{ip}	0.004	0.009	0.000	0.001
M_{op}	0.000	0.001	0.000	0.002
N + M_{ip}	0.449	0.505	0.857	0.156
N + M_{op}	0.118	0.256	0.311	0.111
Total	0.449	0.505	0.857	0.156

Case 1a: K-Joint - members - Damage contribution N, M_{ip}, M_{op}

K1 (t_{br1} = 11mm, t_{ch1} = 40.5mm, t_{br2} = 12.5mm, t_{ch2} = 44.5mm)

Front plane

V_{wind} [m/s	Brace 1 Max	Brace 2 Max	Chord 1 Max	Chord 2 Max
N	0.066	0.144	0.629	0.640
M_{ip}	0.002	0.001	0.000	0.000
M_{op}	0.000	0.000	0.000	0.000
N + M_{ip}	0.142	0.243	0.847	0.830
N + M_{op}	0.138	0.183	0.987	0.992
Total	0.142	0.243	0.987	0.992

Side plane

V_{wind} [m/s	Brace 1 Max	Brace 2 Max	Chord 1 Max	Chord 2 Max
N	0.182	0.388	0.629	0.640
M_{ip}	0.000	0.000	0.000	0.000
M_{op}	0.000	0.000	0.000	0.000
N + M_{ip}	0.264	0.681	0.847	0.830
N + M_{op}	0.340	0.501	0.987	0.992
Total	0.340	0.681	0.987	0.992

K2 (t_{br1} = 9.5mm, t_{ch1} = 33mm, t_{br2} = 11mm, t_{ch2} = 40.5mm)

Front plane

V_{wind} [m/s	Brace 1 Max	Brace 2 Max	Chord 1 Max	Chord 2 Max
N	0.044	0.009	0.565	0.296
M_{ip}	0.000	0.000	0.000	0.000
M_{op}	0.000	0.000	0.000	0.000
N + M_{ip}	0.065	0.014	0.766	0.419
N + M_{op}	0.066	0.015	0.960	0.488
Total	0.066	0.015	0.960	0.488

Side plane

V_{wind} [m/s	Brace 1 Max	Brace 2 Max	Chord 1 Max	Chord 2 Max
N	0.073	0.023	0.565	0.296
M_{ip}	0.000	0.000	0.000	0.000
M_{op}	0.000	0.000	0.000	0.000
N + M_{ip}	0.114	0.033	0.766	0.419
N + M_{op}	0.115	0.034	0.960	0.488
Total	0.115	0.034	0.960	0.488

K3 (t_{br1} = 10mm, t_{ch1} = 27.5mm, t_{br2} = 9.5mm, t_{ch2} = 33mm)

Front plane

V_{wind} [m/s	Brace 1 Max	Brace 2 Max	Chord 1 Max	Chord 2 Max
N	0.036	0.052	0.543	0.372
M_{ip}	0.000	0.000	0.000	0.000
M_{op}	0.000	0.000	0.000	0.000
N + M_{ip}	0.060	0.087	0.715	0.428
N + M_{op}	0.058	0.083	0.931	0.591
Total	0.060	0.087	0.931	0.591

Side plane

V_{wind} [m/s	Brace 1 Max	Brace 2 Max	Chord 1 Max	Chord 2 Max
N	0.044	0.080	0.543	0.372
M_{ip}	0.000	0.000	0.000	0.000
M_{op}	0.000	0.000	0.000	0.000
N + M_{ip}	0.057	0.111	0.715	0.428
N + M_{op}	0.069	0.140	0.931	0.591
Total	0.069	0.140	0.931	0.591

Case 1a: Average damage contribution of N, M_{ip} and M_{ip} to unity check

Extensive table

	N only	M_{ip} only	N + M_{ip}
LEGS			
Level 1 c	24%	0.1%	100%
Level 1 m	77%	0.0%	100%
Level 2 c	41%	0.3%	100%
Level 2 m	72%	0.0%	100%
Level 3 c	28%	0.5%	100%
Level 3 m	80%	0.0%	100%
Level 4 c	29%	0.5%	100%
Level 4 m	76%	0.0%	100%
Average legs	**54%**	**0.2%**	**100%**
BRACES			
Level 1c K	29%	0.6%	100%
Level 1m K	57%	0.0%	100%
Level 1c X	33%	32.6%	100%
Level 1m X	39%	0.0%	100%
Level 2c K	41%	6.1%	100%
Level 2m K	70%	0.0%	100%
Level 2c X	23%	51.0%	100%
Level 2m X	21%	51.0%	100%
Level 3c K	28%	10.2%	100%
Level 3m K	68%	0.0%	100%
Level 3c X	100%	6.8%	100%
Level 3m X	31%	6.8%	100%
Level 4c K	10%	5.3%	100%
Level 4m K	78%	0.0%	100%
Level 4c X	100%	5.1%	100%
Level 4m X	21%	5.1%	100%
Average braces	**47%**	**11.3%**	**100%**
Average tot	**49%**	**8%**	**100%**

	N only	M_{op} only	N + M_{op}
LEGS			
Level 1 c	100%	0.4%	100%
Level 1 m	65%	0.0%	100%
Level 2 c	100%	0.2%	100%
Level 2 m	62%	0.0%	100%
Level 3 c	99%	4.6%	100%
Level 3 m	61%	0.0%	100%
Level 4 c	100%	0.0%	100%
Level 4 m	58%	0.0%	100%
Average legs	**81%**	**0.7%**	**100%**
Braces			
Level 1c K	100%	0.2%	100%
Level 1m K	77%	0.0%	100%
Level 1c X	30%	2.5%	100%
Level 1m X	51%	1.9%	100%
Level 2c K	100%	0.1%	100%
Level 2m K	61%	0.0%	100%
Level 2c X	21%	0.7%	100%
Level 2m X	45%	0.1%	100%
Level 3c K	82%	1.5%	100%
Level 3m K	60%	0.0%	100%
Level 3c X	39%	1.9%	100%
Level 3m X	47%	1.1%	100%
Level 4c K	100%	0.0%	100%
Level 4m K	64%	0.0%	100%
Level 4c X	45%	0.0%	100%
Level 4m X	53%	0.0%	100%
Average braces	**61%**	**0.6%**	**100%**
Average tot	**68%**	**1%**	**100%**

G.3. ULS unwelded structure: Utilisation tables per scenario

In this section, detailed global buckling utilisation factors are given for the mild steel unwelded structure (case 2a). Damage due to three different wind-wave scenarios is given. Those cases can be seen in Fig. 4.4.

Important and maximum values are highlighted.

Highlighted in red: Damage belonging to governing scenario for specific member in structure.

Case 2a: Members - Damage per scenario

Unity check global buckling:

Element description			*Steel thickness [mm]*	*Unity check global buckling*			*Maximum difference scenario 1 vs scenario 2 [%]*
				Scenario 1	*Scenario 2*	*Scenario 3*	
Legs	Level 1	Front	21.5	0.65	0.83	0.86	3%
		Back	21.5	0.99	0.96	0.74	
	Level 2	Front	18.5	0.66	0.85	0.87	15%
		Back	18.5	0.97	0.84	0.73	
	Level 3	Front	16	0.71	0.94	0.94	5%
		Back	16	0.99	0.80	0.76	
	Level 4	Front	14.5	0.73	0.99	0.99	-2%
		Back	14.5	0.97	0.75	0.76	
	Average			**0.83**	**0.87**	**0.83**	**5%**
Braces	Level 1	Side	9	0.95	0.76	0.79	25%
		Back	9	0.61	0.71	0.50	
	Level 2	Side	6	0.93	0.96	0.79	-3%
		Back	6	0.80	0.81	0.70	
	Level 3	Side	5	0.92	0.98	0.89	-6%
		Back	5	0.84	0.88	0.83	
	Level 4	Side	5.5	0.99	0.84	0.91	18%
		Back	5.5	0.87	0.76	0.74	
	Average			**0.86**	**0.84**	**0.77**	**8%**
Average				**0.85**	**0.85**	**0.80**	**7%**

G.4. ULS unwelded structure: Relative contribution of normal force and bending moments

In this section, the relative contribution of normal force N, in-plane bending moment M_{ip} and out-of-plane bending moment M_{op} to the total global buckling unity check of the unwelded structure (case 2a) is given.

Important and maximum values are highlighted.

Highlighted in red: Value of N, M_{ip} or M_{op} with largest contribution to total damage.

Highlighted in yellow: Value of $N + M_{ip}$ or $N + M_{op}$ with largest damage contribution.

Case 2a: Members - Damage contribution N, M_{ip}, M_{op}

Unity check global buckling:

Element description			*Steel thickness [mm]*	*Unity check global buckling*					
				N	M_{ip}	M_{op}	$N + M_{ip}$	$N + M_{op}$	$N + M_{ip} + M_{op}$
Legs	Level 1	Front	21.5	0.78	0.21	0.12	0.81	0.85	0.86
		Back	21.5	0.89	0.19	0.19	0.96	0.92	0.99
	Level 2	Front	18.5	0.80	0.11	0.07	0.83	0.83	0.87
		Back	18.5	0.88	0.08	0.10	0.92	0.91	0.97
	Level 3	Front	16	0.84	0.07	0.06	0.89	0.89	0.94
		Back	16	0.86	0.07	0.07	0.92	0.93	0.99
	Level 4	Front	14.5	0.80	0.13	0.10	0.91	0.88	0.99
		Back	14.5	0.79	0.11	0.12	0.89	0.86	0.97
Braces	Level 1	Side	9	0.57	0.41	0.14	0.88	0.64	0.95
		Back	9	0.44	0.36	0.20	0.68	0.51	0.71
	Level 2	Side	6	0.54	0.60	0.20	0.88	0.59	0.96
		Back	6	0.38	0.61	0.29	0.78	0.43	0.81
	Level 3	Side	5	0.43	0.74	0.34	0.83	0.65	0.98
		Back	5	0.34	0.69	0.44	0.72	0.61	0.88
	Level 4	Side	5.5	0.42	0.58	0.10	0.94	0.46	0.99
		Back	5.5	0.33	0.54	0.17	0.82	0.37	0.87
			Average	**0.63**	**0.34**	**0.17**	**0.85**	**0.71**	**0.92**

Case 2a: Members - Damage contribution N, M_{ip}, M_{op} in percentage

Element description			*Steel thickness [mm]*	*Contribution to unity check*			
				N	M_{ip}	M_{op}	$N + M_{ip} + M_{op}$
Legs	Level 1	Front	21.5	89%	19%	19%	100%
		Back	21.5				
	Level 2	Front	18.5	91%	9%	10%	100%
		Back	18.5				
	Level 3	Front	16	87%	7%	7%	100%
		Back	16				
	Level 4	Front	14.5	81%	13%	10%	100%
		Back	14.5				
	Average			**87%**	**12%**	**12%**	**100%**
Braces	Level 1	Side	9	60%	43%	15%	100%
		Back	9				
	Level 2	Side	6	57%	63%	21%	100%
		Back	6				
	Level 3	Side	5	44%	75%	35%	100%
		Back	5				
	Level 4	Side	5.5	42%	59%	10%	100%
		Back	5.5				
	Average			**51%**	**60%**	**20%**	**100%**
Average				**69%**	**36%**	**16%**	**100%**

G.5. ULS unwelded structure: Contribution of hydrodynamic forces

In this section, the contribution of hydrodynamic forces (waves and current) to the total global buckling unity check of the mild steel unwelded structure (case 2a) is given. Results differ from App. F, as results are for one seed only (10 minutes), compared to six seeds (60 minutes).

Highlighted in red: Damage belonging to governing scenario for a specific member in the structure.

Case 2a: Average contribution of hydrodynamic forces

Unity check global buckling wind 0 degrees (seed 1 only):

Element description			*Steel thickness [mm]*	*Unity check global buckling*		Contribution hydrodynamic force [%]
				Wind, waves and current (case 1)	*Wind only*	
Legs	Level 1	Front	21.5	0.65	0.67	9%
		Back	21.5	0.94	0.86	
	Level 2	Front	18.5	0.66	0.68	-3%
		Back	18.5	0.84	0.87	
	Level 3	Front	16	0.71	0.72	-6%
		Back	16	0.87	0.92	
	Level 4	Front	14.5	0.73	0.75	-4%
		Back	14.5	0.88	0.92	
	Average			**0.78**	**0.80**	**-1%**
Braces	Level 1	Side	9	0.88	0.51	71%
		Back	9	0.61	0.52	
	Level 2	Side	6	0.91	0.79	14%
		Back	6	0.80	0.70	
	Level 3	Side	5	0.92	0.78	15%
		Back	5	0.81	0.80	
	Level 4	Side	5.5	0.93	0.97	-4%
		Back	5.5	0.77	0.80	
	Average			**0.83**	**0.73**	**24%**
Average				**0.81**	**0.77**	**11%**

Unity check global buckling wind 45 degrees (seed 1 only):

Element description			*Steel thickness [mm]*	*Unity check global buckling*		Contribution hydrodynamic force [%]
				Wind, waves and current (case 2)	*Wind only*	
Legs	Level 1	Front	21.5	0.83	0.85	13%
		Back	21.5	0.96	0.68	
	Level 2	Front	18.5	0.85	0.87	-3%
		Back	18.5	0.84	0.69	
	Level 3	Front	16	0.94	0.96	-2%
		Back	16	0.80	0.72	
	Level 4	Front	14.5	0.99	1.00	-1%
		Back	14.5	0.74	0.70	
	Average			**0.87**	**0.81**	**2%**
Braces	Level 1	Side	9	0.76	0.54	39%
		Back	9	0.71	0.44	
	Level 2	Side	6	0.96	0.67	43%
		Back	6	0.81	0.60	
	Level 3	Side	5	0.98	0.91	7%
		Back	5	0.88	0.63	
	Level 4	Side	5.5	0.82	0.82	0%
		Back	5.5	0.70	0.69	
	Average			**0.83**	**0.66**	**23%**
Average				**0.85**	**0.74**	**12%**